University of Rome Tor Vergata,
Electronic Engineering Department

Ph.D. Dissertation on Sensorial
and Learning Systems

Integrated Control of Active Steering and Electronic Differentials in Four Wheel Drive and Steering Vehicles

Stefano Scalzi

Advisors:
Prof. Riccardo Marino

XXI Cycle (2005-2008)

If I have been able to see
further, it was only because
I stood on the shoulders of
giants.
Sir Isaac Newton

Contents

Preface

This thesis is submitted in partial fulfillment of the requirements for the degree of doctor engineering at the University of Rome Tor Vergata.
My supervisor has been professor Riccardo Marino and the research activity has been developed at the Electronic Engineering Department in the Sensorial and Learning Systems Ph.D. course between october 2005 and october 2008.
From october 2005 to april 2006, within the framework of a doctoral degree, I having been given the opportunity to work on an industrial problem in Ferrari S.p.a in the reliability department (road tests).

Acknowledgment

First, I would like to thank my advisor professor R. Marino for his rich source of ideas, support throughout the entire research and for always having an open door to my troubles. This co-operation has resulted in two published and two submitted journals papers and several conferences.

I would like to acknowledge the cooperative spirit of the department in which I work in this three years: Prof. Santosuosso, Dr. Ing. Verrelli, Dr. Ing. Cinili, Ing. Tiberti and the students that have been done their thesis in collaboration with the department.

I am very grateful for the support from my parents Patrizia and Claudio and my brother Dario; to my extended family and to my beloved Milena who has always been kind and supportive, patient and encouraging. I would like to acknowledge my friends. It has always been a joy to go for treks with them.

Thank you all, this thesis would never have been possible without your contributions.

Chapter 1

Introduction

1.1 Motivation for Automotive Control Research

There are a lot of motivations to make research in the automotive field: safety, comfort, performance and other related issues. Vehicle Safety Technology (VST) is a term used by the automotive industry applied to technologies focused on ensuring safety and performance of vehicle. The car safety problem is a critical issue due to the high number of accidents and life losses (above 6000 per year in Italy); many accidents involve only one vehicle and are caused by loss of control.
The overall driver task is non trivial from a control viewpoint: the driver directly controls only one state variable (or one combination of them) by the front steering angle (the yaw rate when he is negotiating a turn or the lateral deviation, which is directly related to the lateral speed, when he is performing an overtaking); the lateral speed steady state gain changes with longitudinal speed (positive at low speed and negative at medium and high speed); the lateral speed transfer function is minimum-phase at low speed and non minimum-phase at medium and high speed; moreover poorly damped oscillatory modes at high speed can induce resonances when drivers are inexperienced.

Also for this reasons many electronics control systems are introduced with the goal of safety; this target do not always align with those of performance: some employed systems can help the driver to perform greater longitudinal acceleration without taking in to account the stability of the vehicle. For this reason, recently, several papers are focused on the design of integrated chassis control.

1.1.1 Safety

Automobile safety is the avoidance of automobile accidents or the minimization of harmful effects of accidents, in particular as pertaining to human life and health. Numerous safety features have been built into cars for years for the safety of car's occupants only and for the safety of others. The safety systems can be divided in two category: passive and active.
Passive safety refers to:

- Seatbelts (or safety belts) which absorb energy and limit forward motion of an occupant, and help keep occupants from being ejected from the vehicle.
- Shoulder harnesses add additional protection to seatbelts by restraining the upper body, absorbing energy and preventing injuries from second collisions where the moving occupant hits the stationary dashboard or windshield.
- Energy absorbing windshields which had a deformable polymer layer that allows the windshield to deform on impact absorbing energy and preventing penetration of the head through the windshield and the airbags which should be considered supplemental restraint systems used in addition to belts.

Active safety refers to:

- Traction Control System (TCS) which actuates brakes or reduces throttle to restore traction if driven wheels begin to spin.
- Four Wheel Drive (4WD) which, distributing power to all four wheels, lessens the chances of wheel spin.
- Reverse backup sensors, which alert drivers to nearby objects in their path.
- Electronic Stability Control (ESC, also known by ESP and other numerous manufacturer-specific names) which can reduce power from the engine and even applies braking actions to prevent the car from understeering or oversteering.
- Four Wheel Steering (4WS) which gives, at the cost of mechanical complexity, quicker, more accurate maneuvers at high speed and/or decreased turning circle at low speed.
- Anti-lock Braking System (ABS)
- Electronic Brake force Distribution (EBD)
- Lane Departure Warning System (LDW)
- Dynamic Brake Control (DBC)

Many of this control systems were implemented on cars on the market in recent years such as the Anti-lock Braking System, the Acceleration Slip Regulation (ASR), the Electronic Stability Program, the active steering (BMW) and the four wheel steer steering (4WS) technologies (Renault, Honda, Mazda) with the goal of increasing safety.

1.1.2 Comfort

Some electronic control systems are also introduced to improve comfort such as:

Adaptive Cruise Control (ACC); Intelligent Speed Adaptation (ISA) which physically prevents vehicles from being able to exceed the speed limit through electronic throttle control governed by a GPS matched database of speed limits and the Variable Electronic Power Steering (VEPS) which allows assistance while parking and reduces steering effort. Other control systems can be designed to improve comfort and manoeuvrability (the goal is to obtain that the yaw rate and lateral acceleration are in-phase) as will be shown in Chapter 3.

1.1.3 Performance

To increase longitudinal vehicle performance and to avoid wheels spin the mechanical self locking differential is generally introduced. In a power on driving condition a free differential can not transmit the driving torque to the wheel with high adherence and the vehicle does not move while the locking action of the self locking differential can generate an undesired understeer at low speed or a critical oversteer at high speed. Recently, the development of the semiactive and active differential allow to design electronic control system which can help the driver to perform greater longitudinal acceleration taking in to account the stability of the vehicle as will be shown in Chapter 4.

1.2 Goals of this Study and Chapters Overview

The intent of this research is to propose new control strategies to improve vehicle safety and performance integrating: the active front and rear wheel steering; the electronically controlled differentials and the active front steering; or integrating the information given by a vision based vehicle with the active steering.
The thesis is organized as follows. In the remaining part of this chapter a literature review on vehicle dynamics is presented: the four wheel

steering, the active differential and the autonomous vehicle technology is recalled.

In Chapter 2 the vehicle model is presented and analyzed to explore and evaluate the driver effort; in Chapter 3 the Asymptotic Sideslip and Yaw Rate Decoupling Control in Four Wheel Steering Vehicles is presented. In Chapter 4 the Integrated Control of Active Steering and Electronic Differentials in Four Wheel Drive Vehicles is presented. In Chapter 5 a Nested PID Steering Control for Lane Keeping in Vision Based Autonomous Vehicles is designed and finally in Chapter 6 the global chassis integrated control systems that can be examined in the near future are briefly illustrated.

1.3 Literature Review on Vehicle Control

1.3.1 Four Wheel Steering Control

Several cars on the market use four wheel steer steering (4WS) technologies as shown recently by Renault and BMW or in the last years [1]. In the first generation (Honda) of rear steering vehicles [2], the front wheels steering angle δ_f is transmitted to the rear wheels mechanically by a shaft; in this case the control law is given by $\delta_r = K(\delta_f)\delta_f$ with δ_r the rear steering angle. In active rear steering systems a feedback control $\delta_r = K(v)r$ from the yaw rate measurement r is also used with K depending on the vehicle speed. The rear wheels are steered, at low speed, in the opposite direction to the front wheels to improve manoeuvrability for instance during parking. At high speed, the rear wheels are steered in the same direction as the front wheels to improve stability. Also Mazda uses a feed-forward system that steers the rear wheel like the Honda 4WS but the steering ratio depends on vehicle speed while Nissan uses a feedback control depending on the front wheel aligning torque and the vehicle speed to set the maximum rear steering angle.

More recently some patented feedback control laws on the rear axle are based on the yaw tracking error; in [3] a static lookup table determines the desired yaw rate and a PID controller on the yaw rate tracking error is proposed while in [4] a feed-forward control algorithm includes a proper transfer function between driver and rear control signals to reduce the lateral velocity and to increase stability.
Nowadays two important car company such as BMW and Renault work on 4WS technology: Renault develops its new four-wheel steering Active Drive Chassis with the European introduction of the new high-performance GT versions of the new Laguna Hatch and Sport Tourer; the patented work done by Renault on the four wheel steering system is also shown in [16] in which a coordination of selective backing and active rear steering is presented. Also BMW recently present its new Integral-Active-Steering which will be published for the first time on the FISITA 2008 [19]. In Fig. 1.3 and in Fig. 1.4 the Renault active rear steering systems is shown.

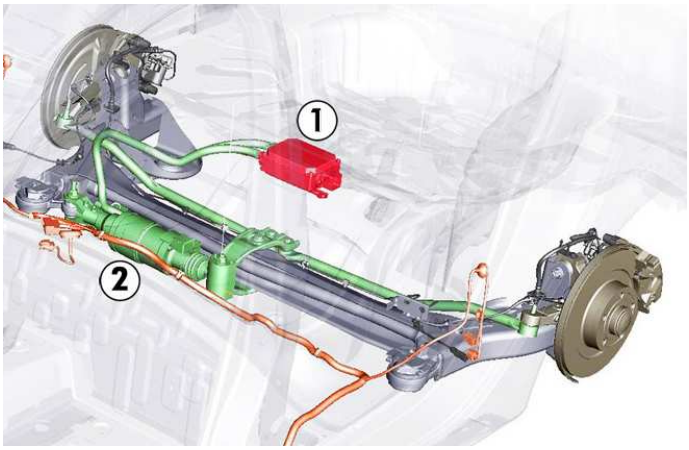

Figure 1.1: Renault active rear steering system.

Also on the front axle many control laws are proposed such as in [11]

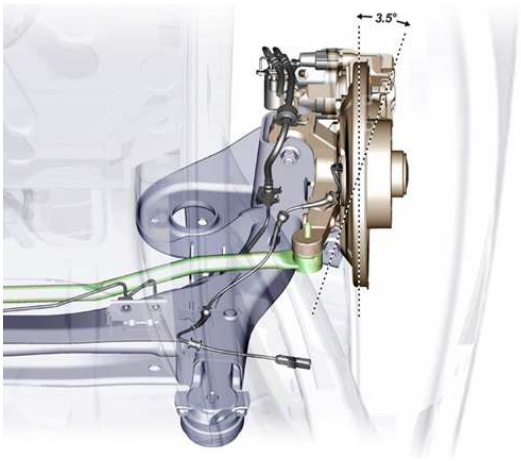

Figure 1.2: Renault active rear steering system detail.

or [12] and implemented on cars such as BMW 5 Series models, or on steer by wire prototypes in which the conventional steering elements are replaced by two electrical actuators which are positioned in the front corners of the vehicle and turn the front wheels. In [11] a PI active front steering control on the yaw rate tracking error with different gains for braked and unbraked driving conditions is used while in [12] a patented method is used to ensure safety during active steering system failure computing the steering wheel angle as the sum of the proposed control law steering angle and the driver steering angle; in Fig. 1.3 and in Fig. 1.4 the BMW active steering systems is shown.

1.3.2 Decoupling Issues

The independent control of the yaw rate and the sideslip angle dynamics improves vehicle handling, comfort, safety and lane keeping. In four wheel steering (4WS) vehicles the decoupling issues are addressed in several papers ([5]-[10]). Decoupling by active front steering was first analyzed in [5]: for a simplified model at constant speed, it is shown

Figure 1.3: Active steering column whit actuator prototype.

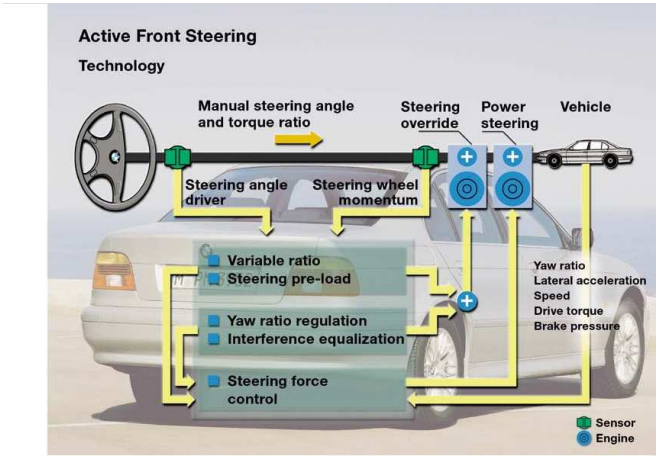

Figure 1.4: BMW Active steering system.

that the dynamics of the front axle acceleration may be robustly triangularly decoupled from the yaw rate dynamics, using only the front wheel steering angle as control input, by feeding back the yaw rate error through an integrator; in four wheel steering vehicles yaw damping can be adjusted (see [6]) so that it becomes velocity independent. In order to achieve exact decoupling between lateral speed and yaw rate dynamics accurate state measurements are needed. While the yaw rate is easily measurable by low cost gyroscopes, the lateral speed measurements require high cost systems such as GPS systems [20] or in-vehicle cameras [21]. To allow low cost measurements of the lateral speed, some estimation techniques have been developed.

In [22] a nonlinear body sideslip angle and yaw rate observer is presented while two different state observer are presented in [23]: the first observer is based on a physical model and produces a noise-free, vehicle parameter dependent lateral speed estimate; the second one is based on a kinematic model relating longitudinal and lateral acceleration, longitudinal and lateral speed and yaw rate. In [24] extended Kalman filters are used to estimate vehicle state and tire forces from noise-corrupted measurements. A study of lateral speed estimation algorithms is presented in [25] in which three different estimation methods are illustrated, simulated and experimentally validated:

- transfer function approach, which is based on the identification of the input-output linearised model for yaw rate and lateral speed;
- state-space approach, which is based on an adaptive algorithm which provides states and unknown parameters of the linearised model for yaw rate and lateral speed dynamics;
- kinematics approach, which is based on the kinematic model proposed in the paper: [23].

In [26] an algorithm for estimation of vehicle yaw rate and sideslip angle using steering wheel angle, wheel speed and lateral acceleration sensors is proposed. A nonlinear observer approach for estimation of lateral and longitudinal speed of a vehicle is proposed in [27]: the nonlinear observers are based on lateral acceleration, yaw rate, wheel speed and steering angle measurements. In [7] the decoupling between yaw and lateral dynamics is studied when longitudinal speed is time-varying and an observer is proposed to estimate the lateral speed from yaw rate measurements only.
In [8] and [9] a decoupling control is proposed using full state measurements (including lateral speed) that can be obtained by non standard automotive sensors in order to track a reference model for both state variables. In [10] it is shown that the lateral speed dynamics and the yaw rate dynamics can be exactly decoupled by feeding back longitudinal speed, yaw rate and lateral acceleration measurements (lateral speed measurements are not required): the yaw rate tracking error dynamics follow a second order reference model with arbitrary poles, while the lateral speed dynamics tend exponentially to zero with a vehicle-dependent time constant and lateral acceleration tends to be proportional to the yaw rate.

In this Ph.D. thesis, in the Chapter 3, it is shown, for a four wheel steering vehicle, that a proportional-integral (PI) active front steering control and a proportional-integral (PI) active rear steering control from the yaw rate error together with an additive feedforward reference signal for the vehicle sideslip angle can asymptotically decouple the lateral velocity and the yaw rate dynamics, that is the control can set arbitrary steady state values for lateral speed and yaw rate at any longitudinal speed; moreover the PI controls can suppress oscillatory behaviours by assigning real stable eigenvalues to a widely used linear model of the

vehicle steering dynamics for any value of longitudinal speed in understeering vehicles. In particular the four PI control parameters are explicitly expressed in terms of the three real eigenvalues to be assigned: this parameterization allows to compute the optimal controlled system eigenvalues by a numerical minimization of a weighted sum of the cross transfer functions H infinity norms so that the influences of the yaw rate and the vehicle sideslip references on the vehicle sideslip angle and the yaw rate respectively are reduced during transient responses. No lateral acceleration and no lateral speed measurements are required.

The controlled system maintains the well-known advantages of both front and rear active steering control: higher controllability, enlarged bandwidth for the yaw rate dynamics, suppressed resonances, new stable cornering manoeuvres and improved manoeuvrability. In addition zero lateral speed may be asymptotically achieved: in this case comfort is improved since the phase lag between lateral acceleration and yaw rate is reduced.

The robustness of the proposed decoupling PI control with respect to tire parameters such as the cornering stiffnesses (which may change due to different adherence conditions and/or low tire pressure), the vehicle mass and the vehicle moment of inertia (that vary from unloaded to full load conditions) is analyzed by means of the eigenvalues displacement and the Bode plots.

A nonlinear reference model is designed to generate the yaw rate reference signal on the basis of the driver steering wheel angle so that the uncontrolled and the controlled vehicle dynamic behaviours may be compared while the vehicle sideslip angle reference is set equal to zero.

Several simulations, including moose tests, are carried out on a standard small SUV CarSim® model to explore the robustness with respect to unmodelled effects such as combined lateral and longitudinal tire forces, pitch, roll and driver dynamics. The simulations show the advantages

obtained by the proposed PI decoupling control: reduced lateral speed, suppressed oscillations, smoother driver commands and new stable trajectories.

1.3.3 Semiactive and Active Differential

The development of electro actuated differentials allows for new control strategies in vehicle systems dynamics control as in [30], [31], [32], [33], [34] and recently in [18] and [17]. In Fig. 1.5 and in Fig. 1.6 a logical scheme of the semiactive and the active differential is shown.

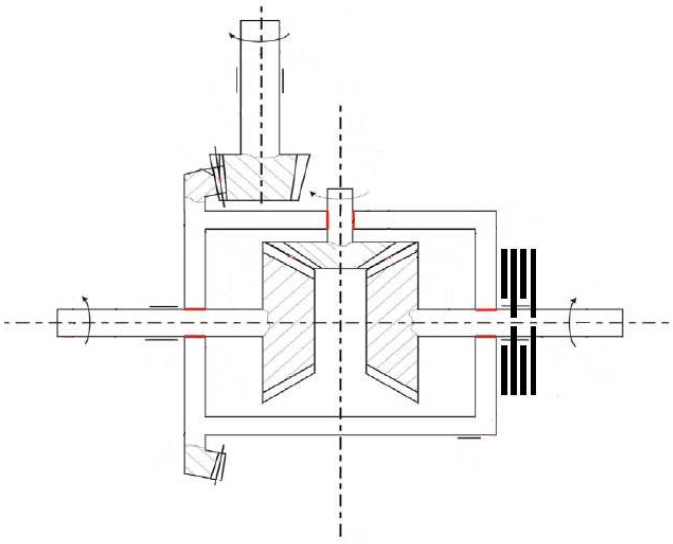

Figure 1.5: Logical scheme of the semiactive differential.

In [32] the control is semiactive since the electronic control system can determine the torque transferred by the differential but not its direction; the torque is transferred from the fastest wheel to the slowest one; the control operates when the rear wheel speed difference exceeds a given threshold and its value is computed by a proportional-integral control law based on the error between the measured and the desired

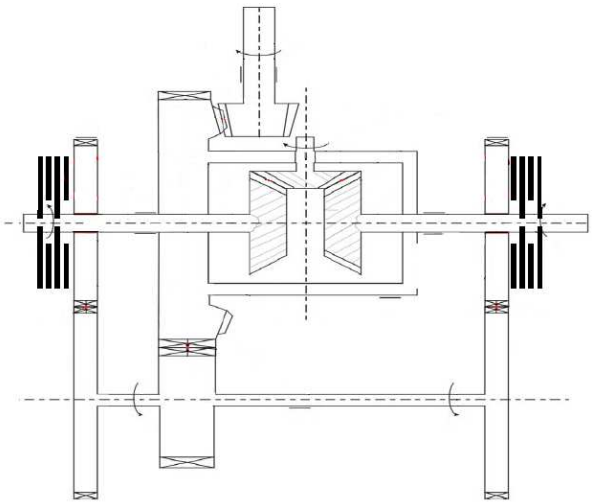

Figure 1.6: Logical scheme of the active differential.

rear wheel speed angular velocity. In [33], the proposed controller is designed following the Internal Model Control approach and it is active since it can generate yaw moments of every amount and direction. In [34] the locking action of the rear semiactive differential is electronically controlled according to a Lyapunov analysis. In [17] the active sport differential is introduced: an innovative regulating system distributes torque from the engine in continuously variable proportions between the rear wheels. This greatly enhances agility, driving pleasure and active driving safety. The controlled power flow enables the car to take corners even more directly and responsively, and to retain its directional stability considerably longer.

1.3.4 Integrated Control Design

Many papers are currently focused on the design of integrated global chassis control systems: in [35] an integrated control of active front

steering and direct yaw moment generated by a distribution of braking forces is designed; in [36] the electronic stability program (ESP) is integrated with the active front wheel steering, the active suspension and an active anti roll bar; in [37] four wheel steering is coordinated with wheel torque distribution using an optimization approach; a non linear optimization approach is followed by [38] to determine the optimal force to be exerted by each tire controlled by active steering and brake pressures distribution; in [39] the global chassis control optimization is obtained by a gradient-based optimal control algorithm approach: the active rear steering and the active rear differential are used as actuators. In [42] a feasibility study on optimization based coordination of active front steering, active rear steering and active roll stabilizer is presented; a risk calculator determines the probability of an accident in any given situation and help the control systems to coordinate and allocate the active systems action. In [43] the active front steering, the active rear differential and the active brake are integrated by an allocation algorithm which distributes the requested global yaw torque based on the torque potential of each actuator. In [44] the active front steering, the electronic stability control and the continuous damping control are integrated to produce a defined compensation moment while minimizing the electronic stability control range of action. In [45] the integration of active steering and electronic stability program have been developed using a supervisory and a Characteristic Locus method showing that the integrated controls can improve vehicle performances that are superior with respect to the individual control modules without any integration scheme.

In this Ph.D. thesis, in the Chapter 4, the front and rear active or semiactive electronically controlled differentials and an active front steering control are designed and integrated: the goal is to improve ve-

hicle dynamics by suppressing resonances and enlarging the bandwidth for the yaw rate tracking dynamics so that the driver effort is reduced and to improve safety. Moreover the control law on the electronically controlled differentials is designed in order to improve safety by reducing the drawbacks due to the mechanical self-locking differential action which may cause undesired understeering and oversteering behaviours especially in critical manoeuvres such as braking or standing start conditions on surfaces with different adherence between the left and the right side of the vehicle. The control strategy for the electronic differentials is not only aimed at keeping the wheel speed differences at desired values but it is also integrated with the active steering control action (a PI control on the yaw rate error) to produce a yaw moment, based on the yaw rate error, which improves the vehicle steering dynamics since the corresponding eigenvalues can be placed to be all real at every speed to prevent oscillations. The stability analysis is performed using both singular perturbation and Lyapunov techniques in the presence of small parameters which are due to the ratio between the moments of inertia of the wheels and of the vehicle.

The proposed active differential control law is adapted to a semiactive differential and the stability of the integrated hybrid control law is investigated.

Several simulations are carried out on a CarSim® small SUV model to explore the robustness with respect to unmodelled dynamics such as pitch, roll and nonlinear combined lateral and longitudinal tire forces according to combined slip theory. In response to sudden direction changes the simulations show suppressed oscillations, enlarged bandwidth for the yaw rate dynamics while new stable manoeuvres are allowed especially in critical conditions. In standing start or brake manoeuvres when the vehicle wheels on one side are on low adherence surface the proposed integrated control shows new stable manoeuvres with improved perfor-

mance (greater accelerations) and reduced driver effort. Comparisons between active and semiactive differentials are also performed.

1.3.5 Vision Based Autonomous Vehicles

Intelligent vehicles and automated highway systems have attracted a growing attention in the last years with the aim of increasing safety and comfort: see for instance [54], [55], [56], [57], [63], [64], [66], [67], [53], [58], [59], [60], [61], [62], [68], [11] and [12]. In [54, 55] a feedback from lateral and longitudinal vehicle speed, yaw angle and yaw rate is used to help the driver to steer back to the lane the vehicle during diminished driving capability due to inattention. The control strategy is based on the Lyapunov theory and LMI optimization by defining polytopic and hypercubic state space regions, where if the driver stays in, the driving task is considered safe; the main idea is to approximate these regions by standard and composite Lyapunov level curves. In [56] a H_∞ controller is designed to minimize the effect of the disturbances on the measured lateral offset and the desired yaw angle. In [57] a steering controller, which uses finite preview optimal control methods, is proposed to control the measured lateral offset, the yaw angle and their derivatives. In [63] a closed loop control strategy is analyzed on the basis of a feedback from the lateral offset: an automatic lane keeping is combined with the driver's steering without any switching strategy. In [64] a control system based on the loop shaping technique is tested by experiments using a feedback from the lateral offset. In [66] a non linear observer based control strategy is investigated by measuring the lateral offset, its derivative, the yaw angle and the yaw rate. In [67] a combined control system, which integrates Active Cruise Control and Lane Keeping Control is analyzed by using Model Predictive Control (MPC) to define a lane changing algorithm. In [53] a model predictive steering controller is used to emulate the driver behaviour in the CarSim environment: it

is designed on the basis of a simplified linear model and on longitudinal and lateral speed, yaw angle and yaw rate measurements to predict the error with respect to a given target path. Also in [58] a model predictive control approach is followed: the controlled outputs are the lateral offset, the yaw rate and the yaw angle; the controller is designed both on a nonlinear and a linear vehicle model using lateral and longitudinal vehicle speed, yaw angle and yaw rate measurements. In [59] a feedforward and a feedback action on the lateral offset and the yaw angle error is experimented. In [60] a gain scheduling based proportional feedback from the lateral offset is experimented. In [61] a feedforward term from road curvature and a PID on a weighted sum of the heading error and the lateral offset are used as steering controller in the DARPA Grand Challenge. In the same competition the yaw angle and a nonlinear term proportional to the lateral offset are used in [62] as measurements to design the steering controller.Furthermore, to improve safety, driver comfort and vehicle performance, several driver assistance systems are investigated in the literature. In [68] a steering assistance control system with a feedback from the lateral offset and lateral speed is designed to follow the desired path while an assistance torque is applied in order to improve the vehicle handling and steering feel. In [11] and [12] the active front steering is proposed and implemented on cars such as BMW 5 Series models. In [11] a PI active front steering control on the yaw rate tracking error with different gains for braked and unbraked driving condition is used while in [12] a patented method is proposed to ensure safety during active steering system failure computing the steering wheel angle as the sum of the proposed control law steering angle and the driver steering angle. Most control algorithms employed in lane keeping make use of pole placement, model predictive and observer based techniques or require difficult measurements of lateral speed, vehicle absolute position and orientation. The simplest algorithm [60] only implements a

proportional feedback from the lateral offset; since in addition to lateral offset measurements from vision systems the yaw rate measurements are easily obtained by an on board gyroscope, in this paper we propose a control scheme which integrates the active steering action based on the yaw rate error with the lane keeping action based on lateral offsets.

In this Ph.D. thesis, in the Chapter 5, a nested PID steering control for lane keeping in vision based autonomous vehicles is designed to perform path following in the case of roads with a curvature which increases linearly with respect to time. No lateral speed measurement is used since it can be hardly measured with high cost and low accuracy and reliability. The designed control input is the steering wheel angle: it is computed on the basis of yaw rate measured by a gyroscope and the lateral offset measured by the vision system as the distance between the road centerline and a virtual point at a fixed distance from the vehicle. A PI active front steering control on the yaw rate tracking error is used to reject constant disturbances and the effect of uncertain parameters while improving vehicle steering dynamics. To integrate the additional lateral offset measure the yaw rate reference is viewed as the control signal in an external control loop: it is designed using a PID control (with an additive double integral action) on the lateral offset to reject the disturbances on the curvature which increase linearly with respect to time. The robustness is proved, by using the theorem presented in [69, 70], with respect to speed variation and uncertainties on vehicle physical parameters such as the front and rear cornering stiffnesses and the vehicle mass. It is shown how the robustness of the controlled system decreases as speed increases. The asymptotical stability is however ensured for all perturbations in the range of interest. Several simulations, such as the tracking of a CarSim environment default path and a standard sudden braking action on surfaces with different adherence conditions (μ-split braking manoeuvre), are carried out on a standard big sedan CarSim

vehicle model to explore the robustness with respect to unmodelled effects, such as combined lateral and longitudinal tire forces, pitch and roll. The simulations show reduced lateral offsets and new stable μ-split braking manoeuvres with respect to the CarSim model predictive steering controller which requires lateral speed.

Chapter 2

Vehicle Model

In this section the commonly used nonlinear and linear single track vehicle models are considered to capture the essential steering vehicle dynamics. More detailed models of a car can also be found in [13, 28, 29].

2.1 Model Derivation

The essential features of car steering dynamics in a horizontal plane are described by the well-known single track model. It is obtained by lumping the two front wheels into one wheel in the longitudinal axis of the car, the same is done with the two rear wheels. Since the vehicle center of gravity is assumed at road level and no suspensions model is included, there are no roll, pitch and heave motion: the car can be considered as a rigid body with three degree of freedom. Two reference frames are considered as shown in Fig. 2.1 [13]:

- $\Re(X, Y, Z)$ is an inertial reference frame .
- $\Re(x, y, z)$ is an non-inertial reference frame fixed to the vehicle centre of gravity. The x axis corresponds to the longitudinal axis of the car while the y axis coincides with the lateral axis. The yaw

angle, denoted with ϕ, is the angle between the X axis and the x axis.

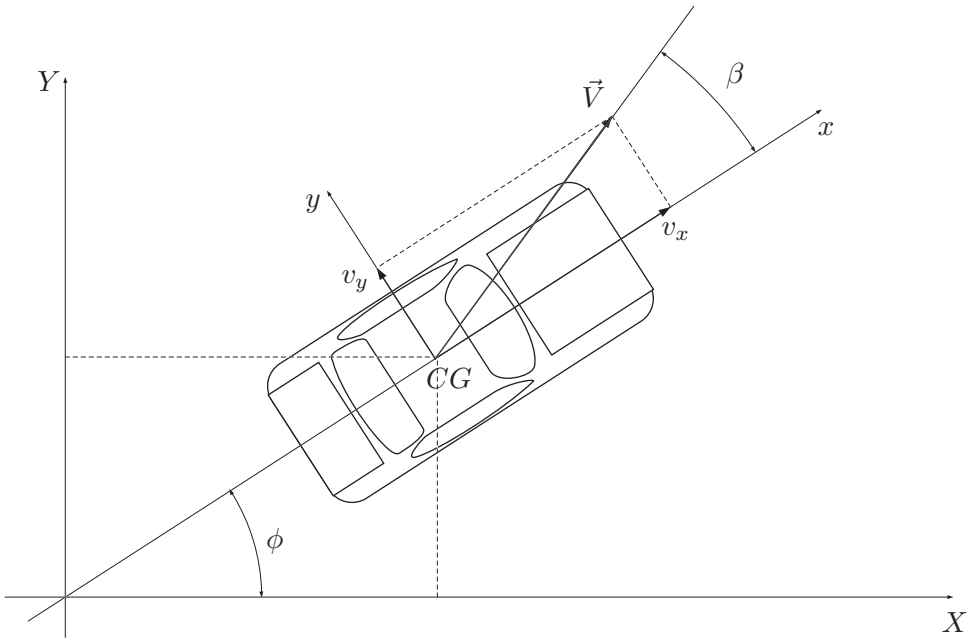

Figure 2.1: Reference frames used to derive the vehicle model.

The coordinates X, Y and ϕ are the state variables of the vehicle model in the inertial frame. The equations of motion are

$$m\ddot{X} = m\dot{V}_x = F_x \tag{2.1a}$$

$$m\ddot{Y} = m\dot{V}_y = F_y \tag{2.1b}$$

$$J\ddot{\phi} = J\dot{r} = M_z \tag{2.1c}$$

where F_x, F_y are the total forces acting on the vehicle center of gravity expressed in the $X-Y$ reference frame and M_z is the total yaw torque. They can be obtained by the following relation

$$\vec{F} = \begin{bmatrix} F_x \\ F_y \end{bmatrix} = \begin{bmatrix} \cos(\phi) & -\sin(\phi) \\ \sin(\phi) & \cos(\phi) \end{bmatrix} \begin{bmatrix} f_x \\ f_y \end{bmatrix} = R_z^{-1}(\phi)\vec{f} \tag{2.2}$$

where f_x and f_y are the total forces in the vehicle reference frame. Also vehicle speeds in the two frames are related by a similar relation:

$$\vec{V} = \begin{bmatrix} V_x \\ V_y \end{bmatrix} = R_z^{-1}(\phi) \begin{bmatrix} v_x \\ v_y \end{bmatrix} = R_z^{-1}(\phi)\vec{v} \tag{2.3}$$

where $\vec{v}$ is the vehicle velocity vector in the vehicle reference frame. From (2.1), (2.2) and (2.3) the vehicle equations of motion, written in the inertial frame, are

$$m\frac{d\vec{V}}{dt} = m\frac{dR_z^{-1}(\phi)\vec{v}}{dt} = \tag{2.4}$$

$$= mR_z^{-1}(\phi)\frac{d\vec{v}}{dt} + m\frac{dR_z^{-1}(\phi)}{d\phi}\dot{\phi}\vec{v} = R_z^{-1}(\phi)\vec{f}. \tag{2.5}$$

Multiplying both members of (2.5) by $R_z(\phi)$ yields

$$m\frac{d\vec{v}}{dt} + mSr\vec{v} = \vec{f}, \tag{2.6}$$

where

$$S = \begin{bmatrix} 0 & -1 \\ 1 & 0 \end{bmatrix},$$

and the equations of motion in the vehicle coordinate system are

$$m(\dot{v}_x - rv_y) = f_x + d_x \tag{2.7a}$$

$$m(\dot{v}_y + rv_x) = f_y + d_y \tag{2.7b}$$

$$J\dot{r} = M_z + T_z \tag{2.7c}$$

where d_x, d_y and T_z are the external forces and torques disturbances acting on the vehicle. The forces transmitted from the road to the car via the tires are represented in Fig. 2.2 for a single track vehicle model; each tire has a lateral force f_s, which is responsible of the cornering

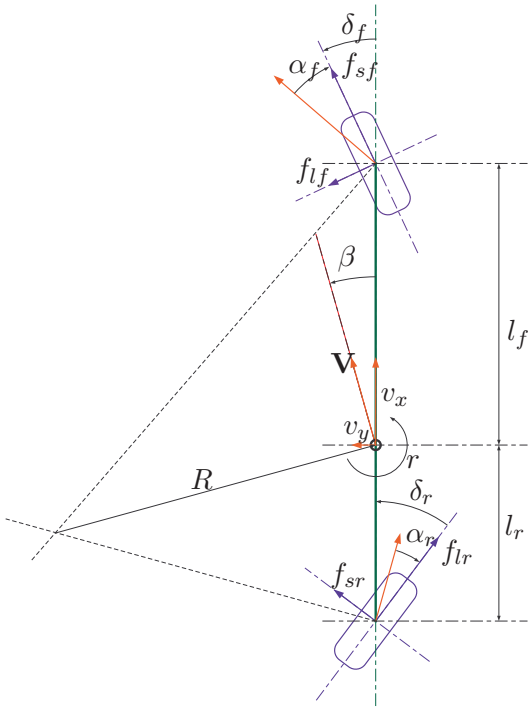

Figure 2.2: Single-track car model.

motion of the car, and a longitudinal force f_l which is responsible of the longitudinal (accelerating and braking) motion of the car.

Other forces and torques result from aerodynamics, gravity (on slopes and on roads with non-zero bank angle), aligning moment of the wheels and so on. In this approach, the forces generated by tires are included in the model; other forces will be handled as external disturbances. The expressions of the x and y force components of each axle are (see Fig. 2.2):

$$\begin{aligned} f_{xf} &= f_{lf}\cos(\delta_f) - f_{sf}\sin(\delta_f) \\ f_{xr} &= f_{lr}\cos(\delta_r) - f_{sr}\sin(\delta_r) \\ f_{yf} &= f_{lf}\sin(\delta_f) + f_{sf}\cos(\delta_f) \\ f_{yr} &= f_{lr}\sin(\delta_r) + f_{sr}\cos(\delta_r). \end{aligned}$$

From these expressions, it easy to obtain the expressions of f_x, f_y and M_z since results

$$\begin{aligned} f_x &= f_{xf} + f_{xr} \\ f_y &= f_{yf} + f_{yr} \\ M_z &= l_f f_{yf} - l_r f_{yr} \end{aligned}$$

where l_f and l_r are the distance between the vehicle center of gravity and the front and rear axle respectively. Finally the three degree-of-freedom single track nonlinear car model is given by the following equations:

$$m\,(\dot{v}_x - r v_y) = f_{lf}\cos\delta_f - f_{sf}\sin\delta_f + f_{lr}\cos\delta_r - f_{sr}\sin\delta_r + d_x \quad (2.8a)$$

$$m\,(\dot{v}_y + r v_x) = f_{lf}\sin\delta_f + f_{sf}\cos\delta_f + f_{lr}\sin\delta_r + f_{sr}\cos\delta_r + d_y \quad (2.8b)$$

$$J\dot{r} = l_f(f_{lf}\sin\delta_f + f_{sf}\cos\delta_f) - l_r(f_{lr}\sin\delta_r + f_{sr}\cos\delta_r) \quad (2.8c)$$

2.1.1 Tire Forces

Several tire friction models describing the nonlinear behaviour of the tire forces are reported in the literature. There are static models as well as dynamic models, models which are constructed based on heuristic data as well as others which have been derived from physical behaviour. The most reputed tire model is the Pacejka tire model, also known as "magic formula" and it is derived heuristically from experimental data. The "magic formula" has been shown to suitably match experimental data and is on the form:

$$f_{si}(\alpha_i) = D_y \sin\{C_y \text{atan}[(1-E_y)B_y\alpha_i + E_y \text{atan}(B_y\alpha_i)]\} \tag{2.9}$$

$$f_{li}(\lambda_i) = D_x \sin\{C_x \text{atan}[(1-E_x)B_x\lambda_i + E_x \text{atan}(B_x\lambda_i)]\}. \tag{2.10}$$

where f_{si} (f_{li}) are the lateral (longitudinal) forces of the $i-$th tire (i =front, rear) given by Pacejka tire model and the basics parameters that appear in the Pacejka magic formula are the following: D is the peak value of the curve (except for addition/shift), C is the shape factor (determines the shape of the peak) and B, C, D and E variables are functions of the wheel load, slip angle, slip ratio and camber. The lateral forces depend on the term α_i which represents the side slip angle α_f, α_r which are defined as:

$$\alpha_f = \delta_f - \beta_f \tag{2.11a}$$

$$\alpha_r = \delta_r - \beta_r \tag{2.11b}$$

$$\beta_f = \arctan\left(\frac{v_y + l_f r}{v_x}\right) \tag{2.12a}$$

$$\beta_r = \arctan\left(\frac{v_y - l_r r}{v_x}\right) \tag{2.12b}$$

The longitudinal forces depend on the term λ_i which represents the longitudinal slip λ_f, λ_r which are defined as:

$$\begin{cases} \lambda_i = (\omega_i R_w - V_i)/V_i \\ V_i = \left((v_y \pm r l_f)^2 + (v_x \pm r T_f/2)^2\right)^{1/2} \end{cases} \tag{2.13}$$

in which V_i are the wheels velocities in the ideal case of free rolling.

2.2 Linear Single Track Vehicle Model

The state variables in (2.8) are (v_x, v_y, r) while (δ_f, δ_r) are the input variables in four wheel steering (4WS) vehicles. The linearized model around the operating condition $\mathbf{x}^* = 0$ ($v_y = 0$, $r = 0$), $\mathbf{u}^* = 0$ ($\delta_f = 0$, $\delta_r = 0$) when the longitudinal speed is kept constant is given by the following widely used equations [6] (see Fig. 2.2)

$$\begin{aligned} \dot{v}_y &= \frac{f_{sf}(\alpha_f)}{m}\cos\delta_f + \frac{f_{sr}(\alpha_r)}{m}\cos\delta_r - rV \\ \dot{r} &= \frac{f_{sf}(\alpha_f) l_f}{J}\cos\delta_f - \frac{f_{sr}(\alpha_r) l_r}{J}\cos\delta_r \end{aligned}$$

which can be written in the following vectorial form:

$$\dot{\mathbf{x}} = \mathbf{f}(\mathbf{x}, \mathbf{u}) \tag{2.14}$$

Linearizing the function $\mathbf{f}(\mathbf{x}, \mathbf{u})$ by a Taylor series about $\mathbf{x}^* = 0$ e $\mathbf{u}^* = 0$

$$\dot{\mathbf{x}} = \mathbf{f}(\mathbf{x}, \mathbf{u}) \approx \mathbf{f}(\mathbf{x}^*, \mathbf{u}^*) + \left.\frac{\partial \mathbf{f}}{\partial \mathbf{x}}\right|_{\substack{\mathbf{x}=\mathbf{x}^* \\ \mathbf{u}=\mathbf{u}^*}} (\mathbf{x} - \mathbf{x}^*) + \left.\frac{\partial \mathbf{f}}{\partial \mathbf{u}}\right|_{\substack{\mathbf{x}=\mathbf{x}^* \\ \mathbf{u}=\mathbf{u}^*}} (\mathbf{u} - \mathbf{u}^*) \tag{2.15}$$

$$\dot{\mathbf{x}} = \left.\frac{\partial \mathbf{f}}{\partial \mathbf{x}}\right|_{\substack{\mathbf{x}=\mathbf{x}^* \\ \mathbf{u}=\mathbf{u}^*}} \mathbf{x} + \left.\frac{\partial \mathbf{f}}{\partial \mathbf{u}}\right|_{\substack{\mathbf{x}=\mathbf{x}^* \\ \mathbf{u}=\mathbf{u}^*}} \mathbf{u} = A\mathbf{x} + B\mathbf{u} \tag{2.16}$$

the matrices A and B are computed as follows:

$$\frac{\partial \mathbf{f}}{\partial \mathbf{x}} = \begin{bmatrix} a_{11} & a_{12} \\ a_{21} & a_{22} \end{bmatrix}$$

$$a_{11} = \left(\frac{\partial f_{sf}}{\partial \alpha_f}\frac{\partial \alpha_f}{\partial v_y}\right)\frac{\cos\delta_f}{m} + \left(\frac{\partial f_{sr}}{\partial \alpha_r}\frac{\partial \alpha_r}{\partial v_y}\right)\frac{\cos\delta_r}{m}$$

$$a_{12} = \left(\frac{\partial f_{sf}}{\partial \alpha_f}\frac{\partial \alpha_f}{\partial r}\right)\frac{\cos\delta_f}{m} + \left(\frac{\partial f_{sr}}{\partial \alpha_r}\frac{\partial \alpha_r}{\partial r}\right)\frac{\cos\delta_r}{m} - V$$

$$a_{21} = \left(\frac{\partial f_{sf}}{\partial \alpha_f}\frac{\partial \alpha_f}{\partial v_y}\right)\frac{l_f\cos\delta_f}{J} - \left(\frac{\partial f_{sr}}{\partial \alpha_r}\frac{\partial \alpha_r}{\partial v_y}\right)\frac{l_r\cos\delta_r}{J}$$

$$a_{22} = \left(\frac{\partial f_{sf}}{\partial \alpha_f}\frac{\partial \alpha_f}{\partial r}\right)\frac{l_f\cos\delta_f}{J} - \left(\frac{\partial f_{sr}}{\partial \alpha_r}\frac{\partial \alpha_r}{\partial r}\right)\frac{l_r\cos\delta_r}{J}$$

in which

$$\left.\frac{\partial f_{sf}}{\partial \alpha_f}\right|_{\alpha_f=0} = c_f \tag{2.17}$$

$$\left.\frac{\partial f_{sr}}{\partial \alpha_r}\right|_{\alpha_r=0} = c_r \tag{2.18}$$

$$\left.\frac{\partial \alpha_f}{\partial v_y}\right|_{\alpha_f=0} = -\frac{1}{V} \tag{2.19}$$

$$\left.\frac{\partial \alpha_r}{\partial v_y}\right|_{\alpha_r=0} = -\frac{1}{V} \tag{2.20}$$

$$\left.\frac{\partial \alpha_f}{\partial r}\right|_{\alpha_f=0} = -\frac{l_f}{V} \tag{2.21}$$

$$\left.\frac{\partial \alpha_r}{\partial r}\right|_{\alpha_r=0} = +\frac{l_r}{V}. \tag{2.22}$$

$$\left.\frac{\partial \mathbf{f}}{\partial \mathbf{x}}\right|_{\substack{\mathbf{x}=\mathbf{x}^* \\ \mathbf{u}=\mathbf{u}^*}} = A = \begin{bmatrix} -\frac{c_f}{mV} - \frac{c_r}{mV} & -\frac{c_f l_f}{mV} + \frac{c_r l_r}{mV} - V \\ -\frac{c_f l_f}{JV} + \frac{c_r l_r}{JV} & -\frac{c_f l_f^2}{JV} - \frac{c_r l_r^2}{JV} \end{bmatrix}$$

$$\left.\frac{\partial \mathbf{f}}{\partial \mathbf{u}}\right|_{\substack{\mathbf{x}=\mathbf{x}^* \\ \mathbf{u}=\mathbf{u}^*}} = \begin{bmatrix} b_{11} & b_{12} \\ b_{21} & b_{22} \end{bmatrix}$$

$$\begin{aligned}
b_{11} &= \frac{\partial f_{sf}}{\partial \alpha_f}\frac{\partial \alpha_f}{\partial \delta_f}\frac{\cos\delta_f}{m} - \frac{f_{sf}}{m}\sin\delta_f + \frac{\partial f_{sr}}{\partial \alpha_r}\frac{\partial \alpha_r}{\partial \delta_f}\frac{\cos\delta_r}{m} \\
b_{12} &= \frac{\partial f_{sf}}{\partial \alpha_f}\frac{\partial \alpha_f}{\partial \delta_r}\frac{\cos\delta_f}{m} + \frac{\partial f_{sr}}{\partial \alpha_r}\frac{\partial \alpha_r}{\partial \delta_r}\frac{\cos\delta_r}{m} - \frac{f_{sr}}{m}\sin\delta_r \\
b_{21} &= \frac{\partial f_{sf}}{\partial \alpha_f}\frac{\partial \alpha_f}{\partial \delta_f}\frac{l_f\cos\delta_f}{J} - \frac{l_f f_{sf}}{J}\sin\delta_f - \frac{\partial f_{sr}}{\partial \alpha_r}\frac{\partial \alpha_r}{\partial \delta_f}\frac{l_r\cos\delta_r}{J} \\
b_{22} &= \frac{\partial f_{sf}}{\partial \alpha_f}\frac{\partial \alpha_f}{\partial \delta_r}\frac{l_f\cos\delta_f}{J} - \frac{\partial f_{sr}}{\partial \alpha_r}\frac{\partial \alpha_r}{\partial \delta_r}\frac{l_r\cos\delta_r}{J} + \frac{l_r f_{sr}}{J}\sin\delta_r
\end{aligned}$$

in which

$$\begin{aligned}
\frac{\partial \alpha_f}{\partial \delta_f} &= 1 & \frac{\partial \alpha_r}{\partial \delta_f} &= 0 \\
\frac{\partial \alpha_f}{\partial \delta_r} &= 0 & \frac{\partial \alpha_r}{\partial \delta_r} &= 1
\end{aligned}$$

$$\left.\frac{\partial \mathbf{f}}{\partial \mathbf{u}}\right|_{\substack{\mathbf{x}=\mathbf{x}^* \\ \mathbf{u}=\mathbf{u}^*}} = B = \begin{bmatrix} \frac{c_f}{m} & \frac{c_r}{m} \\ \frac{c_f l_f}{J} & -\frac{c_r l_r}{J} \end{bmatrix}$$

The linearized system $\dot{x} = Ax + Bu$ is equal to:

$$\begin{bmatrix} \dot{v}_y \\ \dot{r} \end{bmatrix} = \begin{bmatrix} a_{11} & a_{12} \\ a_{21} & a_{22} \end{bmatrix} \begin{bmatrix} v_y \\ r \end{bmatrix} + \begin{bmatrix} b_{11} & b_{12} \\ b_{21} & b_{22} \end{bmatrix} \begin{bmatrix} \delta_f \\ \delta_r \end{bmatrix} \tag{2.23}$$

where

$$\begin{array}{rcl} a_{11} & = & -(c_f + c_r)/mV \\ a_{12} & = & -V - (c_f l_f - c_r l_r)/mV \\ a_{21} & = & -(c_f l_f - c_r l_r)/JV \\ a_{22} & = & -(c_f l_f^2 + c_r l_r^2)/JV \end{array} \tag{2.24}$$

$$\begin{array}{rclrcl} b_{11} & = & c_f/m & b_{12} & = & c_r/m \\ b_{21} & = & c_f l_f/J & b_{22} & = & -c_r l_r/J \end{array} \tag{2.25}$$

and c_f e c_r are the lateral front and rear cornering stiffness. The linear model can be also rewritten considering the vehicle sideslip angle

$$v_y = v \sin \beta \tag{2.26}$$

obtaining the following linear system:

$$\begin{bmatrix} \dot{\beta} \\ \dot{r} \end{bmatrix} = \begin{bmatrix} a_{11} & a_{12} \\ a_{21} & a_{22} \end{bmatrix} \begin{bmatrix} \beta \\ r \end{bmatrix} + \begin{bmatrix} b_{11} & b_{12} \\ b_{21} & b_{22} \end{bmatrix} \begin{bmatrix} \delta_f \\ \delta_r \end{bmatrix} \tag{2.27}$$

where

$$\begin{array}{rcl} a_{11} & = & -\frac{(c_f + c_r)}{mv}, \\ a_{12} & = & -1 - \frac{(c_f l_f - c_r l_r)}{mv^2}, \\ a_{21} & = & -\frac{(c_f l_f - c_r l_r)}{J}, \\ a_{22} & = & -\frac{(c_f l_f^2 + c_r l_r^2)}{Jv}, \\ b_{11} & = & \frac{c_f}{mv}, \qquad b_{12} = \frac{c_r}{mv}, \\ b_{21} & = & \frac{c_f l_f}{J}, \qquad b_{22} = -\frac{c_r l_r}{J}. \end{array} \tag{2.28}$$

The linearized steering dynamics will be considered to design the control laws presented in this thesis.

2.3 The Driver Task

To capture the essential vehicle steering dynamic and to better understand the driver task a brief single track vehicle analysis is carried out.

2.3.1 Vehicle Dynamics Analysis

The transfer matrix of the second order system (2.23) are given by

$$\begin{bmatrix} v_y(s) \\ r(s) \end{bmatrix} = \begin{bmatrix} \phi_{11}(s) & \phi_{12}(s) \\ \phi_{21}(s) & \phi_{22}(s) \end{bmatrix} \begin{bmatrix} \delta_f(s) \\ \delta_r(s) \end{bmatrix}. \tag{2.29}$$

Each single transfer function of the matrix given before is:

$$\phi_{11}(s) = \frac{v_y(s)}{\delta_f(s)} = \frac{b_{11}s - b_{11}a_{22} + a_{12}b_{21}}{s^2 - (a_{22} + a_{11})s + a_{11}a_{22} - a_{12}a_{21}} \tag{2.30}$$

$$\phi_{12}(s) = \frac{v_y(s)}{\delta_r(s)} = \frac{b_{12}s - b_{12}a_{22} + a_{12}b_{22}}{s^2 - (a_{22} + a_{11})s + a_{11}a_{22} - a_{12}a_{21}} \tag{2.31}$$

$$\phi_{21}(s) = \frac{r(s)}{\delta_f(s)} = \frac{b_{21}s + a_{21}b_{11} - b_{21}a_{11}}{s^2 - (a_{22} + a_{11})s + a_{11}a_{22} - a_{12}a_{21}} \tag{2.32}$$

$$\phi_{22}(s) = \frac{r(s)}{\delta_r(s)} = \frac{b_{22}s + a_{21}b_{12} - b_{22}a_{11}}{s^2 - (a_{22} + a_{11})s + a_{11}a_{22} - a_{12}a_{21}} \tag{2.33}$$

where a_{11}, a_{12}, a_{21}, a_{21}, b_{11}, b_{12}, b_{21} and b_{21} are given in the previous section; each transfer function has relative degree one.
The expressions of the zeroes of the four transfer function are:

$$\begin{aligned} z_{11} &= -\frac{l_f c_r l_r - l_f m V^2 + c_r l_r^2}{JV} \\ z_{12} &= -\frac{l_r c_f l_f + l_r m V^2 + c_f l_f^2}{JV} \\ z_{21} &= -\frac{c_r(l_r + l_f)}{V m l_f} \\ z_{22} &= -\frac{c_f(l_r + l_f)}{V m l_r} \end{aligned}$$

The bode diagram of the transfer function between the driver steering wheel angle δ_f and the lateral velocity v_y and between δ_f and the yaw

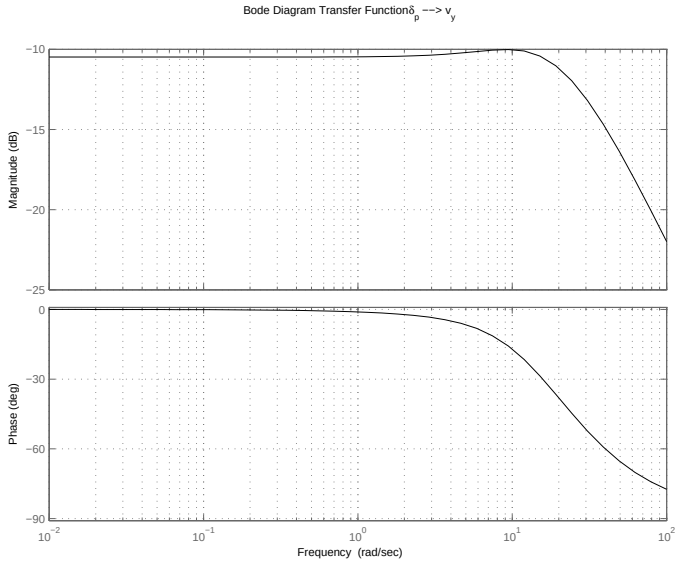

Figure 2.3: Bode diagram of the transfer function between δ_f and v_y at $V = 10\ [m/s]$.

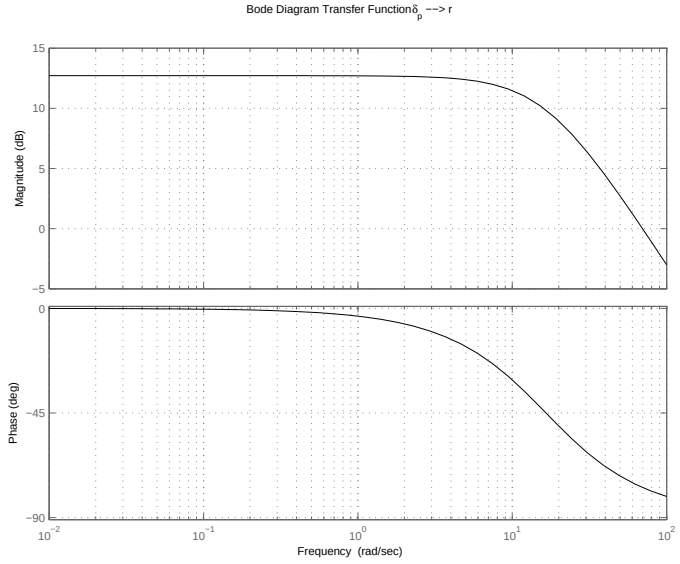

Figure 2.4: Bode diagram of the transfer function between δ_f and r at $V = 10\ [m/s]$.

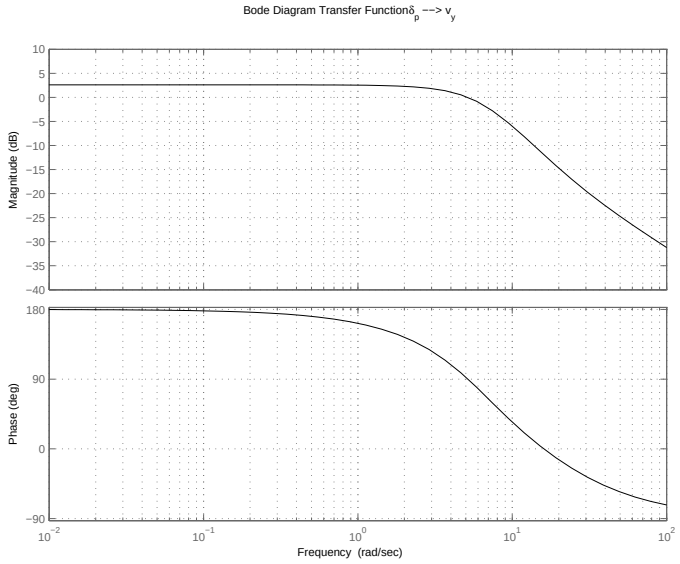

Figure 2.5: Bode diagram of the transfer function between δ_f and v_y at $V = 30\ [m/s]$.

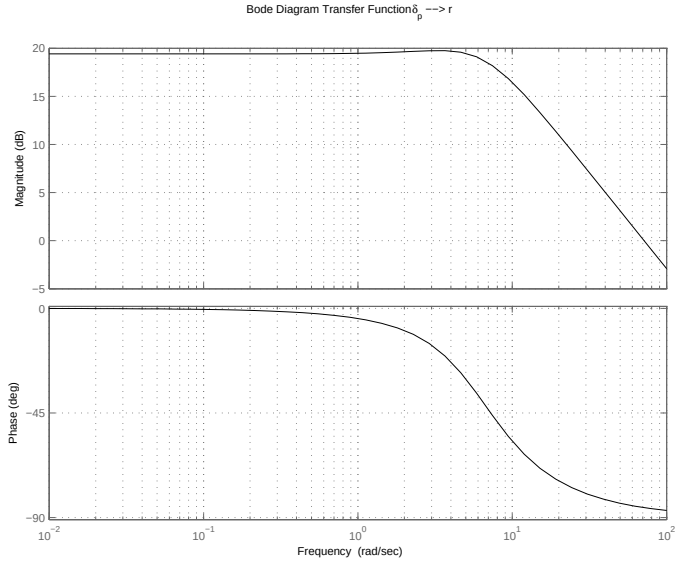

Figure 2.6: Bode diagram of the transfer function between δ_f and r at $V = 30\ [m/s]$.

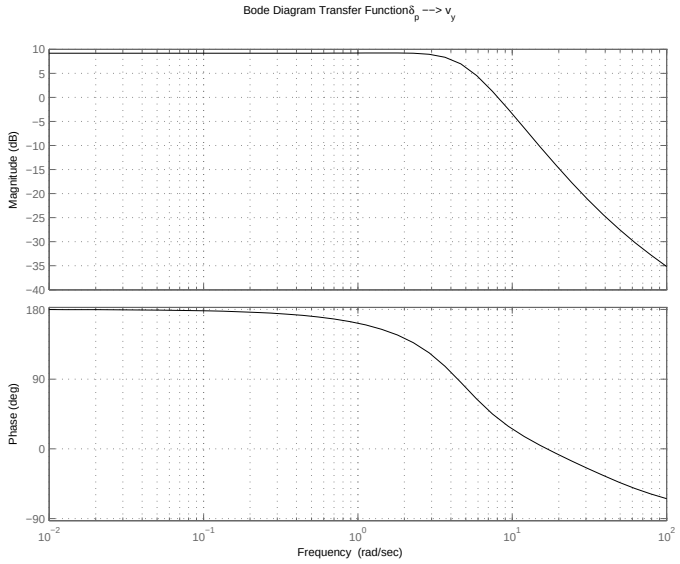

Figure 2.7: Bode diagram of the transfer function between δ_f and v_y at $V = 50\ [m/s]$.

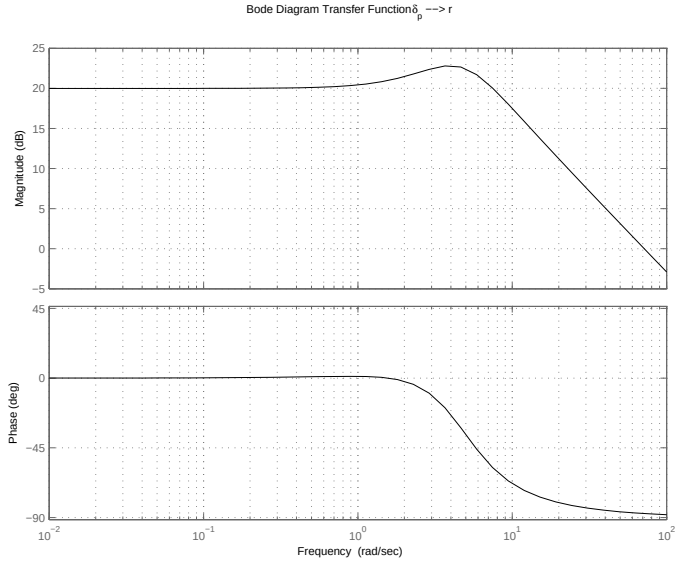

Figure 2.8: Bode diagram of the transfer function between δ_f and r at $V = 50\ [m/s]$.

rate r for different speed are shown in Fig. 2.3, Fig. 2.4, Fig. 2.5, Fig. 2.6, Fig. 2.7 and Fig. 2.8.

As shown in Fig. 2.3 and Fig. 2.5, the zero z_{11} of the transfer function $\phi_{11}(s)$ from δ_f to v_y changes its sign with respect to the longitudinal speed. The system (2.23) is minimum phase at low speed ($V < 10$ m/s) and becomes non-minimum-phase at medium and high speed so that the drive should compensate different lateral vehicle behaviours at different speed. In Fig. 2.6 and Fig. 2.8 it is depicted that the yaw rate response shows increasing resonances for increasing speed.
The steady-state values of r and v_y, obtained from (2.23), are given by

$$\begin{bmatrix} v_y \\ r \end{bmatrix} = - \begin{bmatrix} a_{11} & a_{12} \\ a_{21} & a_{22} \end{bmatrix}^{-1} \begin{bmatrix} b_{11} & b_{12} \\ b_{21} & b_{22} \end{bmatrix} \begin{bmatrix} \delta_f \\ \delta_r \end{bmatrix} \tag{2.34}$$

Expanding expression (2.34) using (2.24) and (2.25) yields:

$$\begin{aligned} v_y &= V \frac{-c_f c_r l_r^2 - c_f l_f c_r l_r + m V^2 c_f l_f}{-c_f c_r l_r^2 - c_r c_f l_f^2 - 2 c_f l_f c_r l_r + m V^2 c_f l_f - m V^2 c_r l_r} \delta_f \\ &\quad + V \frac{-c_r c_f l_f^2 - c_f l_f c_r l_r - m V^2 c_r l_r}{-c_f c_r l_r^2 - c_r c_f l_f^2 - 2 c_f l_f c_r l_r + m V^2 c_f l_f - m V^2 c_r l_r} \delta_r \qquad (2.35) \\ r &= \frac{-V c_f c_r (l_r + l_f)}{-c_f c_r l_r^2 - c_r c_f l_f^2 - 2 c_f l_f c_r l_r + m V^2 c_f l_f - m V^2 c_r l_r} (\delta_f - \delta_r). \qquad (2.36) \end{aligned}$$

In a standard 2WS vehicle the steady-state values of r and v_y are function of the front steering angle only

$$\begin{aligned} v_y &= V \frac{-c_f c_r l_r^2 - c_f l_f c_r l_r + m V^2 c_f l_f}{-c_f c_r l_r^2 - c_r c_f l_f^2 - 2 c_f l_f c_r l_r + m V^2 c_f l_f - m V^2 c_r l_r} \delta_f \\ r &= \frac{-V c_f c_r (l_r + l_f)}{-c_f c_r l_r^2 - c_r c_f l_f^2 - 2 c_f l_f c_r l_r + m V^2 c_f l_f - m V^2 c_r l_r} \delta_f \qquad (2.37) \end{aligned}$$

and are drawn for different vehicle speed in Fig. 2.9 and Fig. 2.10.

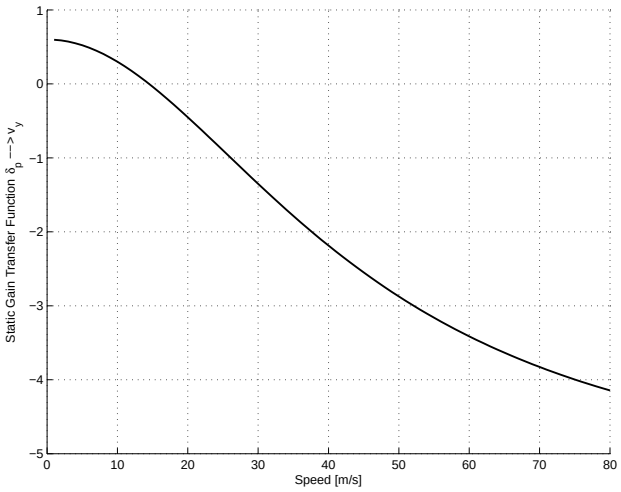

Figure 2.9: Steady state values of v_y for different values of the longitudinal speed.

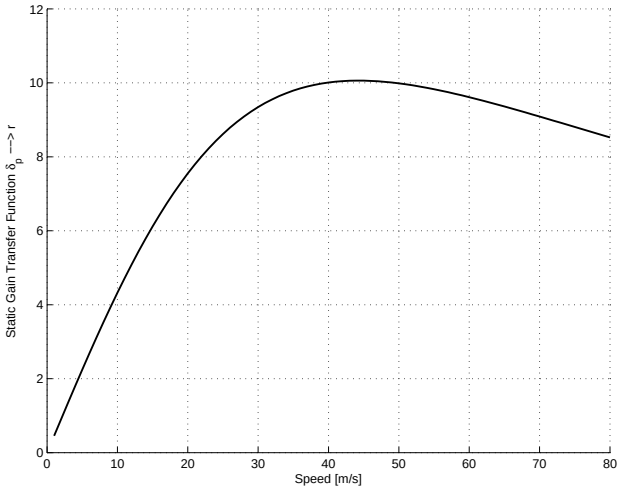

Figure 2.10: Steady state values of r for different values of the longitudinal speed.

The plot of eigenvalues versus longitudinal speed is given in Fig. 2.11. It is shown that the eigenvalues of an understeering vehicle become complex conjugates, with negative real part, as the longitudinal speed V increases. The damping factor of the eigenvalues tends to decrease as shown in Fig. 2.11. This results in an undesirable poorly damped oscillatory behaviour at medium and high speed that may lead to instability involving the driver's reaction delay.

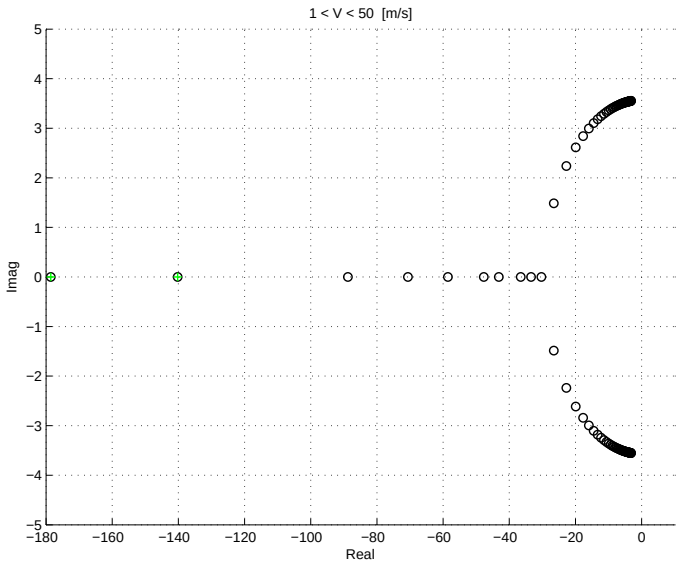

Figure 2.11: Uncontrolled vehicle eigenvalues for different speed ($1 < v < 50$ $[m/s]$).

Moreover the phase portrait of the system

$$m(\dot{v}_y + rV) = f_{sf}(\alpha_f) + f_{sr}(\alpha_r) \tag{2.38a}$$

$$J\dot{r} = l_f f_{sf}(\alpha_f) - l_r f_{sr}(\alpha_r) \tag{2.38b}$$

for $\delta_f = 0$ shows that the origin ($v_y = 0$, $r = 0$) is the stable and attractive equilibrium point. This equilibrium point corresponds to a rectilinear uniform motion for a given longitudinal speed. In Fig.

2.12 it is shown the phase portrait at $v = 30$ $[m/s]$; the oscillating behaviour near the equilibrium points indicates that the linearized model has complex conjugate eigenvalues.

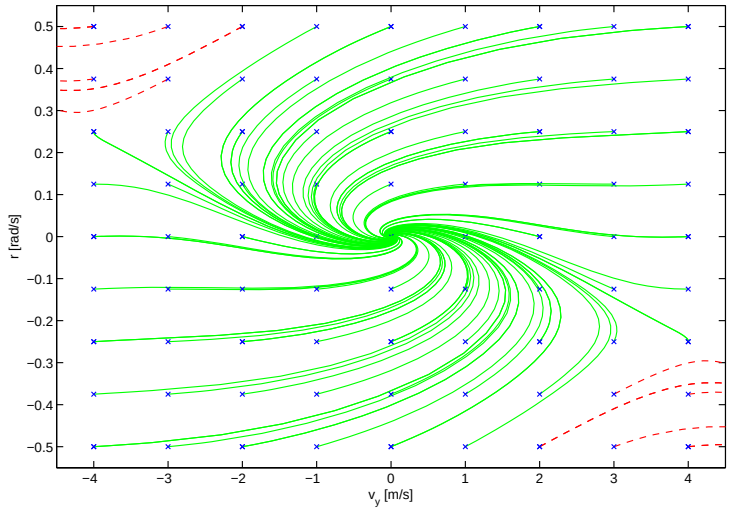

Figure 2.12: Phase portrait of the nonlinear single track model (2.38) when δ_f=0 [rad], v=30 $[m/s]$.

The phase portrait for different initial conditions and constant front steering angle δ_f=0.01 rad is given in Fig. 2.13. The corresponding stable equilibrium point has $r > 0$ and $v_y < 0$ and its domain of attraction is reduced.

Increasing the front steering angle results in a new stable equilibrium point closer to the unstable one as shown in Fig. 2.14. The domain of attraction of the stable equilibrium point is greatly reduced if compared with the one shown in Fig. 2.12 since some stable initial conditions in Fig. 2.12 becomes unstable.

In conclusion, the driver directly controls only one state variable (or one combination of them) by the front steering angle: he controls the yaw rate when he is negotiating a turn or he controls the lateral devi-

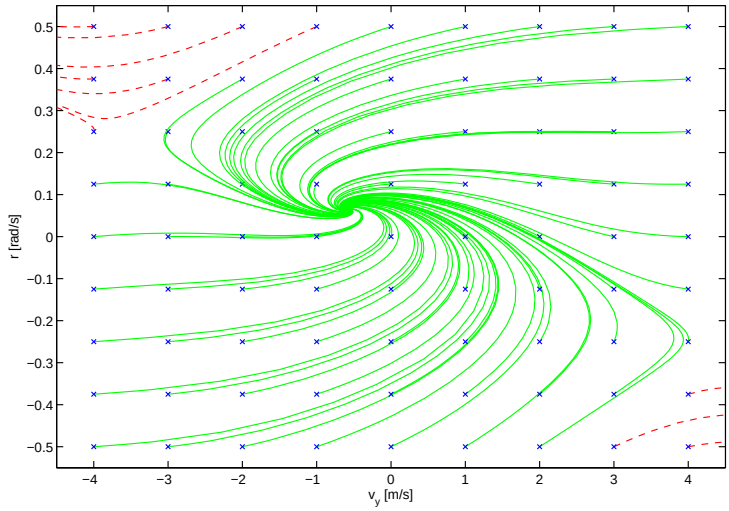

Figure 2.13: Phase portrait of the nonlinear single track model (2.38) when δ_f=0.01 [rad], v=30 $[m/s]$.

ation (directly related to the lateral speed) when he is performing an overtaking. Moreover the driver should compensate different lateral behaviours at different speed both in transient and stedy state: the lateral speed steady state gain changes with longitudinal speed (positive at low speed and negative at medium and high speed); the lateral speed transfer function is at minimum-phase at low speed and non minimum-phase at medium and high speed. Furthermore poorly damped oscillatory modes at high speed can induce resonances when drivers are inexperienced so that the overall driver task is non trivial from a control viewpoint.

2.3.2 Driver Simulations

The difficult driver task can be observed also analyzing the following of a given road curvature at a given constant longitudinal speed by means of the driver steering wheel angle (δ_f) and an external longitudinal force (f_m).

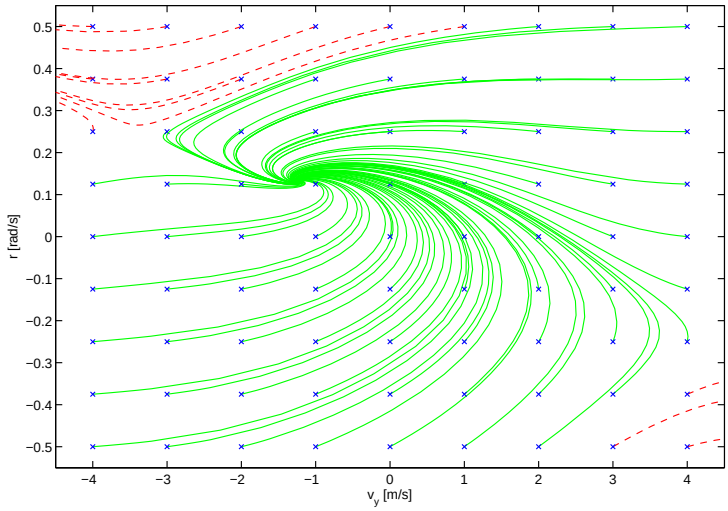

Figure 2.14: Phase portrait of the nonlinear single track model (2.38) when δ_f=0.02 [rad], v=30 $[m/s]$.

$$m\left(\dot{v}_x - r v_y\right) = f_{lf}\cos\delta_f - f_{sf}\sin\delta_f + f_{lr} \tag{2.39a}$$

$$m\left(\dot{v}_y + r v_x\right) = f_{lf}\sin\delta_f + f_{sf}\cos\delta_f + f_{sr} \tag{2.39b}$$

$$J\dot{r} = l_f(f_{lf}\sin\delta_f + f_{sf}\cos\delta_f) - l_r f_{sr} \tag{2.39c}$$

in which the longitudinal forces f_{lf} and f_{lr} are computed as follows:

$$f_{lf} = \gamma f_m \tag{2.40a}$$

$$f_{lr} = (1-\gamma) f_m \tag{2.40b}$$

where γ is a repartition parameter of the total longitudinal force. The following simulation is computed inverting the non linear 3DOF vehicle model for a giver road curvature (1/R) equal to 0.01 $[m^{-1}]$. In Fig. 2.15 it is shown that the desired longitudinal speed and road

curvature are followed. In Fig. 2.16 the required driver steering wheel angle and longitudinal traction forces are shown. To avoid the typical vehicle oscillations the driver must give a countersteer to track a ramp reference on the yaw rate; the same behaviour can be observed for the longitudinal traction force.

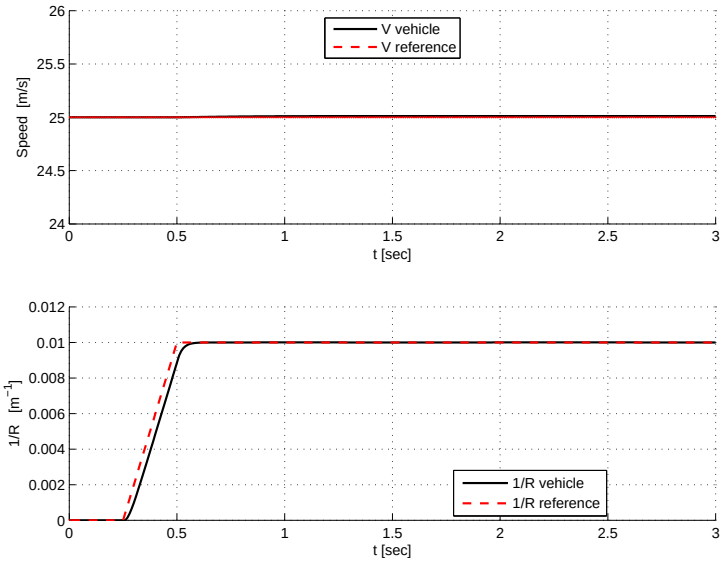

Figure 2.15: References and vehicle dynamics for the yaw rate and the longitudinal speed.

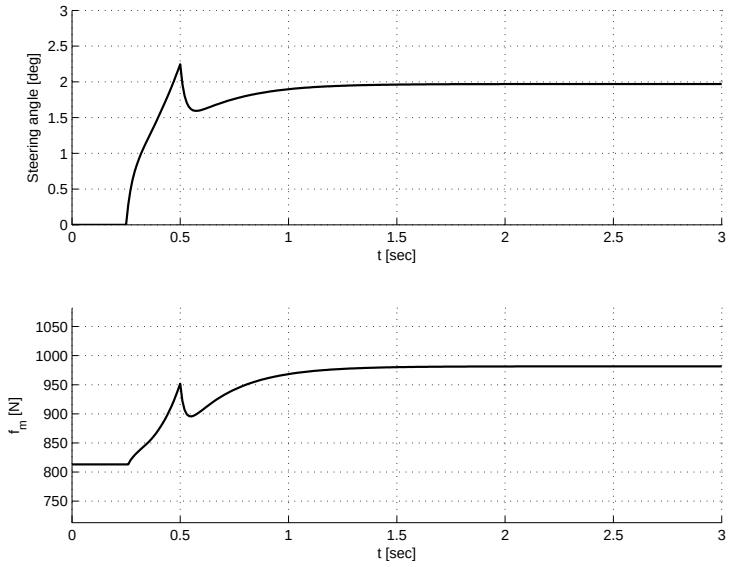

Figure 2.16: Driver inputs to follow a ramp for the yaw rate and a constant speed of $v = 25$ $[m/s]$.

Chapter 3

Asymptotic Decoupling Control in Four Wheel Steering Vehicles

3.1 Control Design

The asymptotic decoupling feedback control law acting on the front and rear steering angles is presented in this section. For a desired vehicle sideslip angle β_d and for a desired yaw rate reference r_d the simple functional scheme of the control system which is designed in Theorem 1 is described in Fig. 3.1.

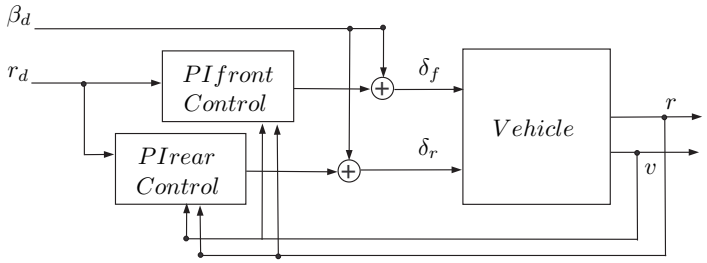

Figure 3.1: Functional scheme for the controlled system.

Theorem 1 *Consider the model (2.27) and let* (β_d, r_d) *be the constant*

reference signals for (β, r) *and* $\tilde{r} = r - r_d$ *the yaw rate tracking error; the controller*

$$\left\{\begin{array}{lcl} \delta_f &=& -K_{pf}\tilde{r} - K_{if}\alpha_0 + \beta_d \\ &=& -K_{pf}\tilde{r} - K_{if}\int_0^t \tilde{r}\,(\tau)\,d\tau + \beta_d \\ \delta_r &=& -K_{pr}\tilde{r} - K_{ir}\alpha_0 + \beta_d \\ &=& -K_{pr}\tilde{r} - K_{ir}\int_0^t \tilde{r}\,(\tau)\,d\tau + \beta_d \\ \dot{\alpha}_0 &=& \tilde{r} \end{array}\right. \tag{3.1}$$

with

$$\begin{array}{rcl} K_{pr} &=& (-b_{11}a_{21}a_{11}a_{22}^2 + (a_{12}b_{11}a_{21}^2 + (a_{12}a_{11}b_{21} \\ &-& b_{11}a_{11}^2 - (\lambda_3+\lambda_1+\lambda_2)b_{11}a_{11})a_{21} + a_{11}^3 b_{21} \\ &+& (\lambda_3+\lambda_1+\lambda_2)b_{21}a_{11}^2 + (\lambda_1\lambda_3 + \lambda_1\lambda_2 \\ &+& \lambda_3\lambda_2)b_{21}a_{11} + b_{21}\lambda_1\lambda_2\lambda_3)a_{22} + (-b_{21}a_{12}^2 \\ &+& (a_{11}+\lambda_1+\lambda_3+\lambda_2)b_{11}a_{12})a_{21}^2 + (-a_{11}^2 b_{21} \\ &-& (\lambda_3+\lambda_1+\lambda_2)b_{21}a_{11} - b_{21}(\lambda_1\lambda_2 + \lambda_1\lambda_3 \\ &+& \lambda_3\lambda_2))a_{12}a_{21})/(-a_{21}(a_{11}a_{22} - a_{21}a_{12})(b_{22}b_{11} \\ &-& b_{21}b_{12})) \end{array} \tag{3.2}$$

$$\begin{array}{rcl} K_{pf} &=& ((-a_{22}^2 a_{21}a_{11}b_{12} + (a_{21}^2 b_{12}a_{12} + (a_{11}a_{12}b_{22} \\ &-& a_{11}^2 b_{12} - (\lambda_3+\lambda_2+\lambda_1)b_{12}a_{11})a_{21} + b_{22}a_{11}^3 \\ &+& (\lambda_3+\lambda_2+\lambda_1)b_{22}a_{11}^2 + (\lambda_1\lambda_3 + \lambda_3\lambda_2 \\ &+& \lambda_1\lambda_2)b_{22}a_{11} + b_{22}\lambda_1\lambda_2\lambda_3)a_{22} + (-b_{22}a_{12}^2 \\ &+& (\lambda_1+\lambda_2+a_{11}+\lambda_3)b_{12}a_{12})a_{21}^2 + (-b_{22}a_{11}^2 \\ &-& (\lambda_2+\lambda_1+\lambda_3)b_{22}a_{11} - b_{22}(\lambda_3\lambda_2 + \lambda_1\lambda_2 \\ &+& \lambda_1\lambda_3))a_{12}a_{21})/(a_{21}(a_{11}a_{22} - a_{21}a_{12})(-b_{21}b_{12} \\ &+& b_{22}b_{11})) \end{array} \tag{3.3}$$

$$K_{if} = -\frac{\lambda_3\lambda_2\lambda_1(a_{12}b_{22} - b_{12}a_{22})}{(a_{11}a_{22} - a_{21}a_{12})(-b_{21}b_{12} + b_{22}b_{11})} \tag{3.4}$$

$$K_{ir} = -\frac{K_{if}(a_{22}b_{11} - a_{12}b_{21})}{a_{22}b_{12} - a_{12}b_{22}} \tag{3.5}$$

and $\lambda_1 < 0, \lambda_2 < 0, \lambda_3 < 0$ *arbitrary negative real eigenvalues, achieves:*

- *Asymptotic Decoupling, i.e.*
  arbitrary steady state values for vehicle sideslip angle $\left(\lim_{t\to\infty} |\beta\,(t) - \beta_d| = 0\right)$
  and yaw rate $\left(\lim_{t\to\infty} |r\,(t) - r_d| = 0\right)$ *at any constant speed* v*;*

- *Eigenvalues Assignment, i.e.*
  the real stable eigenvalues λ_i, $1 \leq i \leq 3$, *for the controlled system (2.27,3.1) are arbitrarily placed at every constant speed* v *if the vehicle has an understeering behaviour* ($c_f l_f < c_r l_r$).

Proof

Asymptotic Decoupling:
denoting by $x_c = [\ \beta,\ r,\ \alpha_0\ ]^T$ the extended state variables, the controlled linearized system (2.27,3.1) can be written in the state space form $\dot{x}_c = A_c x_c + B_{c1} r_d + B_{c2} \beta_d$, by introducing the matrices:

$$A_c = \begin{bmatrix} a_{11} & \bar{a}_{12} & \bar{a}_{13} \\ a_{21} & \bar{a}_{22} & \bar{a}_{23} \\ 0 & 1 & 0 \end{bmatrix},$$

$$B_{c1} = \begin{bmatrix} b_{11}K_{pf} + b_{12}K_{pr} \\ b_{21}K_{pf} + b_{22}K_{pr} \\ -1 \end{bmatrix},\ B_{c2} = \begin{bmatrix} b_{11} + b_{12} \\ b_{21} + b_{22} \\ 0 \end{bmatrix} \tag{3.6}$$

in which

$$\begin{aligned} \bar{a}_{12} &= a_{12} - b_{11}K_{pf} - b_{12}K_{pr}, \\ \bar{a}_{13} &= -b_{11}K_{if} - b_{12}K_{ir}, \\ \bar{a}_{22} &= a_{22} - b_{21}K_{pf} - b_{22}K_{pr}, \\ \bar{a}_{23} &= -b_{21}K_{if} - b_{22}K_{ir}. \end{aligned}$$

The equilibrium point $x_c^e = -A_c^{-1}B_{c1}r_d - A_c^{-1}B_{c2}\beta_d$ for the controlled system is equal to:

$$x_c^e = \begin{bmatrix} \frac{K_{if}(a_{12}b_{21} - a_{22}b_{11}) + K_{ir}(a_{12}b_{22} - a_{22}b_{12})}{K_{if}(a_{21}b_{11} - a_{11}b_{21}) + K_{ir}(a_{21}b_{12} - a_{11}b_{22})} \\ 1 \\ \frac{-a_{11}a_{22} + a_{21}a_{12}}{K_{if}(a_{21}b_{11} - a_{11}b_{21}) + K_{ir}(a_{21}b_{12} - a_{11}b_{22})} \end{bmatrix} r_d$$

$$+ \begin{bmatrix} \frac{K_{if}(b_{12}b_{21} - b_{11}b_{22}) + K_{ir}(b_{11}b_{22} - b_{12}b_{21})}{K_{if}(a_{21}b_{11} - a_{11}b_{21}) + K_{ir}(a_{21}b_{12} - a_{11}b_{22})} \\ 0 \\ 0 \end{bmatrix} \beta_d. \tag{3.7}$$

Substituting (2.28,3.5) in (3.7) the controlled system equilibrium point is equal to:

$$x_c^e = \begin{bmatrix} 0 \\ 1 \\ -\frac{l_r m v^2 + c_f(l_r l_f + {l_f}^2)}{v(l_r + l_f) c_f K_{if}} \end{bmatrix} r_d + \begin{bmatrix} 1 \\ 0 \\ 0 \end{bmatrix} \beta_d. \tag{3.8}$$

According to (3.8) the equilibrium values of the sideslip angle β and the yaw rate r are β_d and r_d respectively. The exponential stability of x_c^e is shown in the following.

Eigenvalues Assignment:
substituting (3.5) in (3.6) the characteristic polynomial of the matrix A_c is given by:

$$det(sI - A_c) = (s^3 + d_2 s^2 + d_1 s + d_0) \tag{3.9}$$

The coefficients in (3.9) are related to the control parameters as:

$$\begin{array}{rcl} d_2 & = & b_{21}K_{pf} + b_{22}K_{pr} - (a_{22} + a_{11}) \\ d_1 & = & \left(\frac{b_{22}(a_{11}(a_{12}b_{22} - b_{12}a_{22}) - a_{21}b_{12}a_{12})}{-a_{12}b_{22} + b_{12}a_{22}} + \frac{a_{21}{b_{12}}^2 a_{22}}{-a_{12}b_{22} + b_{12}a_{22}}\right) K_{pr} \\ & - & \left(\frac{a_{21}b_{11}(a_{12}b_{22} - b_{12}a_{22})}{-a_{12}b_{22} + b_{12}a_{22}} + \frac{a_{11}b_{21}(b_{12}a_{22} - a_{12}b_{22} +)}{-a_{12}b_{22} + b_{12}a_{22}}\right) K_{pf} \\ & - & \left(\frac{a_{22}b_{22}b_{11} - b_{21}b_{12}a_{22}}{-a_{12}b_{22} + b_{12}a_{22}}\right) K_{if} - a_x \\ d_0 & = & \left(\frac{a_{11}a_{22}(b_{22}b_{11} - b_{12}b_{21})}{-a_{12}b_{22} + b_{12}a_{22}} + \frac{a_{21}a_{12}(b_{12}b_{21} - b_{11}b_{22})}{-a_{12}b_{22} + b_{12}a_{22}}\right) K_{if} \end{array} \tag{3.10}$$

where

$$a_x = \frac{(a_{11}a_{22} - a_{12}a_{21})(a_{12}b_{22} - b_{12}a_{22})}{-a_{12}b_{22} + b_{12}a_{22}}.$$

Equation (3.10) may be rewritten in matrix form as

$$M \begin{bmatrix} K_{if} \\ K_{pr} \\ K_{pf} \end{bmatrix} = \begin{bmatrix} d_0 \\ d_1 + a_x \\ d_2 + (a_{11} + a_{22}) \end{bmatrix}$$

by introducing the matrix M given in Appendix (Table 7.4); since:

$$\det[M] = \frac{(b_{22}b_{11} - b_{21}b_{12})^2 (a_{11}a_{22} - a_{21}a_{12}) a_{21}}{-a_{12}b_{22} + b_{12}a_{22}}$$

$$= \frac{mv^2(c_f l_f - c_r l_r) - c_r c_f L^2}{J^3 v^2 m^2 \left(l_r m v^2 + l_r c_f l_f + c_f {l_f}^2\right)} {c_f}^2 c_r L^2 \left(c_f l_f - c_r l_r\right) \tag{3.11}$$

det[M] $\neq 0$ if and only if

$$(c_f l_f \neq c_r l_r) \tag{3.12}$$

and

$$(c_r l_r - c_f l_f) m v^2 + c_r c_f L^2 \neq 0. \tag{3.13}$$

Since by assumption $(c_f l_f < c_r l_r)$ then (3.12) and (3.13) hold and therefore det[M] $\neq 0$: the controlled system eigenvalues, which are the zeros of the characteristic polynomial (3.9), can be arbitrarily placed at $\lambda_1, \lambda_2, \lambda_3$ by a proper choice of the control parameter as follows

$$\begin{bmatrix} K_{if} \\ K_{pr} \\ K_{pf} \end{bmatrix} = M^{-1} \begin{bmatrix} \lambda_1\lambda_2\lambda_3 \\ \lambda_1\lambda_2 + \lambda_1\lambda_3 + \lambda_2\lambda_3 + a_x \\ \lambda_1 + \lambda_2 + \lambda_3 + (a_{11} + a_{22}) \end{bmatrix}, \tag{3.14}$$

where:

$$\begin{aligned} d_0 &= \lambda_1\lambda_2\lambda_3; \\ d_1 &= \lambda_1\lambda_2 + \lambda_1\lambda_3 + \lambda_2\lambda_3; \\ d_2 &= \lambda_1 + \lambda_2 + \lambda_3. \end{aligned}$$

The computation of M^{-1} in (3.14) leads to (3.2,3.3,3.4).

Remark 1 *According to (3.11) det[M]=0 in the following two cases:*

1. *if $c_f l_f = c_r l_r$ (neutral vehicle) then, substituting $c_f = c_r l_r / l_f$, two eigenvalues can be arbitrarily placed since rank[M]=2, while the third eigenvalue is negative real for every velocity and is equal to:*

$$\frac{c_f(l_f + l_r)}{l_r m v}. \tag{3.15}$$

2. *if $(c_r l_r - c_f l_f) m v^2 + c_r c_f L^2 = 0$, which may happen only when $c_f l_f > c_r l_r$ (oversteering vehicle), then for the following velocity*

$$v^* = \sqrt{\frac{c_f c_r L^2}{(c_f l_f - c_r l_r)\, m}} \tag{3.16}$$

the characteristic polynomial of the matrix A_c is given by:

$$\lambda(s) = (s^2 + d_1 s + d_0)s \tag{3.17}$$

According to (3.17) the controlled system has an eigenvalue in zero while two eigenvalues can be arbitrarily placed since rank[M]=2. The velocity v^* (3.16) is equal to the critical speed defined in [14] as the velocity above which an oversteering vehicle is unstable. If v^* is above the vehicle maximal speed then det[M]$\neq$ 0 for every speed below v^* so that in this case the eigenvalues of A_c may be assigned according to (3.14) for oversteering vehicles as well.

Remark 2 *The linearized model of a small SUV vehicle taken from CarSim®, whose values are given in Appendix (Table 7.2 and Table 7.3), has an understeering behavior ($c_f l_f < c_r l_r$). The uncontrolled vehicle eigenvalues are computed from matrix A in (2.27) and are shown in Fig. 3.2 when v ranges between 5 and 40 $[m/s]$. The possibility of allocating real stable eigenvalues by the coordinated action of a PI controller in rear steering and a proportional controller in front steering from yaw rate error was established in [47]: this is a crucial property since the appearance of poorly damped oscillatory modes at high speed and/or low adherence makes the vehicle difficult to control. The contribution of Theorem 1 with respect to [47] is to show that if a coordinated integral action is also used for front wheel steering, (β, r) can be driven to arbitrary constant references (β_d, r_d) including $(0, r_d)$ and $(\beta_d, 0)$: the reference model which generates (β_d, r_d) from driver inputs or external inputs can be freely designed while in [47] zero lateral speed is achieved only at low longitudinal speed by a careful design of the reference model. Moreover Theorem 1 gives an explicit parameterization of the PI decoupling control strategy.*

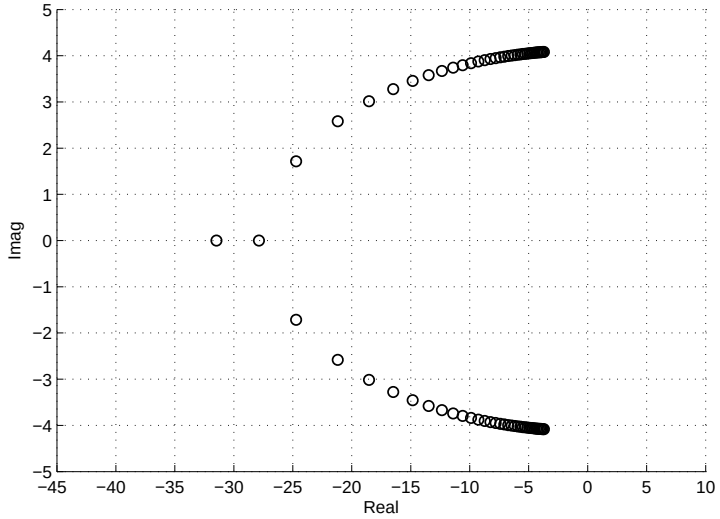

Figure 3.2: Uncontrolled vehicle eigenvalues for different velocities $5 \leq v \leq 40$ $[m/s]$.

Remark 3 *The steady state values of the front and rear steering angle are obtained from (2.27) as follows:*

$$\begin{bmatrix} \beta_d \\ r_d \end{bmatrix} = -\begin{bmatrix} a_{11} & a_{12} \\ a_{21} & a_{22} \end{bmatrix}^{-1} \begin{bmatrix} b_{11} & b_{12} \\ b_{21} & b_{22} \end{bmatrix} \begin{bmatrix} \delta_f \\ \delta_r \end{bmatrix} =$$

$$= \begin{bmatrix} \frac{a_{12}b_{21}-a_{22}b_{11}}{a_{11}a_{22}-a_{12}a_{21}} & \frac{a_{12}b_{22}-a_{22}b_{12}}{a_{11}a_{22}-a_{12}a_{21}} \\ \frac{a_{21}b_{11}-a_{11}b_{21}}{a_{11}a_{22}-a_{12}a_{21}} & \frac{a_{21}b_{12}-a_{11}b_{22}}{a_{11}a_{22}-a_{12}a_{21}} \end{bmatrix} \begin{bmatrix} \delta_f \\ \delta_r \end{bmatrix};$$

the values of δ_f and δ_r for a given equilibrium point (β_d, r_d) are:

$$\delta_f^e = \beta_d - \frac{(a_{12}b_{22} - a_{22}b_{12})\, r_d}{b_{22}b_{11} - b_{12}b_{21}} \tag{3.18}$$

$$\delta_r^e = \beta_d - \frac{(a_{22}b_{11} - a_{12}b_{21})\, r_d}{b_{22}b_{11} - b_{12}b_{21}}. \tag{3.19}$$

The steady state values of the front and rear steering angle (3.18) and (3.19) are equal to the steady state values of the computed steering angles for the proposed control law (3.1).

The advantages introduced by the designed control law (3.1) with respect to the feed forward control action (3.18) and (3.19) are given by the feedback: the lateral speed and the yaw rate references are asymptotically tracked with exponential modes, constant disturbances on the yaw rate dynamics are rejected by the integral part of the control law and more robustness with respect to parameters variations, including speed, is achieved.
Moreover, according to Theorem 1, the computed parameterization (3.14) of the proposed control law in terms of the desired eigenvalues to be assigned allows to place the controlled systems eigenvalues so that a specific index (rise time, bandwidth, controllability or a combination) can be min/maximized.

3.2 H_∞ Optimized Decoupling

Theorem 1 guarantees at steady state the decoupling between the desired vehicle sideslip angle and the desired yaw rate and gives a parameterization of the PI control parameters with respect to the desired eigenvalues. To improve the transient responses a numerical optimization of a weighted sum of the cross transfer functions H infinity norms is performed with respect to the desired eigenvalues. Recall that the H infinity norm is defined as:

$$\|H(j\omega)\|_\infty = \sup_{\omega\in\Re} \|H(j\omega)\|_2 \tag{3.20}$$

where $H(j\omega)$ is a generic transfer function. Let $W_{\beta,r_d}(j\omega)$ be the transfer function between the desired yaw rate and the sideslip angle, $W_{r,\beta_d}(j\omega)$ the transfer function between the desired sideslip angle and the yaw rate and (γ_1, γ_2) two positive arbitrary weights such that $\gamma_1 + \gamma_2 = 1$; the numerical minimization, on a compact set of negative real eigenvalues Ω

of interest, is defined as:

$$\min_{\lambda\in\Omega}\left(\gamma_1\left\|W_{\beta,r_d}(j\omega)\right\|_\infty+\gamma_2\left\|W_{r,\beta_d}(j\omega)\right\|_\infty\right); \tag{3.21}$$

since the controlled system is exponentially stable for each value of $\lambda_1,\lambda_2,\lambda_3$ according to Theorem 1, the two cross H infinity norms in (3.21) exist and are finite for every $\lambda\in\Omega$.
According to (3.21) the H infinity norm of the transfer function $W_{\beta,r_d}(j\omega)$ may be minimized ($\gamma_1=1$) so that, for zero lateral speed reference, the yaw rate reference influence on the lateral dynamics is minimized. If a non zero reference for the vehicle sideslip angle is chosen, a compromise between the numerical optimization on both the cross transfer functions $W_{\beta,r_d}(j\omega)$ and $W_{r,\beta_d}(j\omega)$ may be obtained by a suitable choice of the weights γ_1 and γ_2. In this paper the weights γ_1 and γ_2 are chosen to be equal ($\gamma_1=\gamma_2=0.5$) while the admissible set Ω is chosen as $\Omega=\{-20\le\lambda_1\le-1,\ -20\le\lambda_2\le-1,\ -300\le\lambda_3\le-100\}$; the minimum (3.21) is achieved at

$$\lambda_1=-4,\quad \lambda_2=-4,\quad \lambda_3=-200. \tag{3.22}$$

In Fig. 3.3 the weighted sum of the cross transfer functions H infinity norms (3.21) with $\gamma_1=\gamma_2=0.5$ for different values of λ_1 and λ_2 and for a given $\lambda_3=-200$ is reported: the strict minimum in Fig. 3.3 occurs at $\lambda_1=-4,\ \lambda_2=-4,\ \lambda_3=-200$.

The Bode diagrams of the four transfer functions between the reference signals (β_d,r_d) and (β,r) of the controlled system (2.27,3.1), for the chosen parameters (3.22), are shown in Fig. 3.4 and in Fig. 3.5: recalling Fig. 3.2, Fig. 3.4 shows that the resonances are suppressed; in Fig. 3.5 the Bode diagrams of the cross transfer functions $W_{\beta,r_d}(j\omega)$ and $W_{r,\beta_d}(j\omega)$ are given: attenuation greater than 20db for all frequencies is obtained showing an almost decoupled behavior during transients as

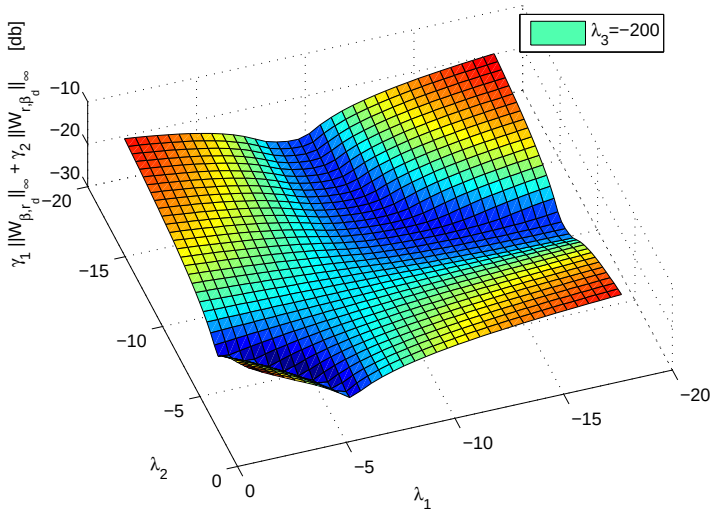

Figure 3.3: Weighted sum of the cross transfer functions H infinity norms for the controlled vehicle at $v = 30$ $[m/s]$.

well.

3.2.1 Zero Yaw Rate Reference

To analyze the achieved dynamic decoupling two different sideslip angle references are given to the nonlinear controlled vehicle (2.8),(3.1) while a zero yaw rate reference is set. Fig. 3.6 shows that the steady state values of the front and the rear steering angles are equal: this is consistent with equations (3.18) and (3.19) when r_d is set equal to zero. Fig. 3.6 also shows that a substantial decoupling is maintained also during transients: in particular the dependence of the yaw rate dynamics from the vehicle sideslip angle reference is greatly reduced and the sideslip reference signals are tracked with no oscillations.

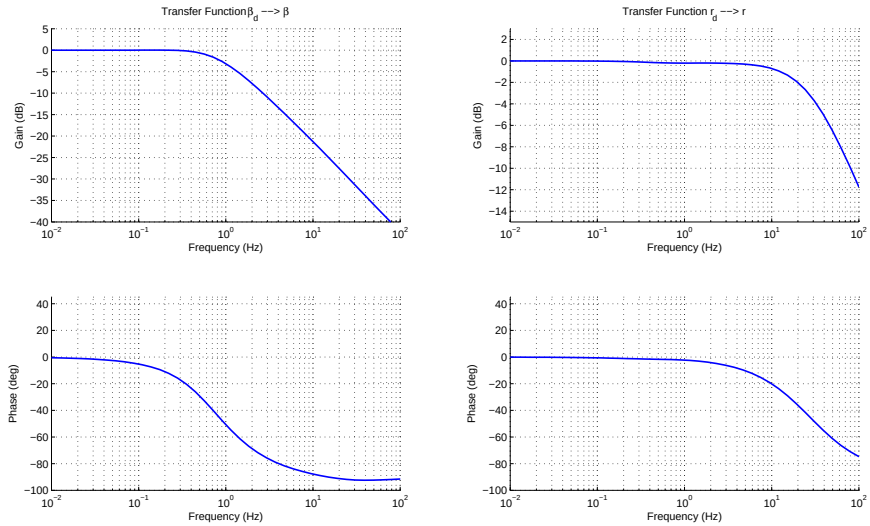

Figure 3.4: Bode diagrams of $W_{\beta,\beta_d}(j\omega)$ and $W_{r,r_d}(j\omega)$ for the controlled vehicle at $v = 30\ [m/s]$.

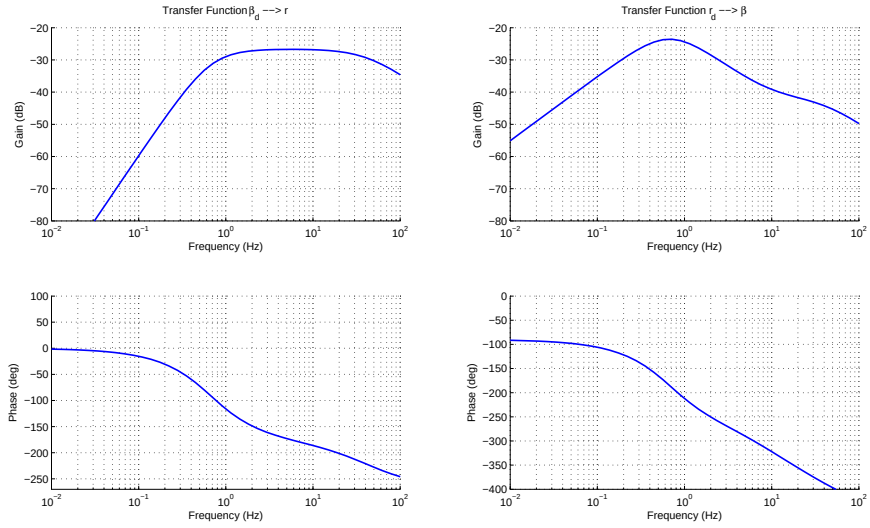

Figure 3.5: Bode diagrams of $W_{r,\beta_d}(j\omega)$ and $W_{\beta,r_d}(j\omega)$ for the controlled vehicle at $v = 30\ [m/s]$.

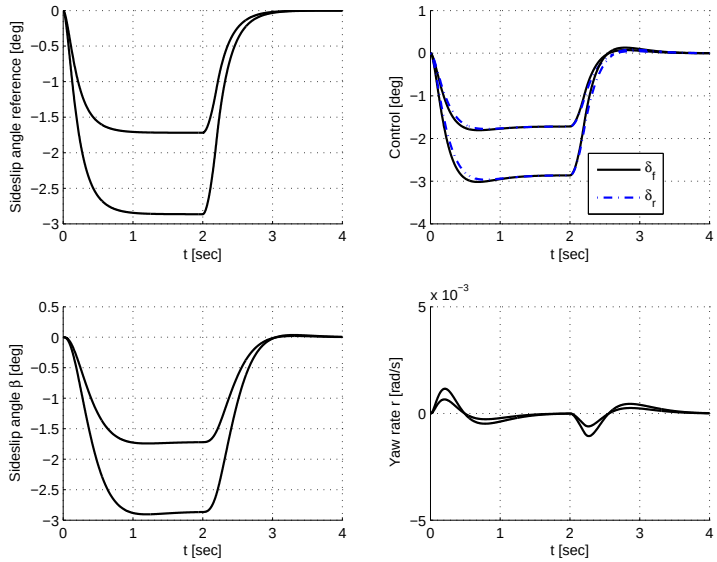

Figure 3.6: Responses to two increasing vehicle sideslip angle references for the controlled vehicle at $v = 30$ $[m/s]$.

3.2.2 Zero Lateral Speed Reference

While zero yaw rate may be desirable during lane keeping, in many four wheel steering control systems ([1], [4]) the steady state value of the lateral velocity is set to zero to improve comfort and manoeuvrability since in this case the yaw rate and lateral acceleration are in-phase according to the following equation:

$$a_y = \dot{v}_y + r v_x \ . \tag{3.23}$$

Setting β_d equal to zero from (3.18) and (3.19) it follows:

$$\delta_r = \ -\frac{a_{22}b_{11}-a_{12}b_{21}}{a_{22}b_{12}-a_{12}b_{22}}\delta_f = \frac{c_f\left(l_f m v^2 - c_r {l_r}^2 - l_f c_r l_r\right)}{c_r\left(l_r c_f l_f + c_f {l_f}^2 + l_r m v^2\right)}\delta_f \tag{3.24}$$

which implies:

$$G_n = \frac{r_d}{\delta_f} = \frac{b_{22}b_{11} - b_{21}b_{12}}{a_{22}b_{12} - a_{12}b_{22}}. \tag{3.25}$$

Equation (3.24), (see also [1] and [4]), guarantees, at steady state, zero lateral speed: it implies that it is impossible to achieve zero lateral speed by using only the front wheel steering angle as control input when $\delta_f = 0$. Equation (3.25) gives the ratio between yaw rate and the front steering angle when $\beta = 0$. Fig. 3.7 shows that the static gain G_n in (3.25) which is compatible with zero lateral speed is different from the uncontrolled vehicle ($\delta_r = 0$) static gain G_u between δ_f and r which is given by:

$$\begin{aligned} G_u &= \lim_{s\to 0} C\left(sI - A\right)^{-1} B \\ &= \frac{a_{21}b_{11} - b_{21}a_{11}}{a_{11}a_{22} - a_{12}a_{21}} \end{aligned} \tag{3.26}$$

where:

$$C = [0 \qquad 1].$$

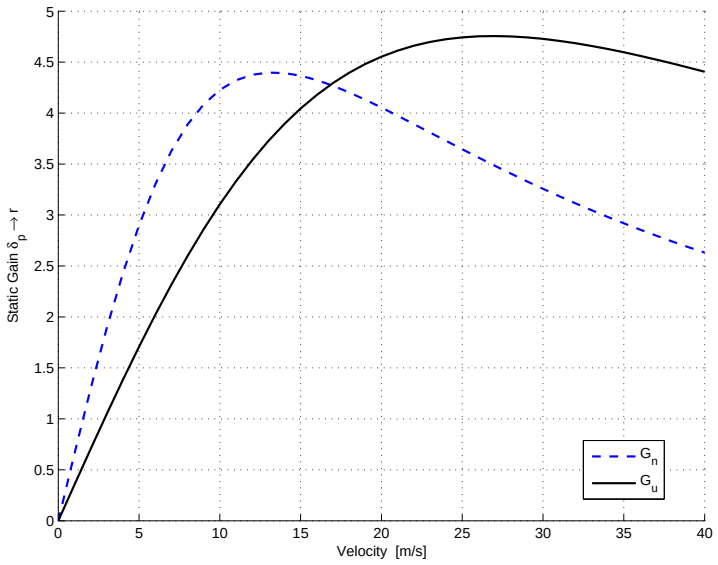

Figure 3.7: Static gain of the transfer function from δ_f to r.

In the proposed control law (3.1) zero lateral speed can be obtained by setting β_d equal to zero. Consequently the ratio of the steady state values of the computed steering angles for the controlled vehicle is equal

to (3.24); however an arbitrarily static gain from the driver wheel input to the yaw rate may be chosen which gives an additional degree of freedom to the designer.

To compare the driveability and the handling of both the uncontrolled and the controlled vehicle, the ratio between the steering wheel and the yaw rate reference is chosen as in (3.26) (*i.e.* $r_d = G_u\delta_p$). The Bode diagrams of the transfer functions from δ_p to v_y and r are first compared and then the responses to a step input of the controlled nonlinear model (2.8),(3.1) and of the uncontrolled model (2.8) in which the steering wheel angle is equal to a fixed steering gear ratio multiplied by the driver steering wheel angle ($\delta_f = 1/18\delta_p$) are analyzed.

According to (3.5) the numerator of the transfer function between the driver steering wheel input and the lateral velocity (3.27) is given by

$$\begin{array}{l} num(\delta_p \rightarrow v_y) = G_u \left(K_{pr} b_{12}(a_{12}b_{22} - b_{12}a_{22})\right. \\ \left. + K_{pf} b_{11}(a_{12}b_{22} - b_{12}a_{22})\right) s^2 \\ +G_u \left(K_{if} a_{12}(b_{11}b_{22} - b_{12}b_{21}) + K_{pr}({b_{12}}^2{a_{22}}^2\right. \\ \left. +{a_{12}}^2{b_{22}}^2 - 2a_{22}a_{12}b_{22}b_{12}) + K_{pf}(b_{12}{a_{22}}^2 b_{11}\right. \\ \left. -a_{22}a_{12}b_{22}b_{11} + {a_{12}}^2 b_{22}b_{21} - a_{12}b_{12}a_{22}b_{21})\right)s \end{array} \tag{3.27}$$

which vanishes at $s = 0$. The reduction of the lateral velocity is confirmed, for the range of frequencies of interest, by comparing the Bode diagrams for the controlled and uncontrolled vehicle of the transfer function between the driver input and the lateral velocity in Fig. 3.8. This analysis confirms that the previously defined steady state benefit for the lateral dynamics is extended to the frequency range of interest. The lateral velocity reduction increases also the comfort: in fact the Bode diagram in Fig. 3.9 of the transfer function between yaw rate and lateral acceleration ($W_{a_y,r}(j\omega)$) shows an improved comfort since the phase lead and the magnitude are reduced over a wide range of frequencies. Fig. 3.10 shows the suppressed resonances and the enlarged bandwidth for the transfer function between δ_p and r for the controlled vehicle.

To confirm the achieved dynamic decoupling a yaw rate reference

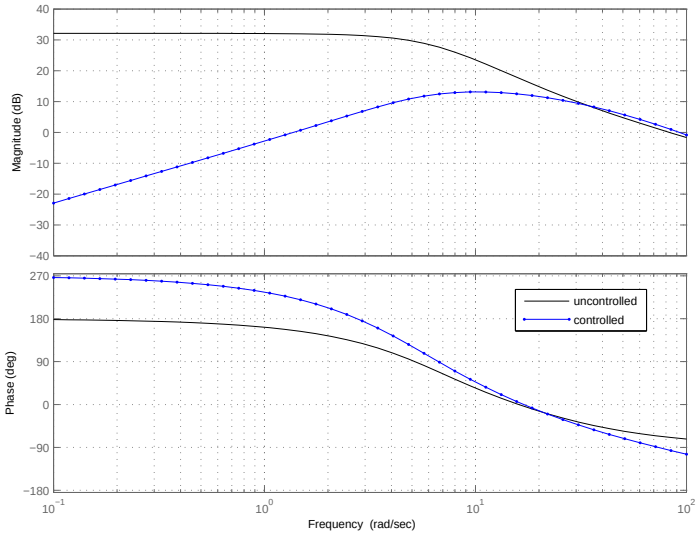

Figure 3.8: Bode diagrams of the transfer functions between δ_p and v_y for the uncontrolled and the controlled vehicle at $v = 30$ $[m/s]$.

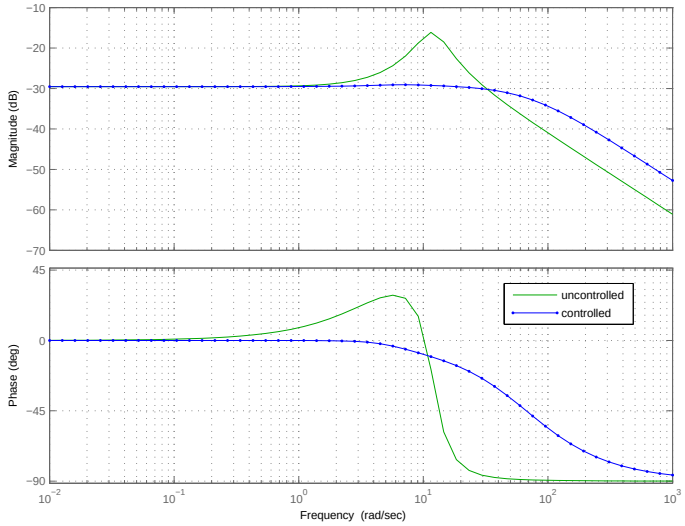

Figure 3.9: Bode diagrams of $W_{a_y,r}(j\omega)$ for the uncontrolled and the controlled vehicle at $v = 30$ $[m/s]$.

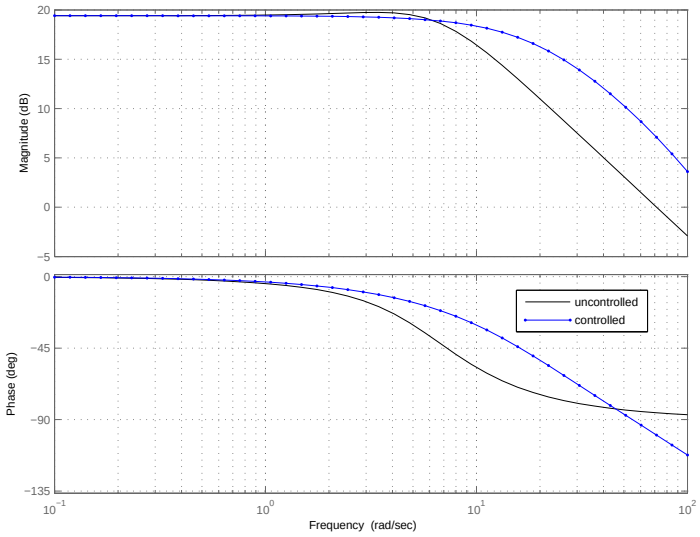

Figure 3.10: Bode diagrams of the transfer functions between δ_p and r for the uncontrolled and the controlled vehicle at $v = 30$ $[m/s]$.

$(r_d = G_u \delta_p)$ is given to the nonlinear controlled vehicle (2.8),(3.1) while a zero vehicle sideslip angle reference is set. Both the uncontrolled and the controlled vehicle responses to a step steering angle are shown in Fig. 3.11 for the non linear model (2.8): the suppression of overshoot in the yaw rate response, the zero steady state value and the reduced transient response of the lateral velocity to a driver steering angle are clearly shown in Fig. 3.11.

3.3 Robustness Analysis

Many variations may occur from the nominal vehicle parameters: the cornering stiffnesses may change due to different road adherence conditions and/or low tire pressure, the vehicle mass and moment of inertia change from unloaded to full load conditions. Setting a variation of

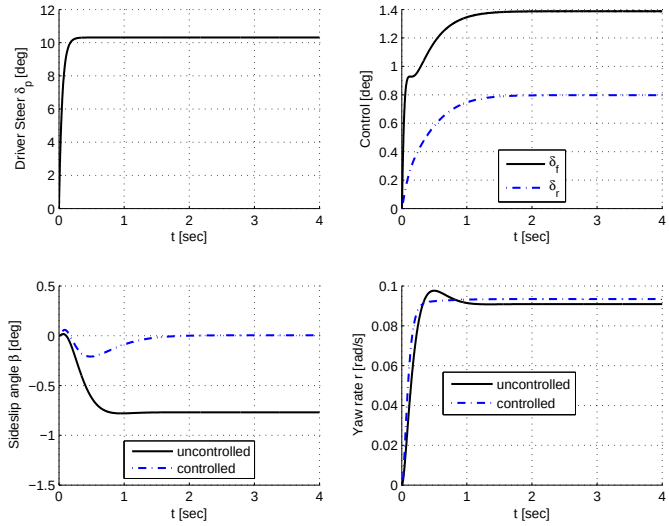

Figure 3.11: Sudden direction changes for the uncontrolled and the controlled vehicle at $v = 30\ [m/s]$.

$\pm 20\%$ for c_f, c_r, m and J with respect to the nominal parameters, the controlled system is analyzed by means of the eigenvalues displacement and the Bode diagrams of both the uncontrolled and the controlled systems. The improvements shown for the nominal parameters are maintained for variations from nominal values in the range $(0, \pm 20\%)$ for c_f, c_r, m, J as far as the eigenvalues assignment is concerned: the controlled vehicle has real modes or complex modes with a damping coefficient greater than 0.7 while the uncontrolled vehicle may have poorly damped oscillations with a damping coefficient smaller than 0.7 as shown in Fig. 3.12 in which 3^4 eigenvalues displacements are reported corresponding to three variations for each parameter. In Fig. 3.13 and Fig. 3.14 the transfer functions between δ_p and v_y, between δ_p and r and between a_y and r are plotted for nine combinations of front cornering stiffness c_f ($c_{f(nominal)} \pm 20\%$) and rear cornering stiffness c_r ($c_{r(nominal)} \pm 20\%$). Fig. 3.13 shows that the lateral velocity is greatly reduced also in corrispondence to vehicle parameters variations while the oscillations and

the static gain variations are suppressed while the bandwidth is enlarged for the yaw rate dynamics. In Fig. 3.14 the improved comfort is also confirmed by the reduced phase lead for the transfer function $W_{a_y,r}(j\omega)$. More robustness with respect to parameters variations is obtained by the the proposed feedback control strategy.

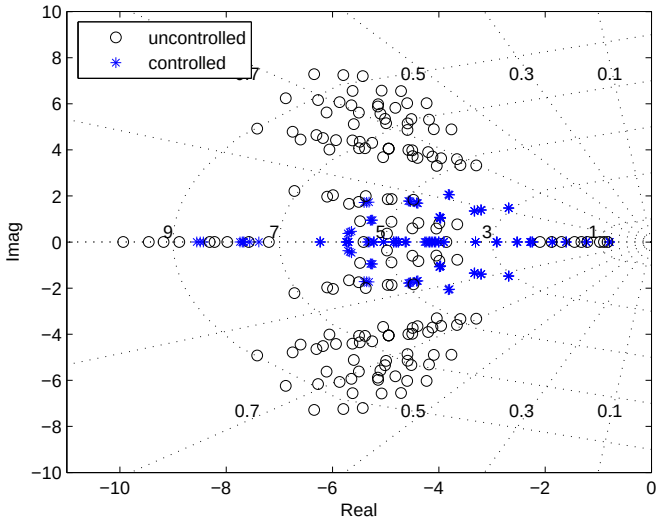

Figure 3.12: Uncontrolled and controlled vehicle eigenvalues for parameters variations at $v = 30$ $[m/s]$.

3.4 Nonlinear Reference Model Design

The generation of the desired reference signals β_d and r_d is an important issue for the control system in Fig. 3.1. As in [47], the steering wheel angle given by the driver is the input δ_p to a non linear first order reference model which, according to the velocity v, generates the yaw rate references signal r_d or equivalently, for a given velocity, the lateral

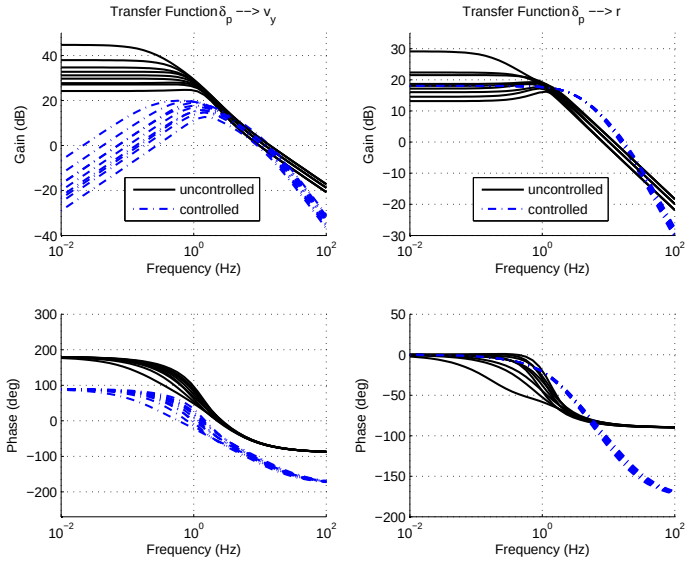

Figure 3.13: Bode diagrams of the transfer functions between δ_p and v_y and between δ_p and r with respect to nine cornering stiffnesses pairs at $v = 30\ [m/s]$.

acceleration reference a_{yd}. The reference model is defined as:

$$\begin{aligned} \dot{a}_{yd} &= -\lambda_{ref}(v)\left(a_{yd} - \underset{a_{y\,\max}}{sat}\left[G\left(\delta_p, v\right)\delta_p v\right]\right) \\ r_d &= \frac{a_{yd}}{v} \end{aligned} \tag{3.28}$$

where $\lambda_{ref}(v)$ is a positive design parameter and $G(\delta_p, v)$ is the imposed static gain between δ_p and r which may depend on δ_p and on tire-road adherence conditions. The gain $G(\delta_p, v)$ is obtained from the uncontrolled vehicle by storing the steady state yaw rate values in a lookup table for different steering angles, vehicle velocities and adherence conditions; the yaw rate references $G(\delta_p, v)\delta_p$ for the vehicle used in this paper in dry conditions are shown in (Fig. 3.15).

In (3.28) the saturation with respect to the lateral acceleration a_{ymax} is used to increase safety and to avoid unstable vehicle behaviours due to inadmissible driver steering inputs. The values of a_{ymax} can be set

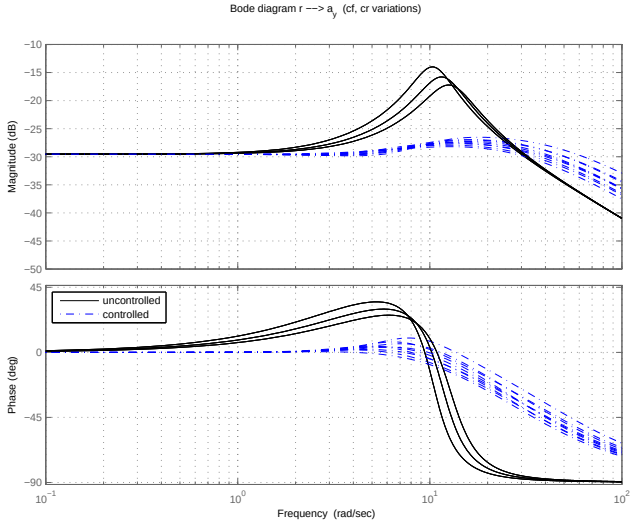

Figure 3.14: Bode diagrams $W_{a_y,r}(j\omega)$ with respect to nine cornering stiffnesses pairs at $v = 30$ $[m/s]$.

greater than the maximum uncontrolled vehicle lateral acceleration to improve the performance of the controlled vehicle. The driver could change the set-up of the vehicle by changing the nonlinear reference model by means of a selector on the steering wheel: the map $G(\delta_p, v)$ may be changed to adapt to different road conditions and different vehicle performance limits.

Similarly to the yaw rate reference the sideslip angle reference can be computed from uncontrolled vehicle measurements by storing the steady state lateral velocity value in a lookup table for different steering angles and vehicle velocities. Furthermore the desired sideslip angle can be related to external inputs such as an auxiliary driver input or can be received from collision avoidance radar information systems, artificial visual systems or instrumented roads equipped with info structures [15] for instance to perform an automated lane keeping.

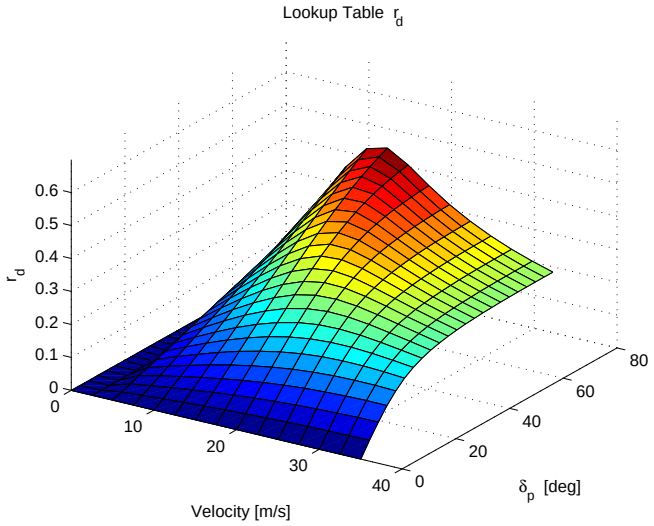

Figure 3.15: Yaw rate references for different driver steering wheel input and velocities.

3.5 Simulation Results on a CarSim® Vehicle

A full vehicle model of a standard CarSim® small SUV (see Fig. 3.16) is used to analyze the responses of both the uncontrolled and the controlled vehicle and to check robustness with respect to combined lateral and longitudinal tire forces effects and to unmodelled dynamics such as pitch and roll. The simulated vehicle has independent front suspension system and a rear solid axle; the front and rear wheel are 205/70R15; the transmission is automatic which has five gears and the engine is a 2.5L (118KW) four wheel drive. CarSim® vehicle takes into account the major kinematics and compliance effects of the suspensions (nonlinear spring models) and steering systems and uses detailed nonlinear tire models according to combined slip theory.

The simulations are performed using in (3.28) the uncontrolled vehicle static gain $G(\delta_p, v)$ obtained from CarSim® by storing the steady state yaw rate values in a lookup table for different steering angles and

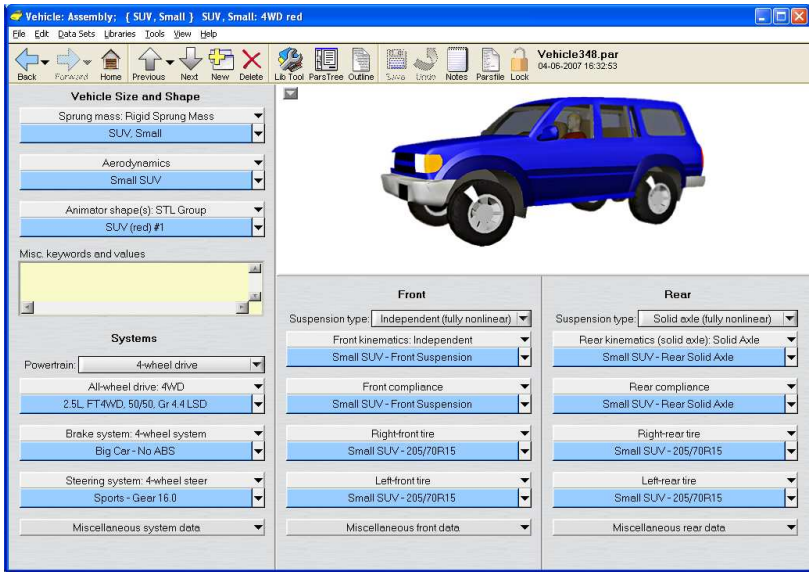

Figure 3.16: CarSim user interface.

vehicle velocities on dry roads. The controller (3.1) with $\beta_d = 0$ is parametrized according to (3.22).

3.5.1 Sudden Direction Changes

Two canonical manoeuvres, such as sudden direction changes, are simulated for two increasing driver steering wheel angles. Fig. 3.17 shows: the two increasing driver inputs; the corresponding two computed front and rear control steering angles, the two uncontrolled and controlled vehicle sideslip angles and the two yaw rate controlled and uncontrolled signals. The proposed control counteracts the yaw rate tracking errors so that the oscillations are suppressed and lateral speed is reduced both during transients and in steady state.

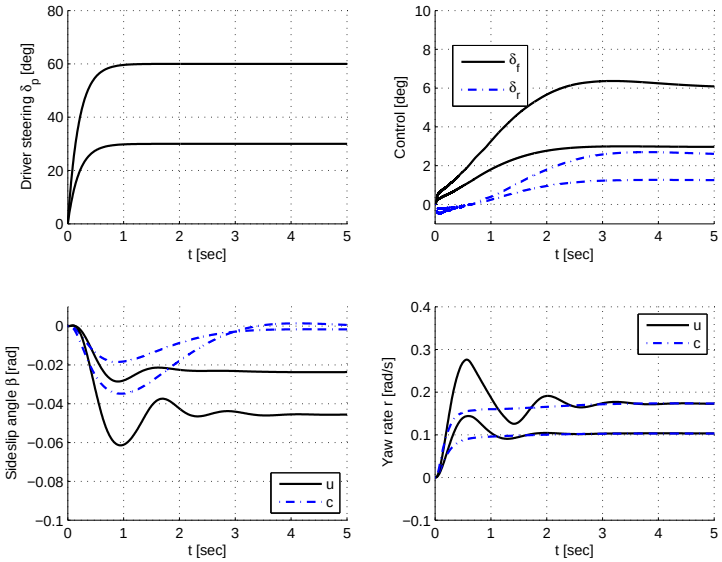

Figure 3.17: Sudden direction changes for the uncontrolled(u) and the controlled(c) CarSim® vehicle model at $v = 30\ [m/s]$.

3.5.2 Nonlinear Car Model Inversion

To compare the driver control efforts in driving both the uncontrolled vehicle and the controlled one on the same XY-trajectory the same longitudinal and lateral acceleration profile is set for both vehicles. To set zero longitudinal acceleration CarSim uses a feedback speed controller to simulate the action of a driver whose goal is to maintain a target speed which can be specified either as a function of time or as a function of road position: the speed controller uses the brakes to slow the vehicle down and to reproduce the behaviour of a cruise controller. To set the desired lateral acceleration profile a PI control on the error between the lateral acceleration in the fixed reference system and the desired lateral acceleration reference is used for the driver command

$$\delta_p = P\left(A_{yref} - A_y\right) + I\left(\int_0^t \left(A_{yref} - A_y\right)dt\right). \tag{3.29}$$

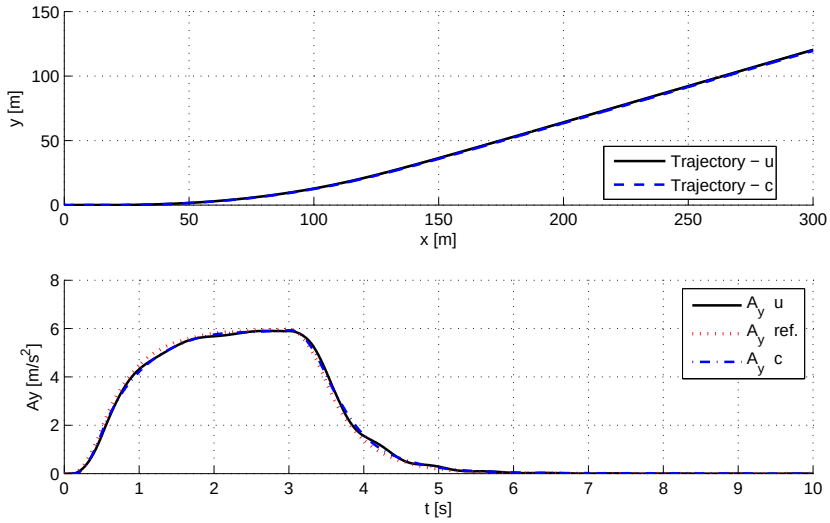

Figure 3.18: Coincident XY-trajectory for the uncontrolled(u) and the controlled(c) CarSim® vehicle model at $v = 30$ $[m/s]$.

The results for both the uncontrolled and the controlled systems, when the driver is modelled according to (3.29), are shown in Fig. 3.18 and Fig. 3.19. The desired lateral acceleration is tracked for both the vehicles as shown in Fig. 3.18 so that the same path in the XY-plane is followed. Fig. 3.19 shows the front and rear steering control actions which suppress the oscillations and reduce the vehicle sideslip angle so that the driver steering angle is much smoother for the controlled vehicle than for the uncontrolled one: a reduced control effort is required to drive the controlled vehicle.

3.5.3 Moose Test

The moose test is finally performed to check the robustness of the proposed control law with respect to a driver controller modelled in CarSim which uses an optimal feedback control strategy to follow a prescribed

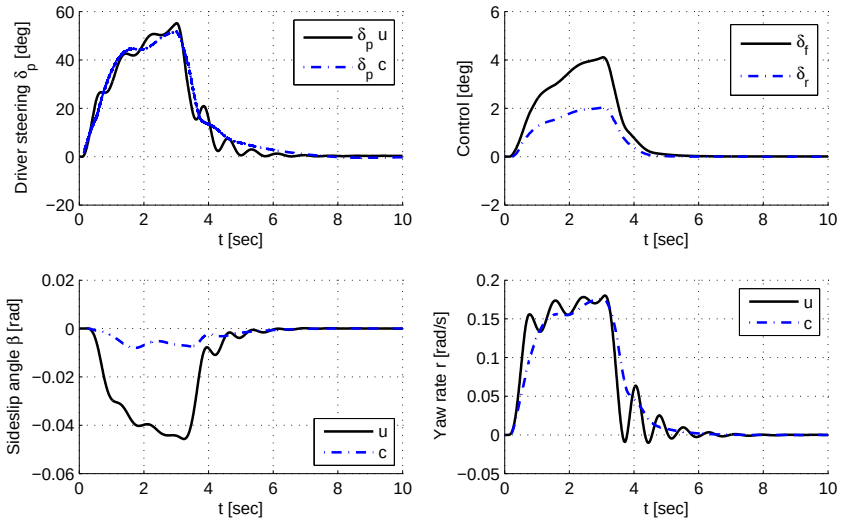

Figure 3.19: Coincident XY-trajectory for the uncontrolled(u) and the controlled(c) CarSim® vehicle model at $v = 30$ $[m/s]$.

path; in this case the path is part of the ISO/DIS 3888 standard. The test is defined by a pre-determined cone placement in the road and the manoeuvre is carried out on a dry surface. To show the improved performance two moose tests are performed at increasing speeds for both the uncontrolled and the controlled vehicle. For the first moose test, carried out at $v = 30$ $[m/s]$, Fig. 3.20 shows the reduced oscillations for the yaw rate dynamics and lateral velocity and the time intervals in which the front and the rear steering angles have opposite sign. The binding test is performed sucessfully for both vehicles: the uncontrolled vehicle reaches a lateral acceleration value equal to $a_{yu} = 7.5$ $[m/s^2]$ while the controlled vehicle has a lower maximal lateral acceleration equal to $a_{yc} = 6.7$ $[m/s^2]$ showing an increased safety margin with respect to the maximum lateral acceleration. For the moose test, carried out at $v = 35$ $[m/s]$, the proposed control reduces, especially during the second direction change, the yaw rate oscillations allowing the driver to

perform successfully the test with a maximum lateral acceleration equal to 8.5 $[m/s^2]$ while the uncontrolled vehicle rolls over. Fig. 3.21 shows the action of the front and rear steering angles in response to the driver steering wheel angle and the needed counter phase action of the rear wheels with respect to the front wheels to obtain a faster response for the yaw rate dynamics.

Several realistic simulations confirm that driveability and safety are improved by the proposed control.

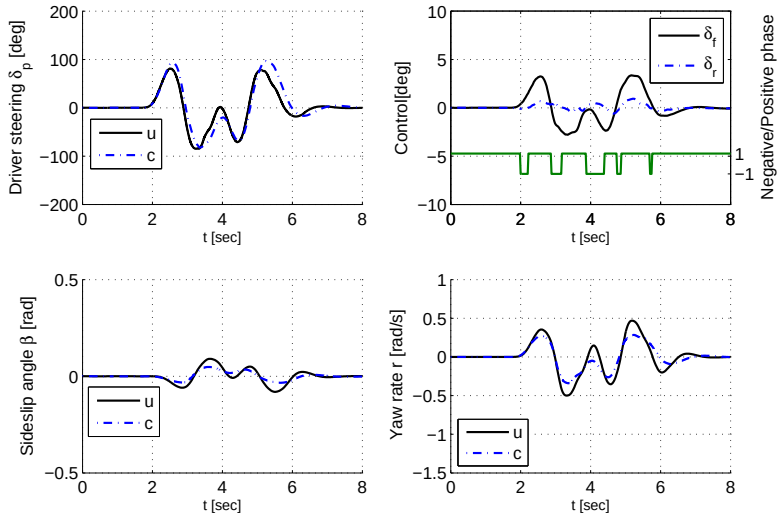

Figure 3.20: Moose test for the uncontrolled(u) and the controlled(c) CarSim® vehicle model at $v = 30$ $[m/s]$.

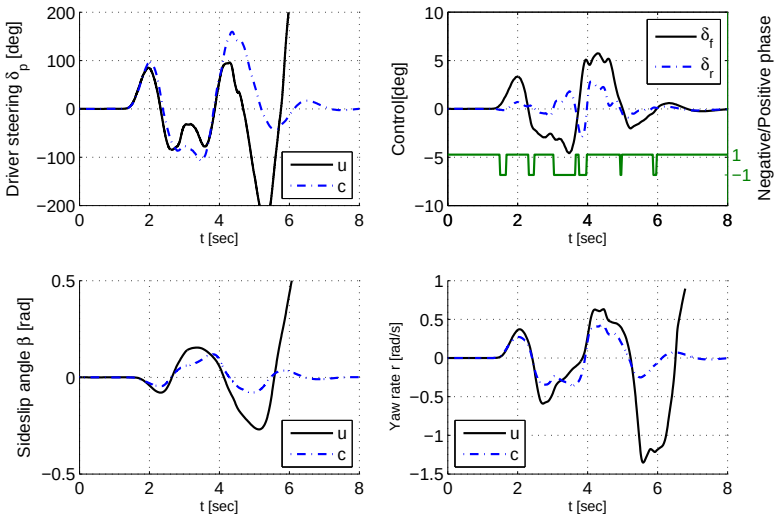

Figure 3.21: Moose test for the uncontrolled(u) and the controlled(c) CarSim® vehicle model at $v = 35$ $[m/s]$.

Chapter 4

Integrated Control of Active Front Steering and Electronic Differentials in Four Wheel Drive Vehicles

4.1 Introduction

In this chapter the integrated control of front and rear active differentials with active front steering is investigated in order to improve vehicle dynamics (i.e. suppress resonances and enlarge the bandwidth of the yaw rate tracking dynamics), safety and to avoid the drawbacks due to the action of a mechanical self-locking differential which may cause undesired understeering or oversteering behaviours in critical manoeuvres.
To design the control a double track vehicle model is introduced to extend the previously defined lumped model.

4.2 Double Track Vehicle Models

A detailed standard CarSim® small SUV model is used in numerical simulations to analyze the responses of both the uncontrolled and the

controlled vehicle. However to capture the essential vehicle steering dynamics and to design the controller a simplified non linear seventh order model is presented and analyzed in this section. The non linear model is described by the following equations:

$$\begin{cases} \dot{v}_x &= rv_y + (F_{lfl}\cos\delta_f + F_{lfr}\cos\delta_f - F_{sfl}\sin\delta_f \\ & \quad -F_{sfr}\sin\delta_f + F_{lrl} + F_{lrr} - c_a {v_x}^2)/m \\ \dot{v}_y &= -rv_x + (F_{lfl}\sin\delta_f + F_{lfr}\sin\delta_f + F_{sfl}\cos\delta_f \\ & \quad +F_{sfr}\cos\delta_f + F_{srl} + F_{srr})/m \\ \dot{r} &= (l_f(F_{lfl}\sin\delta_f + F_{lfr}\sin\delta_f + F_{sfl}\cos\delta_f \\ & \quad +F_{sfr}\cos\delta_f) - l_r(F_{srl} + F_{srr}) - (F_{lfl}\cos\delta_f \\ & \quad -F_{lfr}\cos\delta_f - F_{sfl}\sin\delta_f + F_{sfr}\sin\delta_f)T_f/2 \\ & \quad (F_{lrl} - F_{lrr})T_r/2)/J \\ \dot{\omega}_{fl} &= -(R_w F_{lfl} - T_{eng_1} + T_{d1})/J_w \\ \dot{\omega}_{fr} &= -(R_w F_{lfr} - T_{eng_2} - T_{d1})/J_w \\ \dot{\omega}_{rl} &= -(R_w F_{lrl} - T_{eng_3} + T_{d2})/J_w \\ \dot{\omega}_{rr} &= -(R_w F_{lrr} - T_{eng_4} - T_{d2})/J_w \end{cases} \tag{4.1}$$

where v_y (v_x) are the vehicle lateral (longitudinal)velocity, v is the vehicle velocity, β is the vehicle slip angle (see Fig. 4.1), r is the vehicle yaw rate, ω_{ij} are the wheel speed, δ_f is the front steer angle, l_f (l_r) is the longitudinal distance from the front (rear) axle to the center of mass, T_f (T_r) is the front (rear) distance from the wheels on the same axle, c_a is the aerodynamics drag coefficient, m is vehicle mass, J is the vehicle inertia with respect to the vertical axle through to the center of mass, J_w are the wheels inertia, R_w are the wheels radius, T_{eng_i} is the net torque due to the engine to the wheels, T_{d1} and T_{d2} are the transferred torque between the front and rear wheels respectively and F_s (F_l) are the lateral (longitudinal) forces given by Pacejka tire model, [13], and

are defined as in (2.9,2.10). The lateral forces (2.9) depend on the front (rear) wheel sideslip angle α_f (α_r) which are defined, for a double track vehicle model, as:

$$\begin{cases} \alpha_{fl} = \delta_f - \beta_{fl}; & \alpha_{rl} = -\beta_{rl}; \\ \alpha_{fr} = \delta_f - \beta_{fr}; & \alpha_{rr} = -\beta_{rr} \end{cases} \tag{4.2}$$

in which

$$\begin{cases} \beta_{fl} &= \left((v_y + rl_f) \,/\, (v_x - rT_f/2)\right) \\ \beta_{fr} &= \left((v_y + rl_f) \,/\, (v_x + rT_f/2)\right) \\ \beta_{rl} &= \left((v_y - rl_r) \,/\, (v_x - rT_r/2)\right) \\ \beta_{rr} &= \left((v_y - rl_r) \,/\, (v_x + rT_r/2)\right) \end{cases} \tag{4.3}$$

The longitudinal forces (2.10) depend on the front (rear) longitudinal wheel slip λ_f (λ_r) which are defined as:

$$\begin{cases} \lambda_i = \left(\omega_i R_w - V_i\right) / V_i \\ V_i = \left(\left(v_y \pm rl_f\right)^2 + \left(v_x \pm rT_f/2\right)^2 \right)^{1/2} \end{cases} . \tag{4.4}$$

The system (4.1) is linearized about uniform rectilinear motion ($v_x = v =$ constant, $r = 0$, $v_y = 0$, $\delta_f = 0$, $T_{d1} = 0$, $T_{d2} = 0$): the linearized system, $\dot{x} = Ax + Bu$, is given by:

$$A = \begin{bmatrix} a_{11} & 0 & 0 & a_{14} & a_{15} & a_{16} & a_{17} \\ 0 & a_{22} & a_{23} & 0 & 0 & 0 & 0 \\ 0 & a_{32} & a_{33} & a_{34} & a_{35} & a_{36} & a_{37} \\ a_{41} & 0 & a_{43} & a_{44} & 0 & 0 & 0 \\ a_{51} & 0 & a_{53} & 0 & a_{55} & 0 & 0 \\ a_{61} & 0 & a_{63} & 0 & 0 & a_{66} & 0 \\ a_{71} & 0 & a_{73} & 0 & 0 & 0 & a_{77} \end{bmatrix}, \tag{4.5}$$

$$x = \begin{bmatrix} v_x \\ v_y \\ r \\ \omega_{fl} \\ \omega_{fr} \\ \omega_{rl} \\ \omega_{rr} \end{bmatrix}, \quad B = \begin{bmatrix} 0 & 0 & 0 \\ b_{21} & 0 & 0 \\ b_{31} & 0 & 0 \\ 0 & b_{42} & 0 \\ 0 & b_{52} & 0 \\ 0 & 0 & b_{63} \\ 0 & 0 & b_{73} \end{bmatrix}, \quad u = \begin{bmatrix} \delta_f \\ T_{d1} \\ T_{d2} \end{bmatrix}. \tag{4.6}$$

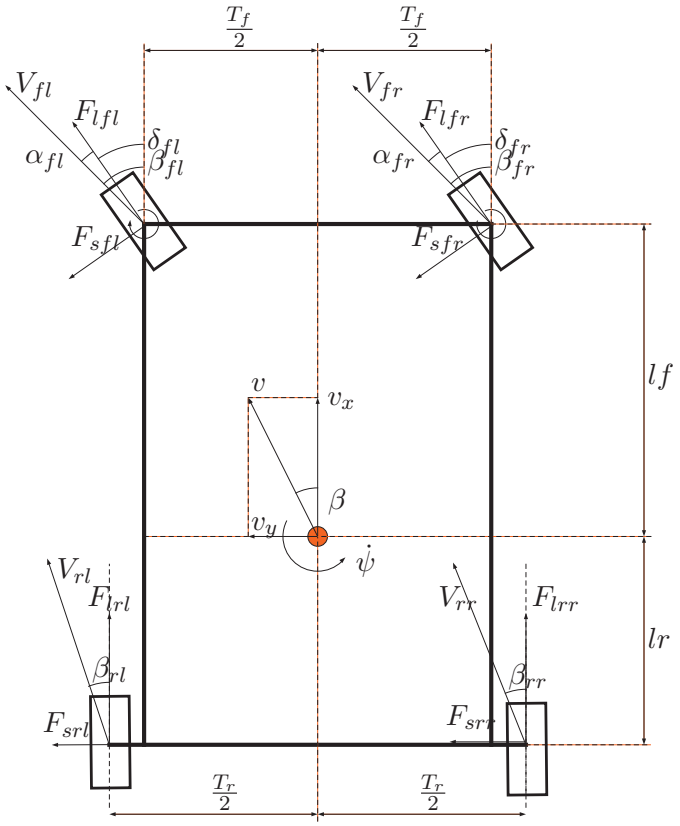

Figure 4.1: Full car model.

where the front steering angle δ_f and the torques T_{d1} and T_{d2} are the control inputs. By introducing the coordinates $\bar{x} = Tx$, we obtain the following linear system, $\dot{\bar{x}} = \bar{A}\bar{x} + \bar{B}u$, in which the new state space variable are the sum and the difference between the front and rear wheel speed:

$$
\begin{aligned}
\bar{x} = Tx = \begin{bmatrix} (\omega_{fl} + \omega_{fr})/2 \\ (\omega_{rl} + \omega_{rr})/2 \\ v_x \\ v_y \\ r \\ \omega_{fl} - \omega_{fr} \\ \omega_{rl} - \omega_{rr} \end{bmatrix} &= \begin{bmatrix} \bar{\omega}_f \\ \bar{\omega}_r \\ v_x \\ \bar{x}_1 \\ \bar{x}_2 \\ \bar{x}_3 \\ \bar{x}_4 \end{bmatrix} \\
\frac{d\bar{x}}{dt} = \begin{bmatrix} \overline{a}_{11} & 0 & \overline{a}_{13} & 0 & 0 & 0 & 0 \\ 0 & \overline{a}_{22} & \overline{a}_{23} & 0 & 0 & 0 & 0 \\ \overline{a}_{31} & \overline{a}_{32} & \overline{a}_{33} & 0 & 0 & 0 & 0 \\ 0 & 0 & 0 & \overline{a}_{44} & \overline{a}_{45} & 0 & 0 \\ 0 & 0 & 0 & \overline{a}_{54} & \overline{a}_{55} & \overline{a}_{56} & \overline{a}_{57} \\ 0 & 0 & 0 & 0 & \overline{a}_{65} & \overline{a}_{66} & 0 \\ 0 & 0 & 0 & 0 & \overline{a}_{75} & 0 & \overline{a}_{77} \end{bmatrix} \bar{x} \\
+ \begin{bmatrix} 0 & 0 & 0 \\ 0 & 0 & 0 \\ 0 & 0 & 0 \\ \overline{b}_{41} & 0 & 0 \\ \overline{b}_{51} & 0 & 0 \\ 0 & \overline{b}_{62} & 0 \\ 0 & 0 & \overline{b}_{73} \end{bmatrix} \begin{bmatrix} \delta_f \\ T_{d1} \\ T_{d2} \end{bmatrix}.
\end{aligned}
\tag{4.7}
$$

The system (4.7) is decoupled in two subsystems: the first one is an autonomous system (neglecting the engine) and describes the third order longitudinal dynamics, and the second one represents the fourth order lateral dynamics. Neglecting the longitudinal dynamics the lateral dynamics becomes

$$\dot{z} = \bar{A}z + \bar{B}u \tag{4.8}$$

with $z = [v_y \quad r \quad \bar{x}_3 \quad \bar{x}_4]^T$. The entries in the matrices $\bar{A}$ and $\bar{B}$, which may depend on v, are:

$$\begin{array}{lll}
\bar{a}_{44} = -\frac{2\left(c_{yf}+c_{yr}\right)}{mv}, & \bar{a}_{45} = -\frac{(mv^2+2c_{yf}l_f-2c_{yr}l_r)}{mv}, & \\
\bar{a}_{54} = -\frac{2\left(c_{yf}l_f-c_{yr}l_r\right)}{Jv}, & \bar{a}_{55} = -\frac{(4l_f^2c_{yf}+4l_r^2c_{yr}+T_f^2c_{xf}+T_r^2c_{xr})}{2Jv}, & \\
\bar{a}_{56} = -\frac{T_f c_{xf} R_w}{2Jv}, & \bar{a}_{57} = -\frac{T_r c_{xr} R_w}{2Jv}, & \bar{a}_{65} = -\frac{T_f c_{xf} R_w}{J_w v}, \\
\bar{a}_{66} = -\frac{R_w^2 c_{xf}}{J_w v}, & \bar{a}_{75} = -\frac{T_r c_{xr} R_w}{J_w v}, & \bar{a}_{77} = -\frac{R_w^2 c_{xr}}{J_w v}, \\
\bar{b}_{41} = \frac{2c_{yf}}{m}, & \bar{b}_{51} = \frac{2c_{yf}l_f}{J}, & \bar{b}_{62} = \bar{b}_{73} = \frac{2}{J_w}.
\end{array} \tag{4.9}$$

The vehicle parameters, whose values are identified from a small SUV CarSim® model used in the simulation paragraph, are given in Appendix (Table 7.5 and Table 7.6).

4.3 Integrated Control with Active Differentials

4.3.1 Control Design

The integrated feedback control law acting on the front steering angle and on the active front and rear differentials is presented in this section. Considering the first two equations of the linear decoupled vehicle model (4.8) the following equations can be written:

$$\begin{bmatrix} \dot{v}_y \\ \dot{r} \end{bmatrix} = \begin{bmatrix} \bar{a}_{44} & \bar{a}_{45} \\ \bar{a}_{54} & \bar{a}_{55} \end{bmatrix} \begin{bmatrix} v_y \\ r \end{bmatrix} + \begin{bmatrix} 0 \\ \bar{a}_{56} \end{bmatrix} z_3 + \begin{bmatrix} 0 \\ \bar{a}_{57} \end{bmatrix} z_4 + \begin{bmatrix} \bar{b}_{41} \\ \bar{b}_{51} \end{bmatrix} \delta_f \tag{4.10}$$

in which the front and the rear wheel speed difference $z_3 = \omega_{fl} - \omega_{fr}$ and $z_4 = \omega_{rl} - \omega_{rr}$ can be viewed as control inputs to generate a yaw moment in addition to the active front steering action. The designed active front steering control for δ_f is a proportional-integral (PI) controller from the yaw rate error as in [11]; the PI feedback control algorithm can be written as follows (K_{pf} and K_{if} are positive parameters):

$$\left\{ \begin{array}{lcl} \delta_f & = & -K_{pf}\tilde{r} - K_{if}\int_0^t \tilde{r}\,(\tau)\,\mathrm{d}\tau = -K_{pf}\tilde{r} - K_{if}\alpha_0 \\ \dot{\alpha}_0 & = & \tilde{r} \end{array} \right. \tag{4.11}$$

where: $\tilde{r} = r - r_d$ and r_d is the desired yaw rate constant reference. Define the variables $\tilde{z}_3$ and $\tilde{z}_4$ as follows:

$$\begin{array}{l} \tilde{z}_3 = z_3 - z_3^* - z_{3d} \\ \tilde{z}_4 = z_4 - z_4^* - z_{4d} \end{array} \tag{4.12}$$

with

$$\begin{array}{rcl} z_3^* & = & \gamma K_{pMz}\,(r - r_d) \\ z_4^* & = & (1-\gamma) K_{pMz}\,(r - r_d)\ , \end{array} \tag{4.13}$$

in which γ, $0 \leq \gamma \leq 1$, is a repartition parameter to assign the percentage of yaw moment to be generated by front and rear wheels and z_{3d} and z_{4d} are the constant desired reference signals for the front and rear wheel speed differences. The error dynamics for the new state space variables $\tilde{z}_3$ and $\tilde{z}_4$ are:

$$\begin{array}{l} \dot{\tilde{z}}_3 = \bar{a}_{65} r + \bar{a}_{66}\tilde{z}_3 + \bar{a}_{66} z_3^* + \bar{a}_{66} z_{3d} + \bar{b}_{62} T_{d1} - \dot{z}_3^* \\ \dot{\tilde{z}}_4 = \bar{a}_{75} r + \bar{a}_{77}\tilde{z}_4 + \bar{a}_{77} z_4^* + \bar{a}_{77} z_{4d} + \bar{b}_{73} T_{d2} - \dot{z}_4^* \end{array} \tag{4.14}$$

in which, from (4.13), $\dot{z}_3^*$ and $\dot{z}_4^*$ are equal to:

$$\begin{array}{l} \dot{z}_3^* = \frac{\partial z_3^*}{\partial r}\frac{\partial r}{\partial t} = \gamma K_{pMz}\dot{r} \\ \dot{z}_4^* = \frac{\partial z_4^*}{\partial r}\frac{\partial r}{\partial t} = (1-\gamma) K_{pMz}\dot{r}. \end{array} \tag{4.15}$$

Substituting (4.15) in (4.14) the error dynamics of the front and rear wheel speed differences are:

$$\begin{array}{rcl} \dot{\tilde{z}}_3 & = & \bar{a}_{65} r + \bar{a}_{66}\tilde{z}_3 + \bar{a}_{66} z_3^* + \bar{a}_{66} z_{3d} + \bar{b}_{62} T_{d1} \\ & - & \gamma K_{pMz}(\bar{a}_{54} v_y + \bar{a}_{55} r + \bar{a}_{56} z_3 + \bar{a}_{57} z_4 + \bar{b}_{51}\delta_f) \\ \dot{\tilde{z}}_4 & = & \bar{a}_{75} r + \bar{a}_{77}\tilde{z}_4 + \bar{a}_{77} z_4^* + \bar{a}_{77} z_{4d} + \bar{b}_{73} T_{d2} \\ & - & (1-\gamma) K_{pMz}(\bar{a}_{54} v_y + \bar{a}_{55} r + \bar{a}_{56} z_3 + \bar{a}_{57} z_4 + \bar{b}_{51}\delta_f). \end{array} \tag{4.16}$$

The active front and rear differentials controls are defined as follows:

$$\left\{ \begin{array}{rcl} T_{d1} & = & -\frac{1}{\bar{b}_{62}}\,[\,\bar{a}_{66} z_3^* - (\gamma K_{pMz}(\bar{a}_{55} r + \bar{a}_{56} z_3 + \bar{a}_{57} z_4 \\ & + & \bar{b}_{51}\delta_f))\,] - K_{p1}\tilde{z}_3 - K_{i1}\alpha_1 \\ T_{d2} & = & -\frac{1}{\bar{b}_{73}}\,[\,\bar{a}_{77} z_4^* - ((1-\gamma) K_{pMz}(\bar{a}_{55} r + \bar{a}_{56} z_3 + \bar{a}_{57} z_4 \\ & + & \bar{b}_{51}\delta_f))\,] - K_{p2}\tilde{z}_4 - K_{i2}\alpha_2 \\ \dot{\alpha}_1 & = & \tilde{z}_3 \\ \dot{\alpha}_2 & = & \tilde{z}_4 \end{array} \right. \tag{4.17}$$

so that the controlled linear system (4.8,4.11,4.17) can be written in the state space form

$$\dot{x}_c = A_c x_c + B_c u_c \tag{4.18}$$

in which:

$$\begin{aligned} A_c &= \begin{bmatrix} 0 & 0 & 1 & 0 & 0 & 0 & 0 \\ a_{c21} & a_{c22} & a_{c23} & 0 & 0 & 0 & 0 \\ a_{c31} & a_{c32} & a_{c33} & a_{c34} & a_{c35} & 0 & 0 \\ 0 & a_{c42} & a_{c43} & a_{c44} & 0 & a_{c46} & 0 \\ 0 & a_{c52} & a_{c53} & 0 & a_{c55} & 0 & a_{c57} \\ 0 & 0 & 0 & 1 & 0 & 0 & 0 \\ 0 & 0 & 0 & 0 & 1 & 0 & 0 \end{bmatrix}, \\ x_c &= \begin{bmatrix} \alpha_0 & v_y & r & \tilde{z}_3 & \tilde{z}_4 & \alpha_1 & \alpha_2 \end{bmatrix}^T, \end{aligned} \tag{4.19}$$

$$\begin{aligned} B_c &= \begin{bmatrix} -1 & 0 & 0 \\ \bar{b}_{41}K_{pf} & 0 & 0 \\ \bar{b}_{51}K_{pf} - K_{pMz}(\bar{a}_{56}\gamma + \bar{a}_{57}(1-\gamma)) & \bar{a}_{56} & \bar{a}_{57} \\ 0 & \bar{a}_{66} & 0 \\ 0 & 0 & \bar{a}_{77} \\ 0 & 0 & 0 \\ 0 & 0 & 0 \end{bmatrix}, \\ u_c &= \begin{bmatrix} r_d & z_{3d} & z_{4d} \end{bmatrix}^T, \end{aligned} \tag{4.20}$$

and the entries in the matrix A_c are:

$$\begin{aligned} a_{c21} &= -\bar{b}_{41}K_{if}, \quad a_{c22} = \bar{a}_{44}, \quad a_{c23} = \bar{a}_{45} - \bar{b}_{41}K_{pf}, \\ a_{c31} &= -\bar{b}_{51}K_{if}, \quad a_{c32} = \bar{a}_{54}, \\ a_{c33} &= \bar{a}_{55} + K_{pMz}(\bar{a}_{57}(1-\gamma) + \bar{a}_{56}\gamma) - \bar{b}_{51}K_{pf}, \\ a_{c34} &= \bar{a}_{56}, \qquad a_{c35} = \bar{a}_{57}, \quad a_{c42} = -\gamma K_{pMz}\bar{a}_{54}, \\ a_{c43} &= \bar{a}_{65}, \qquad a_{c44} = \bar{a}_{66} - K_{p1}\bar{b}_{62}, \qquad a_{c46} = -K_{i1}\bar{b}_{62}, \\ a_{c52} &= (\gamma - 1)K_{pMz}\bar{a}_{54}, \quad a_{c53} = \bar{a}_{75}, \qquad a_{c55} = \bar{a}_{77} - K_{p2}\bar{b}_{73}, \\ a_{c57} &= -K_{i2}\bar{b}_{73}. \end{aligned} \tag{4.21}$$

The error dynamics for the state space variables $\tilde{z}_3$ and $\tilde{z}_4$ of the controlled system are:

$$\begin{cases} \dot{\tilde{z}}_3 &= \left(\bar{a}_{66} - K_{p1}\bar{b}_{62}\right)\tilde{z}_3 - K_{i1}\bar{b}_{62}\int_0^t \tilde{z}_3\left(\tau\right)\mathrm{d}\tau \\ &+ \gamma K_{pMz}\bar{a}_{54}v_y + \bar{a}_{65}r + \bar{a}_{66}z_{3d} \\ \dot{\tilde{z}}_4 &= \left(\bar{a}_{77} - K_{p2}\bar{b}_{73}\right)\tilde{z}_4 - K_{i2}\bar{b}_{73}\int_0^t \tilde{z}_4\left(\tau\right)\mathrm{d}\tau \\ &+ \left(1-\gamma\right)K_{pMz}\bar{a}_{54}v_y + \bar{a}_{75}r + \bar{a}_{77}z_{4d} \end{cases} \tag{4.22}$$

In the design of the controlled system the lateral speed measurement is not used since it can be hardly measured using optical sensors with high cost and low accuracy and reliability, and it can be estimated on line from available signals only with unnegligible errors due to parameters uncertainty.
In order to choose the six control parameters in (4.11) and (4.17) the controlled system (4.18) is investigated using singular perturbation analysis and a Lypunov analysis.

4.3.2 Singular Perturbation Analysis

Since the steering dynamics are physically slower than the wheel speed dynamics a singular perturbation analysis [51] is carried out.
The controlled linear system (4.18) can be written as:

$$\dot{x}_c = A_c \begin{bmatrix} x_{c1} \\ x_{c2} \end{bmatrix} + \begin{bmatrix} b_{c1} \\ b_{c2} \end{bmatrix} u_c \tag{4.23}$$

with:

$$A_c = \begin{bmatrix} A_{c11} & A_{c12} \\ A_{c21} & A_{c22} \end{bmatrix}, \tag{4.24}$$

$$x_{c1} = \begin{bmatrix} \alpha_0 \\ v_y \\ r \end{bmatrix}, \qquad x_{c2} = \begin{bmatrix} \tilde{z}_3 \\ \tilde{z}_4 \\ \alpha_1 \\ \alpha_2 \end{bmatrix}. \tag{4.25}$$

Defining the new time scale $\tau = t/J$ the controlled linear system (4.23), in the error variables $\tilde{x}_c = x_c - x_d$ with $x_d = -A_c^{-1}B_c u_c$,

$$\tilde{x}_c = \begin{bmatrix} \tilde{x}_{c1} \\ \tilde{x}_{c2} \end{bmatrix} = \begin{bmatrix} \tilde{\alpha}_0 \\ \tilde{v}_y \\ \tilde{r} \\ \tilde{z}_3 \\ \tilde{z}_4 \\ \tilde{\alpha}_1 \\ \tilde{\alpha}_2 \end{bmatrix}, \tag{4.26}$$

can be rewritten as follows:

$$\begin{bmatrix} \frac{d}{d\tau}\tilde{x}_{c1} \\ \epsilon\frac{d}{d\tau}\tilde{x}_{c2} \end{bmatrix} = \begin{bmatrix} \tilde{A}_{c11} & \tilde{A}_{c12} \\ \tilde{A}_{c21} & \tilde{A}_{c22} \end{bmatrix} \begin{bmatrix} \tilde{x}_{c1} \\ \tilde{x}_{c2} \end{bmatrix} \tag{4.27}$$

with $\epsilon = J_w/J$ a small positive scalar. The equations (4.27) are written according to [51] in the slow subsystem and the fast subsystem. We recall from [51] p.57-58 the following result which will be applied to (4.27).

Corollary 1

If $\tilde{A}_{c22}^{-1}$ exists and if A_0 and $\tilde{A}_{c22}$ are Hurwitz matrices with $A_0 = \tilde{A}_{c11} - \tilde{A}_{c12}\tilde{A}_{c22}^{-1}\tilde{A}_{c21}$, then there exists an $\epsilon^* > 0$ such that for all $\epsilon \in (0, \epsilon^*]$ the system (4.27) is asymptotically stable.

Moreover as $\epsilon \to 0$ the first three eigenvalues of the system (4.27) tend to fixed positions in the complex plane defined by the eigenvalues of A_0 namely $\tilde{\lambda}_i(A_0)$ while the remaining four eigenvalues of the system (4.27) tend to infinity, with the rate $1/\epsilon$, along asymptotes defined by the eigenvalues of $\tilde{A}_{c22}$ namely $\tilde{\lambda}_i(\tilde{A}_{c22})/\epsilon$. Futhermore, if the eigenvalues of A_0 and $\tilde{A}_{c22}$ are distinct then the eigenvalues of the system (4.27) are approximated as

$$\begin{array}{rcll} \tilde{\lambda}_i & = & \tilde{\lambda}_i(A_0) + O(\epsilon) & i = 1..3 \\ \tilde{\lambda}_i & = & [\tilde{\lambda}_j(\tilde{A}_{c22}) + O(\epsilon)]/\epsilon & i = 4..7,\ j = 1..4 \end{array} \tag{4.28}$$

Eigenvalues Assignment

The aim of the following paragraph is to give a procedure to independently assign the eigenvalues of the steering dynamics and the eigenvalues of the wheel speed dynamics using Corollary 1. The computation of $det(\tilde{A}_{c22})$ gives:

$$det(\tilde{A}_{c22}) = 4J_w^2 K_{i1} K_{i2}. \tag{4.29}$$

Equation (4.29) implies that $\tilde{A}_{c22}^{-1}$ exists while, computing the square matrix $A_0 = \tilde{A}_{c11} - \tilde{A}_{c12}\tilde{A}_{c22}^{-1}\tilde{A}_{c21}$ from (4.27) and obtaining $A_0 = \tilde{A}_{c11}$ we need to guarantee that both the matrix A_0 and $\tilde{A}_{c22}$ are Hurwitz. Using the following two lemmas we satisfy all the hypothesis of Corollary 1 so that ϵ exists such that the eigenvalues of the integrated controlled systems tend to the eigenvalues of A_0 and $\tilde{A}_{c22}$ which are the steering and the wheel dynamics eigenvalues respectively.

Lemma 1

Let $\tilde{\lambda}_1 < 0, \tilde{\lambda}_2 < 0, \tilde{\lambda}_3 < 0$ be arbitrary negative real eigenvalues, if the control parameters K_{pMz}, K_{pf} and K_{if} are chosen as follows:

$$\begin{array}{rcl} K_{pMz} & = & (-\bar{b}_{51}^2\tilde{\lambda}_1\tilde{\lambda}_2\tilde{\lambda}_3 + \bar{b}_{51}^2\bar{a}_{44}(\tilde{\lambda}_1\tilde{\lambda}_2 + \tilde{\lambda}_2\tilde{\lambda}_3 + \tilde{\lambda}_1\tilde{\lambda}_3) \\ & - & \bar{b}_{51}^2\bar{a}_{44}^2(\tilde{\lambda}_1 + \tilde{\lambda}_2 + \tilde{\lambda}_3) - \bar{b}_{51}\bar{b}_{41}(\bar{a}_{54}^2\bar{a}_{45} + 2\bar{a}_{44}^2\bar{a}_{54}) \\ & - & \bar{a}_{54}^2\bar{b}_{41}^2(\tilde{\lambda}_1 + \tilde{\lambda}_2 + \tilde{\lambda}_3 - \bar{a}_{44} - \bar{a}_{55}) + \bar{a}_{54}\bar{a}_{45}\bar{b}_{51}^2\bar{a}_{44} + \bar{b}_{51}^2\bar{a}_{44}^3 \\ & + & 2\bar{b}_{51}\bar{a}_{44}\bar{a}_{54}\bar{b}_{41}(\tilde{\lambda}_1 + \tilde{\lambda}_2 + \tilde{\lambda}_3 - \bar{a}_{55}) \\ & - & \bar{b}_{51}\bar{a}_{54}\bar{b}_{41}(\tilde{\lambda}_2\tilde{\lambda}_3 + \tilde{\lambda}_1\tilde{\lambda}_3 + \tilde{\lambda}_1\tilde{\lambda}_2))/(\bar{a}_{54}\bar{b}_{41}(\bar{a}_{54}\bar{b}_{41}\bar{a}_{57}(1-\gamma) \\ & - & \bar{a}_{56}\gamma(\bar{b}_{51}\bar{a}_{44} - \bar{a}_{54}\bar{b}_{41}) - \bar{b}_{51}\bar{a}_{44}\bar{a}_{57}(1-\gamma))) \end{array} \tag{4.30}$$

$$\begin{array}{rcl} K_{pf} & = & (\bar{a}_{54}\bar{b}_{41}(\tilde{\lambda}_1\tilde{\lambda}_2+\tilde{\lambda}_1\tilde{\lambda}_3+\tilde{\lambda}_2\tilde{\lambda}_3)+\bar{b}_{51}\tilde{\lambda}_1\tilde{\lambda}_2\tilde{\lambda}_3 \\ & + & \bar{b}_{51}\bar{a}_{44}^2(\tilde{\lambda}_1+\tilde{\lambda}_2+\tilde{\lambda}_3)-\bar{b}_{51}\bar{a}_{44}(\tilde{\lambda}_1\tilde{\lambda}_2+\tilde{\lambda}_2\tilde{\lambda}_3+\tilde{\lambda}_1\tilde{\lambda}_3) \\ & + & \bar{a}_{54}^2\bar{a}_{45}\bar{b}_{41}+\bar{a}_{44}^2\bar{a}_{54}\bar{b}_{41}-\bar{b}_{51}\bar{a}_{44}^3-\bar{a}_{54}\bar{a}_{45}\bar{b}_{51}\bar{a}_{44} \\ & - & \bar{a}_{44}\bar{a}_{54}\bar{b}_{41}(\tilde{\lambda}_1+\tilde{\lambda}_2+\tilde{\lambda}_3))/((\bar{a}_{54}\bar{b}_{41}-\bar{b}_{51}\bar{a}_{44})\bar{a}_{54}\bar{b}_{41}) \end{array} \tag{4.31}$$

$$K_{if} = -\tilde{\lambda}_1\tilde{\lambda}_2\tilde{\lambda}_3/(\bar{a}_{54}\bar{b}_{41}-\bar{b}_{51}\bar{a}_{44}); \tag{4.32}$$

the integrated control law (4.11,4.17) arbitrarily assigns real stable eigenvalues $\tilde{\lambda}_i$, $1 \leq i \leq 3$, to the time scaled steering dynamics $\tilde{A}_{c11}$ at every constant speed v provided that the vehicle does not have a neutral behaviour ($c_{yf}l_f \neq c_{yr}l_r$).

Proof

The characteristic polynomial of the matrix $\tilde{A}_{c11}$ is given by:

$$det(sI-\tilde{A}_{c11}) = (s^3+d_2s^2+d_1s+d_0). \tag{4.33}$$

The coefficients in (4.33) are related to the control parameters as:

$$\begin{array}{rcl} d_2 & = & -\bar{a}_{44}-\bar{a}_{55}+\bar{a}_{56}K_{pMz}\gamma+\bar{b}_{51}K_{pf}+\bar{a}_{57}K_{pMz}(1-\gamma) \\ d_1 & = & \bar{a}_{44}\bar{a}_{55}-K_{pf}(\bar{b}_{51}\bar{a}_{44}-\bar{a}_{54}\bar{b}_{41})-\bar{a}_{54}\bar{a}_{45}-K_{pMz}\gamma\bar{a}_{44}\bar{a}_{56} \\ & + & \bar{b}_{51}K_{if}-K_{pMz}\bar{a}_{44}\bar{a}_{57}(1-\gamma) \\ d_0 & = & \bar{b}_{41}K_{if}\bar{a}_{54}-\bar{b}_{51}K_{if}\bar{a}_{44}. \end{array} \tag{4.34}$$

Equation (4.34) may be rewritten in matrix form as

$$M\begin{bmatrix} K_{pMz} \\ K_{pf} \\ K_{if} \end{bmatrix} = \begin{bmatrix} d_0 \\ d_1+(\bar{a}_{54}\bar{a}_{45}-\bar{a}_{44}\bar{a}_{55}) \\ d_2+(\bar{a}_{44}+\bar{a}_{55}) \end{bmatrix}$$

by introducing the matrix M

$$M = \begin{bmatrix} 0 & 0 & \bar{a}_{54}\bar{b}_{41} - \bar{b}_{51}\bar{a}_{44} \\ (\gamma-1)(\bar{a}_{44}\bar{a}_{57}) - \gamma\bar{a}_{44}\bar{a}_{56} & \bar{a}_{54}\bar{b}_{41} - \bar{b}_{51}\bar{a}_{44} & \bar{b}_{51} \\ \bar{a}_{57}(1-\gamma) + \bar{a}_{56}\gamma & \bar{b}_{51} & 0 \end{bmatrix}$$

since:

$$\begin{array}{rcl} \det[M] & = & \gamma\bar{a}_{44}\bar{a}_{56}\bar{a}_{54}\bar{b}_{41}\bar{b}_{51} + \bar{a}_{44}\bar{a}_{57}\bar{a}_{54}\bar{b}_{41}\bar{b}_{51}(1-\gamma) \\ & - & \bar{a}_{54}^2\bar{b}_{41}^2\bar{a}_{56}\gamma - \bar{a}_{54}^2\bar{b}_{41}^2\bar{a}_{57}(1-\gamma). \end{array} \tag{4.35}$$

Substituting the vehicle parameters in 4.35 $det[M]$ is computed as follows:

$$\det[M] = -\frac{8LR_w c_{yf}^2 c_{yr}\left(T_f c_{xf}\gamma + (1-\gamma)T_r c_{xr}\right)\left(c_{yf}l_f - c_{yr}l_r\right)}{m^2V^3J^3} \tag{4.36}$$

$det[M] \neq 0$ if and only if

$$\left(c_{yf}l_f \neq c_{yr}l_r\right). \tag{4.37}$$

Since by assumption $(c_f l_f \neq c_r l_r)$ then (4.37) holds and therefore det[M] $\neq 0$: the eigenvalues of the matrix $\tilde{A}_{c11}$, which are the zeros of the characteristic polynomial (4.33), can be arbitrarily placed at $\tilde{\lambda}_1, \tilde{\lambda}_2, \tilde{\lambda}_3$ by a proper choice of the control parameters as follows

$$\begin{bmatrix} K_{pMz} \\ K_{pf} \\ K_{if} \end{bmatrix} = M^{-1} \begin{bmatrix} d_0 \\ d_1 + (\bar{a}_{54}\bar{a}_{45} - \bar{a}_{44}\bar{a}_{55}) \\ d_2 + (\bar{a}_{44} + \bar{a}_{55}) \end{bmatrix}, \tag{4.38}$$

where:

$$\begin{array}{rcl} d_0 & = & \tilde{\lambda}_1\tilde{\lambda}_2\tilde{\lambda}_3; \\ d_1 & = & \tilde{\lambda}_1\tilde{\lambda}_2 + \tilde{\lambda}_1\tilde{\lambda}_3 + \tilde{\lambda}_2\tilde{\lambda}_3; \\ d_2 & = & \tilde{\lambda}_1 + \tilde{\lambda}_2 + \tilde{\lambda}_3. \end{array}$$

The computation of M^{-1} in (4.38) leads to (4.30,4.31,4.32).

Remark 1 *According to (4.36) $det[M] = 0$ if and only if $c_{yf}l_f = c_{yr}l_r$ (neutral vehicle) then, substituting $c_{yf} = c_{yr}l_r/l_f$, two eigenvalues can be arbitrarily placed since rank[M]=2, while the third eigenvalue is negative real for every velocity and is equal to:*

$$-\frac{2c_{yr}L}{l_f mv}. \tag{4.39}$$

Lemma 2

Let $\tilde{\lambda}_4 < 0, \tilde{\lambda}_5 < 0, \tilde{\lambda}_6 < 0, \tilde{\lambda}_7 < 0$ be arbitrary negative real eigenvalues, if the control parameters K_{p1}, K_{i1}, K_{p2} and K_{i2} are chosen as follows

$$\begin{array}{rclcl} K_{p1} & = & \frac{\bar{a}_{66}-\tilde{\lambda}_4-\tilde{\lambda}_5}{b_{62}}, & K_{i1} = \frac{\tilde{\lambda}_4\tilde{\lambda}_5}{b_{62}}, \\ K_{p2} & = & \frac{\bar{a}_{77}-\tilde{\lambda}_6-\tilde{\lambda}_7}{b_{73}}, & K_{i2} = \frac{\tilde{\lambda}_6\tilde{\lambda}_7}{b_{73}} \end{array} \tag{4.40}$$

the control law (4.11,4.17) arbitrarily assigns real stable eigenvalues $\tilde{\lambda}_i$, $4 \leq i \leq 7$, to the time scaled wheel speed difference dynamics $\tilde{A}_{c22}$ at every constant speed v.

Proof

Lemma 2 can be proved following the same steps of Lemma 1.

Using Lemma 1, Lemma 2 and (4.29) all the hypothesis of Corollary 1 are satisfied; in particular equation (4.29) implies that $\tilde{A}_{c22}^{-1}$ exists.
Lemma 1 shows that $A_0 = \tilde{A}_{c11} - \tilde{A}_{c12}\tilde{A}_{c22}^{-1}\tilde{A}_{c21} = \tilde{A}_{c11}$ is Hurwitz since the eigenvalues, $\tilde{\lambda}_i$, $1 \leq i \leq 3$, of the time scaled matrix $\tilde{A}_{c11}$ are arbitrarily assigned and are equal to the eigenvalues, λ_i, $1 \leq i \leq 3$, of the matrix A_{c11} multiplied by J.
Lemma 2 shows that $\tilde{A}_{c22}$ is Hurwitz since the eigenvalues, $\tilde{\lambda}_i$, $4 \leq i \leq 7$, of the time scaled matrix $\tilde{A}_{c22}$ are arbitrarily assigned and are equal to the eigenvalues, λ_i, $4 \leq i \leq 7$, of the matrix A_{c22} multiplied by J. Using

Corollary 1 we conclude that there exists an ϵ such that the eigenvalues of the integrated controlled system are approximated by the eigenvalues of A_0 and $\tilde{A}_{c22}$ which are the time scaled steering and wheel speed difference dynamics eigenvalues respectively.
The functional scheme of the proposed integrated control system is described in Fig. 4.2.

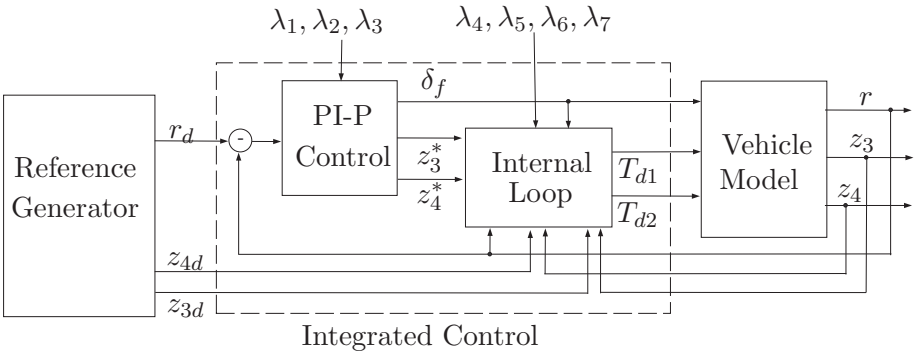

Figure 4.2: Functional scheme for the controlled system.

Remark 4 *For the linearized model of a small SUV vehicle taken from CarSim®, which has an understeering behavior ($c_{yf}l_f < c_{yr}l_r$), the uncontrolled vehicle eigenvalues are computed from matrix $\bar{A}$ in (4.8) and are shown in Fig. 4.3 when v ranges between 5 and 50 $[m/s]$.*

The possibility of allocating real stable eigenvalues by the coordinated action of a PI controller in rear steering and a proportional controller in front steering from yaw rate error was established in [47]. This is a crucial property since the appearance of poorly damped oscillatory modes at high speed and/or low adherence makes the vehicle difficult to control for an unexperienced driver. The contribution of Lemma 1, Lemma 2 and (4.29) with Corollary 1 is to give a simplified procedure to independently assign the steering dynamics eigenvalues and the wheel speed dynamics eigenvalues by an integrated action of the active front steering and the

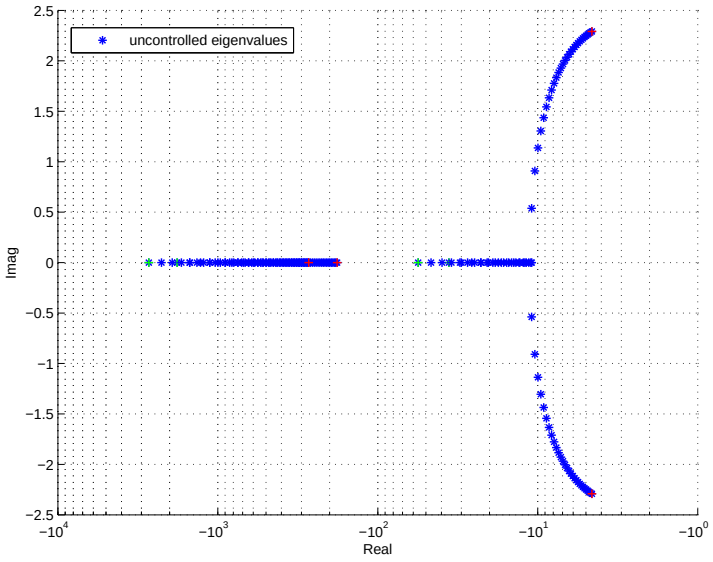

Figure 4.3: Uncontrolled vehicle eigenvalues for different velocities $5 \leq v \leq 50$ $[m/s]$.

active front and rear differentials.

Moreover, according to Lemma 1 and Lemma 2, the computed parameterizations (4.38) and (4.40) of the proposed control law in terms of the desired eigenvalues to be assigned allows the designer to place the controlled system eigenvalues so that a specific index (rise time, bandwidth, controllability or a combination) can be min/maximized.

For the small SUV taken from CarSim® the chosen eigenvalues for the steering dynamics are: $\bar{\lambda}_1 = -30.4, \bar{\lambda}_2 = -8, \bar{\lambda}_3 = -5.5$ *while, for the wheel speed dynamics are* $\bar{\lambda}_4 = -105, \bar{\lambda}_5 = -450, \bar{\lambda}_6 = -105, \bar{\lambda}_7 = -450$*; choosing the control parameters as in (4.38) and (4.40) we obtain that the error between the controlled system eigenvalues* λ_i *and the desired eigenvalues* $\bar{\lambda}_i$ *is:*

$$\max_i \left(\left| \lambda_i - \bar{\lambda}_i \right| / \bar{\lambda}_i \right) \leq 0.05 \tag{4.41}$$

which shows the effectiveness of the proposed approach.

Fig. 4.4 shows, for the chosen parameters, the suppressed resonances and the enlarged bandwidth (4 Hz) for the yaw rate dynamics of the controlled vehicle since the bandwidth of the transfer function between the driver steering wheel input and the yaw rate of the uncontrolled vehicle (4.8) is 1.4 Hz.

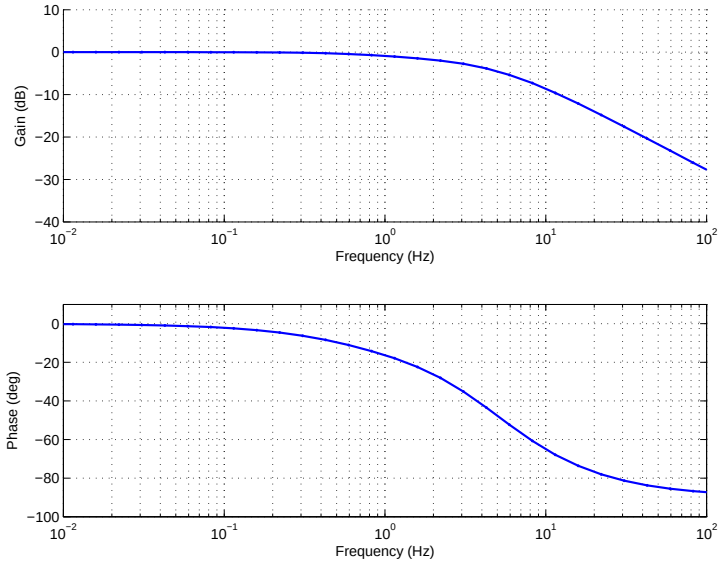

Figure 4.4: Controlled vehicle Bode diagram of the transfer functions between r_d and r at $v = 30$ $[m/s]$.

4.3.3 Lyapunov Analysis

The performed singular perturbation analysis gives a good strategy in the eigenvalues allocation but it does not give a bound for the parameter ϵ^* below which stability is guaranteed; to overcome this drawback the following Lyapunov analysis is carried out. The integrated controlled linear system (4.18) in the error variables can be rewritten as:

$$\dot{\tilde{x}}_c = F_1\tilde{x}_c + \nu F_2\tilde{x}_c \tag{4.42}$$

with:

$$F_1 = A_c - F_2 \qquad F_2 = \begin{bmatrix} 0 & 0 & 0 & 0 & 0 & 0 & 0 \\ 0 & 0 & 0 & 0 & 0 & 0 & 0 \\ 0 & 0 & 0 & 0 & 0 & 0 & 0 \\ 0 & 1 & 0 & 0 & 0 & 0 & 0 \\ 0 & 1 & 0 & 0 & 0 & 0 & 0 \\ 0 & 0 & 0 & 0 & 0 & 0 & 0 \\ 0 & 0 & 0 & 0 & 0 & 0 & 0 \end{bmatrix}, \tag{4.43}$$

and ν is equal to $0.5K_{pMz}\bar{a}_{54}$. Define the following quadratic function V:

$$V = \tilde{x}_c^T P \tilde{x}_c$$

in which P is a positive definite symmetric matrix; the time derivative of V is computed as follows:

$$\begin{array}{rcl} \dot{V} & = & \tilde{x}_c^T \left(PF_1 + F_1^T P\right) \tilde{x}_c \\ & + & \tilde{x}_c^T \left(\nu PF_2 + \nu F_2^T P\right) \tilde{x}_c \, . \end{array} \tag{4.44}$$

Since F_1 is Hurwitz by a proper choice of the control parameters there exist an n x n symmetric positive definite matrix P such that:

$$F_1^T P + PF_1 \;=\; -I \, . \tag{4.45}$$

Equation (4.44) can be rewritten as follows:

$$\begin{array}{rcl} \dot{V} & = & -\tilde{x}_c^T I \tilde{x}_c + \tilde{x}_c^T \left(\nu PF_2 + \nu F_2^T P\right) \tilde{x}_c \\ & = & -\left\|\tilde{x}_c\right\|^2 + \tilde{x}_c^T \left(\nu PF_2 + \nu F_2^T P\right) \tilde{x}_c \\ & \leq & -\left\|\tilde{x}_c\right\|^2 + 2\nu\lambda_{max}(P)\left\|F_2\right\|\left\|\tilde{x}_c\right\|^2 \, . \end{array} \tag{4.46}$$

If $2\nu\lambda_{max}(P)\left\|F_2\right\|\left\|\tilde{x}_c\right\|^2 < 1 - \Gamma$ with $\Gamma > 0$ then

$$\begin{array}{rcc} \dot{V} & \leq & -\left\|\tilde{x}_c\right\|^2 + (1-\Gamma)\left\|\tilde{x}_c\right\|^2 \\ & \leq & -\Gamma\left\|\tilde{x}_c\right\|^2 \end{array} \tag{4.47}$$

so that the controlled system is exponentially stable for

$$|\nu| < \frac{1-\Gamma}{2\lambda_{\max}(P)\left\|F_2\right\|} \,. \tag{4.48}$$

For the chosen control parameters, which assign the eigenvalues given in Remark 2, ν is equal to 0.017 and it satisfies the bound in (4.48) which is equal to 0.081.

4.3.4 Robustness Analysis

Many variations may occur from the nominal vehicle parameters: the cornering stiffnesses may change due to different road adherence conditions and/or low tire pressure, the vehicle mass and moment of inertia change from unloaded to full load conditions. Setting a variation of $\pm 20\%$ for c_{yf}, c_{yr}, c_{xf}, c_{xr}, m and J with respect to the nominal parameters, the controlled system is analyzed by means of the eigenvalues displacement of both the uncontrolled and controlled vehicle. The improvements obtained for the nominal parameters are maintained as far as the eigenvalues assignment is concerned: the controlled vehicle has real modes or complex modes with a damping coefficient greater than the uncontrolled vehicle as shown in Fig. 4.5 in which 3^6 eigenvalues displacements are reported corresponding to three variations for each parameter.

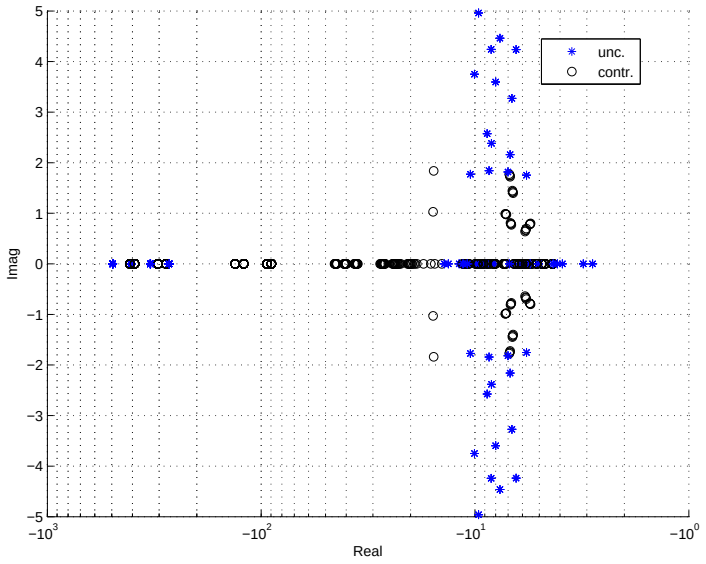

Figure 4.5: Uncontrolled and controlled vehicle eigenvalues for parameters variations at $v = 30$ $[m/s]$.

4.4 Integrated Control with Semiactive Differentials

If the torque T_{di} can be transferred only from the fastest wheel to the slowest one since the employed differential is semiactive the control law (4.17) for the active differential can be modified and simplified as shown in this section. From (4.17) and (4.13) only the terms proportional to the yaw rate error and to the wheel speed difference error are used in the design of the semiactive differential control law to improve stability and performance. Moreover the stability analysis of the switching control system is based on Lyapunov techniques and on the strictly real positive property. For simplicity the proposed control law is extended to a semiactive rear differential but the following analysis can be extended also to semiactive front differentials.

The actuator's power P_{act} is equal to:

$$P_{act} = T_{d2} z_4 \tag{4.49}$$

and the torque T_{di} is transferred only when (4.49) is negative due to the passivity of the actuator. Since the differential is semiactive the control algorithm (4.17) is modified as follows:

$$T_{diff} = \begin{cases} T_{d2} & if \quad T_{d2} z_4 \leq 0 \\ 0 & if \quad T_{d2} z_4 > 0 \, . \end{cases} \tag{4.50}$$

with:

$$T_{d2} = -K_{p2} \tilde{z}_4 - K_{pMz} \tilde{r} \tag{4.51}$$

4.4.1 Stability analysis

The stability of the discontinuous control law (4.50) integrated with the active steering (4.11) is based on Lyapunov techniques and on the strictly real positive property. Defined the controlled system with the active steering $\dot{x}_{as} = A_{as} x_{as} + B_{as} u_{as}$ as follows:

$$\frac{dx_{as}}{dt} = \begin{bmatrix} a_{as11} & a_{as12} & 0 & 0 & a_{as15} \\ a_{as21} & a_{as22} & a_{as23} & a_{as24} & a_{as25} \\ 0 & a_{as32} & a_{as33} & 0 & 0 \\ 0 & a_{as42} & 0 & a_{as44} & 0 \\ 0 & 1 & 0 & 0 & 0 \end{bmatrix} x_{as} + \begin{bmatrix} \overline{b}_{c11} & 0 \\ \overline{b}_{c21} & 0 \\ 0 & 0 \\ 0 & \overline{b}_{c42} \\ -G & 0 \end{bmatrix} u_{as} \tag{4.52}$$

$$x_{as} = \begin{bmatrix} v_y \\ r \\ z_3 \\ z_4 \\ \alpha_0 \end{bmatrix}, \quad u_{as} = \begin{bmatrix} \delta_p \\ T_{d2} \end{bmatrix}. \tag{4.53}$$

where the desired yaw rate r_d is equal to the uncontrolled vehicle steady state yaw rate value and can be written such as $r_d = G\delta_p$ in

which G is the static gain of the transfer function between δ_p and r. The stability of the proposed discontinuous control law is based on the time derivative of the following quadratic function V:

$$V = \tilde{x}_{as}^T P \tilde{x}_{as}$$

in which P is a positive definite symmetric matrix, $\tilde{x}_{as} = x_{as} - x_d$ are the error variables, $x_d = -A_{as}^{-1} b_{as1} \delta_p$ are the reference signals and b_{asi} are the column vectors i-th of the matrix B_{as}. The time derivative of V is computed as follows:

$$\begin{aligned} \dot{V} &= \tilde{x}_{as}^T P \left(A_{as} \tilde{x}_{as} + A_{as} x_d + B_{as} u_{as} \right) \\ &+ \left(\tilde{x}_{as}^T A_{as}^T + x_d^T A_{as}^T + u_{as}^T B_{as}^T \right) P \tilde{x}_{as} \end{aligned}$$

$$\begin{aligned} \dot{V} = \tilde{x}_{as}^T P \left(A_{as} \tilde{x}_{as} + A_{as}(-A_{as}^{-1} b_{as1} \delta_p) + b_{as1} \delta_p + b_{as2} T_{d2} \right) \\ + \left(\tilde{x}_{as}^T A_{as}^T + (-A_{as}^{-1} b_{as1} \delta_p)^T A_{as}^T + b_{as1} \delta_p + b_{as2} T_{d2} \right) P \tilde{x}_{as} \end{aligned}$$

$$\dot{V} = \tilde{x}_{as}^T \left(P A_{as} + A_{as}^T P \right) \tilde{x}_{as} + 2 \tilde{x}_{as}^T P b_{as2} T_{d2} \, . \tag{4.54}$$

Defining:

$$c = [0 \quad K_{pMz} \quad 0 \quad K_{p2} \quad 0] \, , \tag{4.55}$$

so that the output of the controlled system (4.52) is equal to: $y_{as} = c\tilde{x}_{as} = K_{pMz}\tilde{r} + K_{p2}\tilde{z}_4$; we may observe (Fig. 4.6) that the transfer function between T_{d2} and y_{as}, for the nominal vehicle parameters shown in Appendix (Table 7.5) of a small SUV model given by CarSim®, is Strictly Real Positive (see [52] for SPR definition): in fact, for every speed of interest, the Nyquist diagrams belong to the right half plane for every frequency.

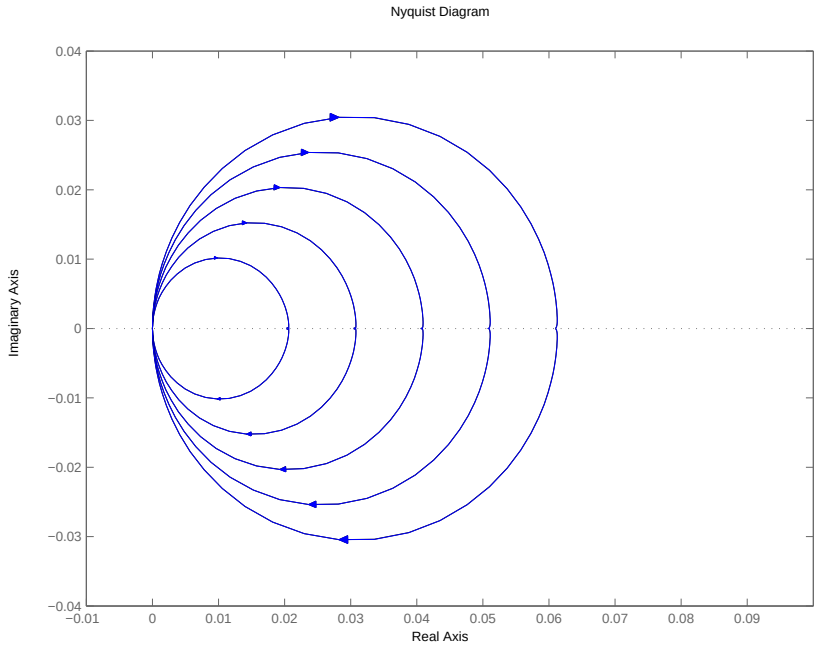

Figure 4.6: Nyquist diagrams for different velocities ($5 < v < 50$ $[m/s]$).

Then, for any symmetric positive define n x n matrix Q there exist an n x n symmetric positive definite matrix P, an n x 1 real vector q and a positive real ε, (see [52] pp. 362-363), such that:

$$\begin{array}{rcl} A_{as}^T P + P A_{as} & = & -qq^T - \varepsilon Q = -Q^* \\ Pb & = & c^T \ . \end{array} \tag{4.56}$$

The equation (4.54) can be rewritten as follows:

$$\dot{V} = -\tilde{x}_{as}^T Q^* \tilde{x}_{as} + 2T_{d2} c \tilde{x}_{as} \ . \tag{4.57}$$

$$\begin{array}{rcl} \dot{V} & = & -\tilde{x}_{as}^T Q^* \tilde{x}_{as} + 2T_{d2} y_{as} \\ & = & -\tilde{x}_{as}^T Q^* \tilde{x}_{as} - 2(K_{p2}\tilde{z}_4 + K_{pMz}\tilde{r})^2 \ . \end{array} \tag{4.58}$$

When the control law (4.50) is on, the speed of convergence of the controlled vehicle is greater than the uncontrolled one while, if the con-

trol law (4.50) is off, the speed of convergence is equal to the uncontrolled one; in fact, form (4.58) we may observe the following relations:

$$V\left(\phi\left(t,x_0\right)\right)_{OFF} \geq V\left(\phi\left(t,x_0\right)\right)_{ON} \ .$$

In the simulation section the performance of the semiactive rear differential integrated with the active steering will be illustrated.

4.5 Simulation Results on a CarSim® Vehicle

4.5.1 Nonlinear Reference Model Design

The generation of the desired reference signals r_d, x_{3d} and x_{4d} is an important issue for the control system in Fig. 4.2. As in [47], the steering wheel angle given by the driver is the input δ_p to a non linear first order reference model which, according to the velocity v, generates the yaw rate references signal r_d or equivalently, for a given velocity, the lateral acceleration reference a_{yd}. The reference model is defined as:

$$\begin{aligned} \dot{a}_{yd} &= -\lambda_{ref}(v)\left(a_{yd} - \underset{a_{y\max}}{sat}\left[G\left(\delta_p, v\right)\delta_p v\right]\right) \\ r_d &= \tfrac{a_{yd}}{v} \end{aligned} \tag{4.59}$$

where $\lambda_{ref}(v)$ is a positive design parameter for the non linear reference model and $G(\delta_p, v)$ is the imposed static gain between δ_p and r which may depend on δ_p (making the reference model nonlinear) and on tire-road adherence conditions. The gain $G(\delta_p, v)$ is obtained from the uncontrolled vehicle by storing the steady state yaw rate values in a lookup table for different steering angles, vehicle velocities and adherence conditions to compare the driveability and the handling of both the uncontrolled and the controlled vehicle so that the ratio between the steering wheel and the yaw rate reference is equal to the uncontrolled one. In (4.59) the saturation with respect to the lateral acceleration

a_{ymax} is used to increase safety and to avoid unstable vehicle behaviours due to inadmissible driver steering inputs. The values of a_{ymax} can be set greater than the maximum uncontrolled vehicle lateral acceleration to improve the performance of the controlled vehicle. The driver could change the set-up of the vehicle by changing the nonlinear reference model by means of a selector on the steering wheel: the map $G(\delta_p, v)$ may be changed to adapt to different road conditions and different vehicle performance limits may be set by changing the parameter $a_{y\,\max}$ in (4.59).

Similarly to the yaw rate reference the wheel speed difference references can be computed from uncontrolled vehicle measurements by storing the steady state front and rear wheel speed difference in a lookup table for different steering angles and vehicle velocities. A standard CarSim® small E-Class SUV is used to analyze the responses of both the uncontrolled and the controlled (4.8,4.11,4.17) vehicle and to check robustness with respect to combined lateral and longitudinal tire forces effects and to unmodelled dynamics such as pitch and roll. The simulated vehicle has independent front and rear suspension systems; the front and rear wheel are 255/75R16; the transmission is automatic which has five gears and the engine is a 2.5L (200KW) four wheel drive with viscous differentials when the active or semiactive differentials are not employed. To distribute torque between the front and the rear axle a full time viscous 50/50 differential is employed: this system in modeled by CarSim as a second order nonlinear system. CarSim® vehicle uses detailed nonlinear tire models according to combined slip theory and takes into account the major kinematics and compliance effects of the suspensions (nonlinear spring models) and steering systems. The uncontrolled vehicle has a nonlinear second order speed depending rack and pinion ratio steering system. For the active steering and the active differentials a realistic actuator with a bandwidth of 10Hz is considered.

The desired eigenvalues and, consequently, the chosen control parameters can be set so that the differential action improves either safety, by providing an additional yaw moment to counteract the yaw rate error, or performance, by avoiding excessive wheel speed difference due to low friction surface.

4.5.2 Sudden Direction Changes

A sudden direction change is simulated to show the suppressed resonances and the faster response of the controlled vehicle at 33 $[m/s]$. The manoeuvre is analyzed on the same vehicle with three different configurations: the uncontrolled vehicle (unc.), a vehicle equipped with the active steering and the semiactive rear differential (semiactive) (4.11, 4.50) and the controlled vehicle with the active steering and the active front and rear differentials integrated control (integr.) (4.11,4.17). Fig. 4.7 shows: the driver inputs; the uncontrolled and the controlled vehicle sideslip, yaw rate and wheel speed differences. Fig. 4.8 shows: the front steer angle and the front and rear differentials actions given by the proposed integrated control law, the uncontrolled and the controlled vehicle X-Y trajectory and longitudinal speed (desired value 33 $[m/s]$). The second plot in Fig. 4.8 illustrates the coordinated control action: the torques of the active differentials both at front and rear wheels are first negative to speed up the response and then positive to reduce the overshoot in coordination with a countersteering action performed by δ_f. The integrated control action succeeds in suppressing the oscillations and the overshoots in the yaw rate and lateral speed responses which are faster in the controlled vehicle as can be seen in Fig. 4.7. In the first part of the manoeuvre the semiactive differential can not improve vehicle performance since it can not give an additional oversteering moment to speed up the vehicle response as shown in the last plot in

Fig. 4.8; moreover the active steering action performed on the controlled semiactive vehicle (4.11, 4.50) is greater than the action performed on the integrated controlled active vehicle (4.11,4.17) as shwon in the first plot in Fig. 4.8. Both the vehicles equipped with the active steering and the active or the semiactive differential show improved performance with respect to the uncontrolled vehicle.

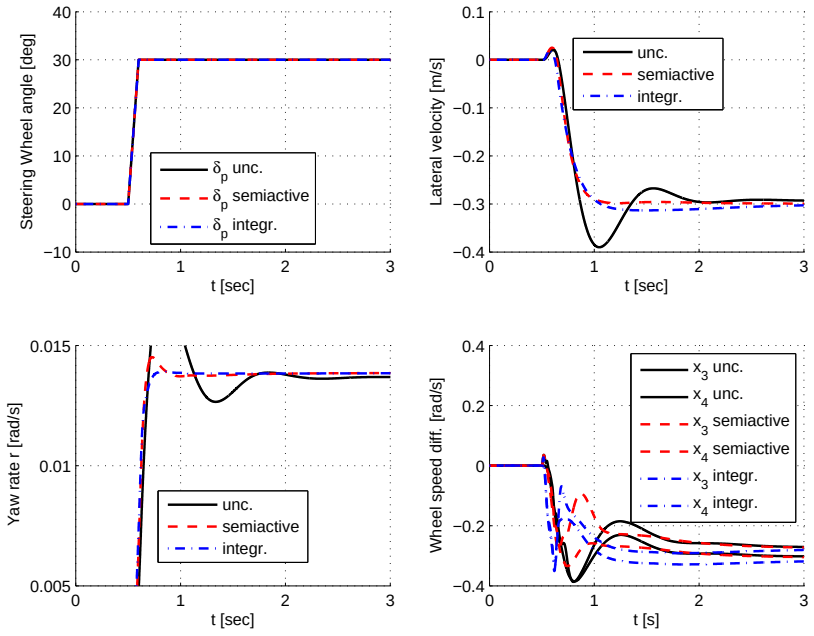

Figure 4.7: Sudden direction change: uncontrolled (unc.), active steering and semiactive differential (semiactive) and integrated controlled (integr.) CarSim® vehicle on dry asphalt at $v = 33$ $[m/s]$.

4.5.3 μ split braking

In a μ split manoeuvre the vehicle wheels on one side are on low adherence surface; in a power on driving condition a free differential can not transmit the driving torque to the wheel with high adherence and the vehicle does not move while the locking of a mechanical differential

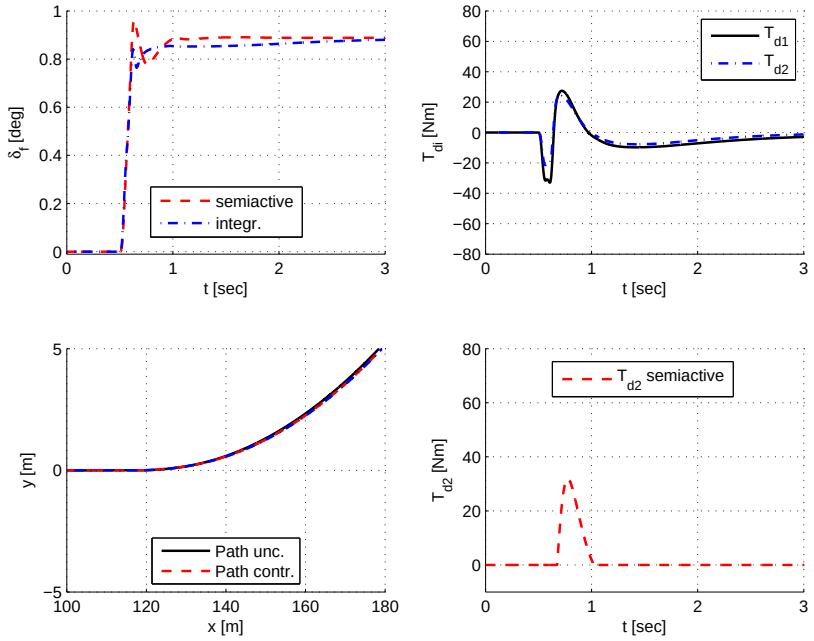

Figure 4.8: Sudden direction change: uncontrolled (unc.), active steering and semiactive differential (semiactive) and integrated controlled (integr.) CarSim® vehicle on dry asphalt at $v = 33$ $[m/s]$.

may generate an undesired oversteering moment due to excessive wheel speed difference. Similarly a μ-split braking action is a critical manoeuvre. Both tests are performed to check the robustness of the proposed integrated control.

In Fig. 4.9 and Fig. 4.10 a μ split braking manoeuvre is analyzed. The simulation is performed setting the high friction coefficient $\mu = 0.85$ on the right hand side and the very low friction coefficient $\mu = 0.1$ on the left hand side. A sudden braking action P_b is given on the same vehicle with three different configurations: the uncontrolled vehicle (unc.); a vehicle equipped with the active steering only (a.s.) (4.11) and the controlled vehicle with the active steering and the active front and rear differentials integrated control (integr.) (4.11) and (4.17). The PI con-

trol parameters of the integrated controlled vehicle related to the wheel speed errors are set equal to zero in (4.17) so that no torque is transferred by the differentials due to wheel speed errors since it can produce an undesired oversteering moment.
In response to the sudden braking action of 1.5 $[MPa]$ shown in Fig. 4.10, both the controlled vehicles keep the track while the uncontrolled vehicle goes out of track. When the proposed integrated control (4.11,4.17) is employed the active steering action and the errors from the desired state variables are reduced (Fig. 4.9, Fig. 4.10) with respect to a vehicle equipped with only the active front steering (4.11). The designed integrated control actions which are reported in Fig. 4.10 counteract the yaw rate error so that the zero yaw rate reference is achieved: notice that the differential torques in Fig. 4.10, second plot, change in sign when the yaw rate error changes sign. The integrated controlled system shows a better performance on the XY plane as shown in Fig. 4.10, third plot, with respect to a vehicle equipped with the active front steering only.

4.5.4 Standing start on μ split

On the same previously defined adherence surface a standing start manoeuvre is carried out. The manoeuvre is performed by the same CarSim® driver model ([53]), whose action δ_p is reported in the first plot of Fig. 4.11, on the same vehicle with two different configurations: the uncontrolled vehicle (unc.) and the controlled vehicle with the active steering and the active front and rear differentials integrated control (contr.) (4.11,4.17). The test shows improved performance for the integrated controlled vehicle: in fact it can reach greater longitudinal accelerations (fourth plot in Fig. 4.12) with respect to the uncontrolled vehicle. To avoid the front and the rear left wheels spin the control (4.11,4.17) applies torque on both the wheels on the surface with higher adherence

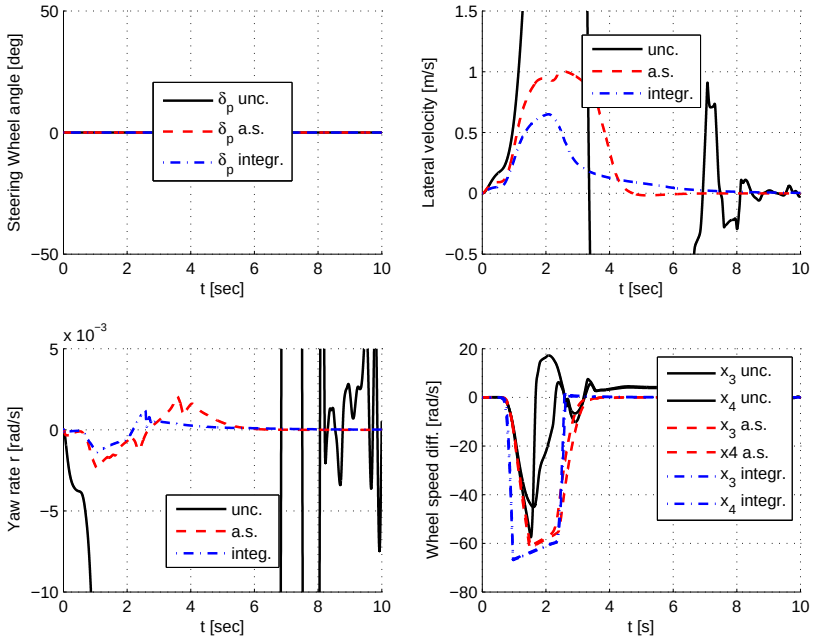

Figure 4.9: μ split braking on the uncontrolled (unc.), integrated controlled (integr.) and controlled by active steering (a.s.) CarSim® car model at $v = 25$ $[m/s]$.

improving traction (see the second plot in Fig. 4.12); since this action generates a counterclockwise yaw moment a negative steering angle is performed by the active steering to obtain zero steady state yaw rate (see the first plot in Fig. 4.12) showing the integrated action of the designed control law. The integrated active control law can greatly reduce the driver effort as shown in Fig. 4.11, first plot, since the CarSim® driver model on the controlled vehicle (4.11,4.17) can perform the manoeuvre giving a much smoother control action.

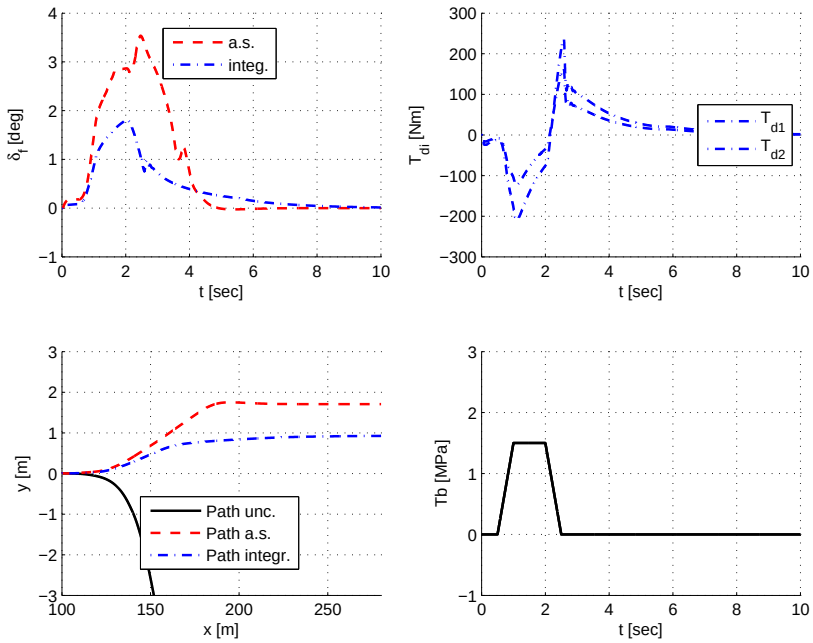

Figure 4.10: μ split braking on the uncontrolled (unc.), integrated controlled (integr.) and controlled by active steering (a.s.) CarSim® car model at $v = 25$ $[m/s]$.

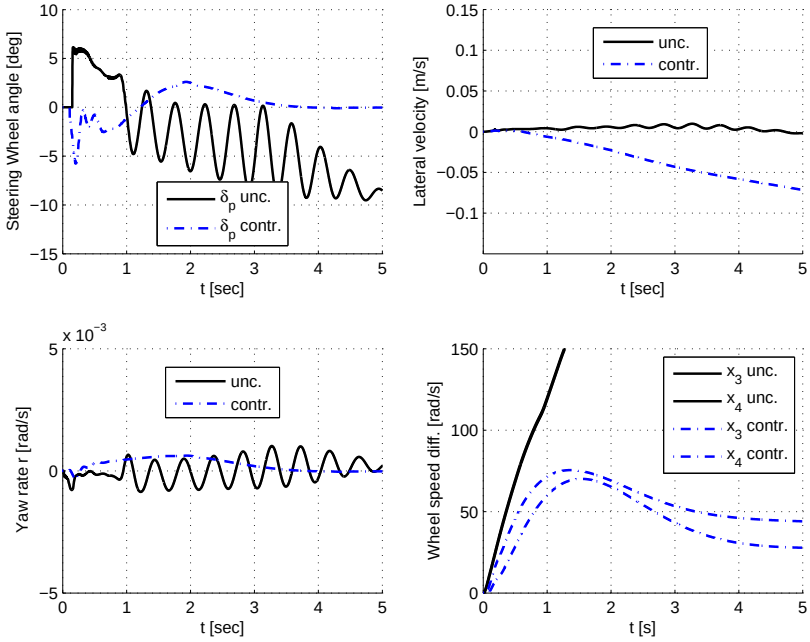

Figure 4.11: μ split standing start on the uncontrolled (unc.) and the integrated controlled (contr.) CarSim® car model.

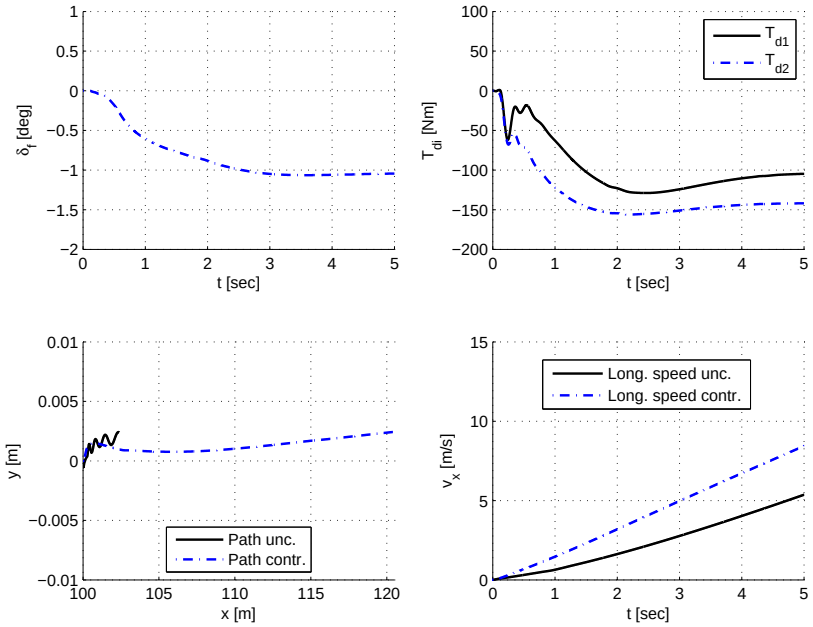

Figure 4.12: μ split standing start on the uncontrolled (unc.) and the integrated controlled (contr.) CarSim® car model.

Chapter 5

Vision Based Autonomous Vehicles

5.1 Introduction

In this chapter a control scheme which integrates the active steering action based on the yaw rate error with the lane keeping action based on lateral offsets is presented.

5.2 Extended Vehicle model

A detailed standard big sedan CarSim® vehicle model is used in numerical simulations to analyze the responses of both the uncontrolled and the controlled vehicle. To design the controller a widely used simplified single track vehicle model (2.27) is considered. The CCD camera measures the lateral deviation of the front preview point y_L that can be modeled [54] as follows:

$$\dot{y}_L = \beta v + l_s r + v\psi \tag{5.1}$$

where ψ is the yaw angle and y_L is the lateral offset from the road centerline at a preview distance l_s (see Fig. 5.1).

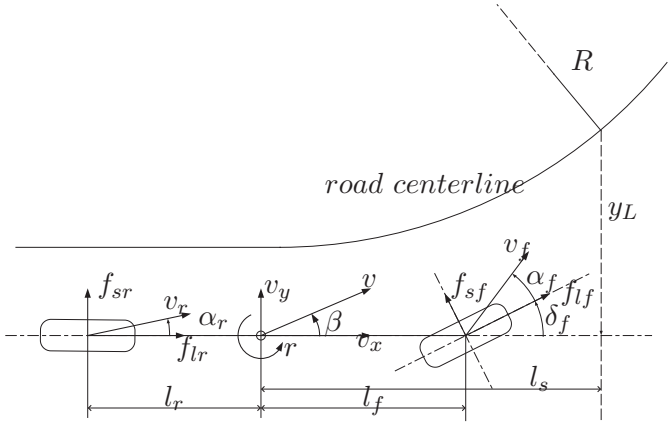

Figure 5.1: Single track vehicle model.

The reduced linear system, $\dot{x} = Ax + Bu$, which includes the lateral offset dynamics (5.1) is given by:

$$\begin{bmatrix} \dot{\beta} \\ \dot{r} \\ \dot{\psi} \\ \dot{y}_L \end{bmatrix} = \begin{bmatrix} a_{11} & a_{12} & 0 & 0 \\ a_{21} & a_{22} & 0 & 0 \\ 0 & 1 & 0 & 0 \\ v & l_s & v & 0 \end{bmatrix} \begin{bmatrix} \beta \\ r \\ \psi \\ y_L \end{bmatrix} + \begin{bmatrix} b_1 \\ b_2 \\ 0 \\ 0 \end{bmatrix} \delta_f + \begin{bmatrix} 0 \\ 0 \\ -v \\ 0 \end{bmatrix} \rho \tag{5.2}$$

where ρ is the road curvature defined as $\rho = 1/R$, with R the curvature radius. The coefficients appearing in systems (5.2), which may depend on v and on uncertain physical parameters are:

$$\begin{array}{llll} a_{11} = -\frac{(c_f+c_r)}{mv}, & a_{12} = -1 - \frac{(c_f l_f - c_r l_r)}{mv^2}, \\ a_{21} = -\frac{(c_f l_f - c_r l_r)}{J}, & a_{22} = -\frac{(c_f l_f^2 + c_r l_r^2)}{Jv}, \\ b_1 = \frac{c_f}{mv}, & b_2 = \frac{c_f l_f}{J}. \end{array} \tag{5.3}$$

where c_f and c_r are the front and the rear tire cornering stiffness which are the linear approximation of Pacejka magic formula. The vehicle parameters for the simplified single track vehicle model (5.2), whose values are identified from a big sedan CarSim® vehicle model used in the simulation paragraph, are given in Appendix (Table 7.7 and Table 7.8).

5.3 Control strategy

5.3.1 Control design

The proposed control strategy is illustrated in Fig. 5.2. It involves the design of two nested control blocks. The first one, called C_1, has to ensure the tracking of a yaw rate reference signal on the basis of the yaw rate tracking error in spite of constant disturbances and parameters uncertainties while the second one, called C_2, has to generate the yaw rate reference signal. The task of C_1 is to steer to zero the difference between the measured yaw rate r and desired yaw rate r_d. Following the active steering approach in [11] a PI control has been used for C_1:

$$\begin{array}{rcl} C1:\ \delta_f & = & -K_{P1}(r-r_d) - K_{I1}\int_0^t (r-r_d)\,d\nu \\ & = & -K_{P1}(r-r_d) - K_{I1}\alpha_0. \end{array} \tag{5.4}$$

The feedback from the yaw rate r improves the transient response, by changing the eigenvalues displacement of the steering dynamics. Substituting (5.4) in (2.27) we obtain:

$$\begin{bmatrix} \dot{\beta} \\ \dot{r} \\ \dot{\psi} \\ \dot{y}_L \\ \dot{\alpha}_0 \end{bmatrix} = \begin{bmatrix} a_{11} & a_{12}-K_{P1}b_1 & 0 & 0 & -b_1K_{I1} \\ a_{21} & a_{22}-K_{P1}b_2 & 0 & 0 & -b_2K_{I1} \\ 0 & 1 & 0 & 0 & 0 \\ v & l_s & v & 0 & 0 \\ 0 & 1 & 0 & 0 & 0 \end{bmatrix} \begin{bmatrix} \beta \\ r \\ \psi \\ y_L \\ \alpha_0 \end{bmatrix}$$

$$+\begin{bmatrix} K_{P1}b_1 \\ K_{P1}b_2 \\ 0 \\ 0 \\ -1 \end{bmatrix} r_d + \begin{bmatrix} 0 \\ 0 \\ -v \\ 0 \\ 0 \end{bmatrix} \rho \tag{5.5}$$

where α_0 is the additional state introduced by the dynamic control (5.4). Once the regulator C_1 is designed, the key idea is to integrate the additional lateral offset measure considering the yaw rate reference signal r_d in (5.5) as the control input to be designed to drive the output y_L to zero. Therefore, to design the desired yaw rate reference, it is necessary to model the dynamics of the road curvature, considering it as a disturbance on the lateral offset. In the case of a constant road curvature one integral term is needed to reject the disturbance; since the road curvature, in the case of non trivial manoeuvres, may be considered as increasing linearly with respect to time an additional integral term is necessary and the regulator C_2 becomes:

$$\begin{aligned} C2: \; r_d &= -K_{P2}y_L - K_{I2}\textstyle\int_0^t y_L \, d\nu \\ &- K_{I3}\int_0^t \int_0^\nu y_L d\eta d\nu - K_d y_{Ld} \\ &= -K_{P2}y_L - K_{I2}\alpha_2 - K_{I3}\alpha_1 - K_d y_{Ld} \; . \end{aligned} \tag{5.6}$$

where:

$$\dot{\alpha}_1 = y_L, \tag{5.7}$$

$$\dot{\alpha}_2 = \alpha_1. \tag{5.8}$$

and the signal y_{Ld} is given by:

$$\dot{\alpha}_3 = -\frac{1}{\tau}\alpha_3 + y_L \tag{5.9}$$

$$y_{Ld} = -\frac{1}{\tau^2}\alpha_3 + \frac{1}{\tau}y_L \tag{5.10}$$

where τ is the filter time constant.

The final structure of the control algorithm is shown in Fig. 5.2 in which C_1 is given by (5.4) and C_2 is given by (5.6).

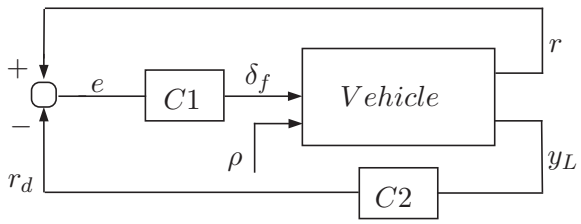

Figure 5.2: Controlled system scheme.

5.3.2 Control properties

To choose the six control gains the closed loop linear system (5.5) and (5.6) is considered assuming an ideal steering actuator. However the control gains are chosen so that the bandwidth of the transfer function between r_d and δ_f is within a typical actuator bandwidth (about 10 Hz). In order to avoid instability phenomena a derivative term has been added and the integral gains are chosen to be small as suggested in [71]. The derivative term gain is small in order to avoid chattering phenomena; the chosen gains are:

$$\begin{array}{c} K_{P1} = 20; \quad K_{I1} = 10; \\ K_{P2} = 30; \quad K_{I2} = 0.01; \quad K_{I3} = 0.01; \quad K_d = 0.05. \end{array} \tag{5.11}$$

In conclusion the controlled system (5.5) and (5.6) $\dot{x}_c = A_c x_c + B_c \rho$ and the equilibrium point x_{ce} are shown below:

$$A_c = \begin{bmatrix} a_{c11} & a_{c12} & 0 & a_{c14} & a_{c15} & a_{c16} & a_{c17} & a_{c18} \\ a_{c21} & a_{c22} & 0 & a_{c24} & a_{c25} & a_{c26} & a_{c27} & a_{c28} \\ 0 & 1 & 0 & 0 & 0 & 0 & 0 & 0 \\ v & l_s & v & 0 & 0 & 0 & 0 & 0 \\ 0 & 1 & 0 & a_{c54} & 0 & a_{c56} & a_{c57} & a_{c58} \\ 0 & 0 & 0 & 1 & 0 & 0 & 0 & 0 \\ 0 & 0 & 0 & 0 & 0 & 1 & 0 & 0 \\ 0 & 0 & 0 & 1 & 0 & 0 & 0 & -\frac{1}{\tau} \end{bmatrix}$$

$$B_c = \begin{bmatrix} 0 & 0 & -v & 0 & 0 & 0 & 0 & 0 \end{bmatrix}^T \tag{5.12}$$

with

$$x_c = \begin{bmatrix} \beta & r & \psi & y_L & \alpha_0 & \alpha_1 & \alpha_2 & \alpha_3 \end{bmatrix}^T \tag{5.13}$$

$$x_{ce} = - \begin{bmatrix} \frac{(b_2 a_{12} - b_1 a_{22})v}{a_{11} b_2 - a_{21} b_1} \\ -v \\ \frac{(a_{11} a_{42} b_2 - a_{21} a_{42} b_1 - a_{41} b_2 a_{12} + a_{41} b_1 a_{22})v}{a_{43}(a_{11} b_2 - a_{21} b_1)} \\ 0 \\ -\frac{(a_{11} a_{22} - a_{21} a_{12})v}{K_{I1}(a_{11} b_2 - a_{21} b_1)} \\ 0 \\ \frac{v}{K_{I2}} \\ 0 \end{bmatrix} \rho, \tag{5.14}$$

where τ is set equal to $\tau = 0.01$ and l_s is chosen equal to $l_s = 13$ $[m]$ while the parameters a_{cij} are shown in the following table.

With the chosen gains (5.11) the controlled system stability is guaranteed since the poles are on the left hand side of the complex plane; this result is confirmed with respect to vehicle parameter variations in the robustness analysis paragraph. Finally the frequency behaviour of

$$
\begin{aligned}
a_{c11} &= a_{11} & a_{c12} &= a_{12} - K_{P1}b_1 \\
a_{c14} &= -\frac{K_{P1}b_1(K_{P2}\tau+K_d)}{\tau} & a_{c15} &= -b_1K_{I1} \\
a_{c16} &= -K_{P1}b_1K_{I3} & a_{c17} &= -K_{P1}b_1K_{I2} \\
a_{c18} &= \frac{K_{P1}b_1(K_d)}{\tau^2} & a_{c21} &= a_{21} \\
a_{c22} &= a_{22} - K_{P1}b_2 & a_{c24} &= -\frac{K_{P1}b_2(K_{P2}\tau+K_d)}{\tau} \\
a_{c25} &= -b_2K_{I1} & a_{c26} &= -K_{P1}b_2K_{I3} \\
a_{c27} &= -K_{P1}b_2K_{I2} & a_{c28} &= \frac{K_{P1}b_2K_d}{\tau^2} \\
a_{c54} &= \frac{K_{P2}\tau+K_d}{\tau} & a_{c56} &= K_{I3} \\
a_{c57} &= K_{I2} & a_{c58} &= -\frac{K_d}{\tau^2}
\end{aligned}
$$

the controlled system has been analyzed. In Fig. 5.3 the behaviour of the controlled system with respect to the road curvature ρ is shown.

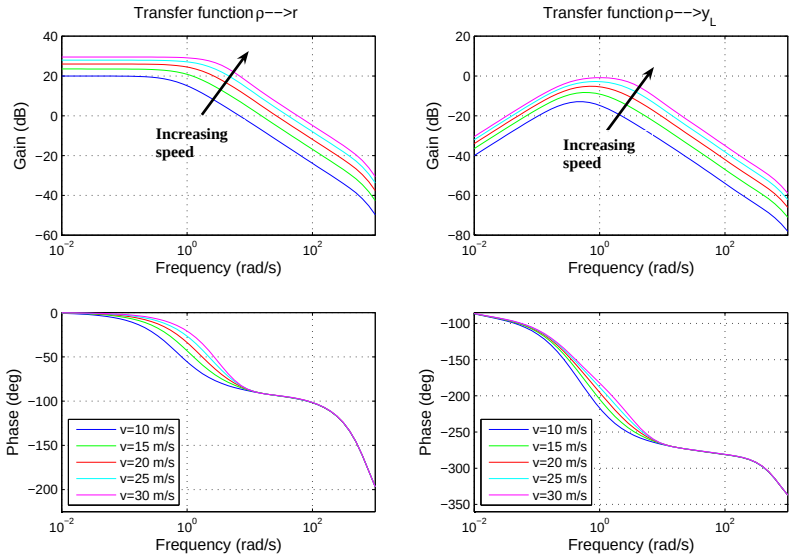

Figure 5.3: Bode diagram of the transfer functions between ρ and y_L and ρ and r.

On the left hand side of Fig. 5.3 the bandwidth of the transfer function from the road curvature to the yaw rate is shown while, on the right hand side of Fig. 5.3, the reduction of the road curvature effect on

the lateral offset is shown.
The transfer function between ρ and y_L for a speed v equal to $v = 36$ m/s is shown below to emphasize the double zeroes at the origin which ensure the rejection of disturbances that increase linearly with respect to time:

$$y_L = -\frac{36s^2\left(36s^4+45\ 10^3s^3+444\ 10^4s^2+2972\ 10^4s+137\ 10^5\right)}{s^8+h_7s^7+h_6s^6+h_5s^5+h_4s^4+h_3s^3+h_2s^2+h_1s+h_0}\rho \tag{5.15}$$

where the coefficients h_i are shown in Table 7.9.

5.3.3 Robustness

Only the robustness of the internal loop, Fig. 5.4, is analyzed since it contains the uncertain parameters of interest c_f, c_r, m and v. As a consequence only the first two dynamical equations in (2.27) along with (5.4) are considered for the robustness analysis.

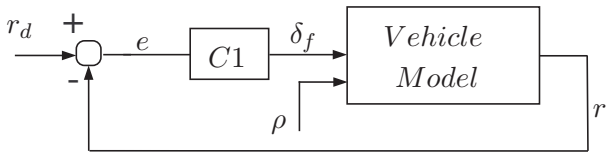

Figure 5.4: Internal loop control scheme.

We define: Σ_0 as the reduced system containing the dynamics of β and r with unperturbed parameters; Σ as the system with perturbations on c_f, c_r and m, $\Delta_P = P - P_0$ as the perturbation on Σ, where P and P_0 are the perturbed and the nominal transfer functions between the δ_f and r respectively; the transfer function between δ_f and r_d $V_0 = C_1(1 + P_0C_1)^{-1}$ as the control sensibility function; $\bar{\sigma}$ as the operator that gives the greater singular value of a transfer function. We

can apply the following theorem.

Theorem 1 *[69, 70]*
If:

α_0) $\lim_{s\to\infty}(1 + P_0C_1) \neq 0$

α_1) Σ_0 *is asymptotically stable*

then Σ *is asymptotically stable for all variations or perturbations of* P *from* P_0 *such that:*

β) *the number of eigenvalues of* A *in* C^- *is equal to the number of eigenvalues of* A_0 *in* C^-

γ) $\lim_{s\to\infty}(1 + PC_1) \neq 0$

δ) $\bar{\sigma}\left[\Delta_P(\omega)\right] < \frac{1}{\bar{\sigma}[V_0(\omega)]}$, $\forall\omega \in$ *Imaginary axis*

Theorem 1 is satisfied for different speeds and perturbations on tire parameters such as the cornering stiffnesses c_r, c_f (which may change due to different adherence conditions and/or low tire pressure) and the vehicle mass m (that vary from unloaded to full load conditions). The robustness decreases as speed increases as shown in the Fig. 5.5, in which a speed variation from 1 m/s to 36 m/s is considered. On the Y-axis of Fig. 5.5 an upper bound for the percentage variations of all the parameters c_r, c_f and m for which the robustness guarantees the asymptotical stability of Σ is shown.

5.4 CarSim simulations

Several simulations in CarSim environment have been performed to compare the CarSim driver model, which is based on a model predictive

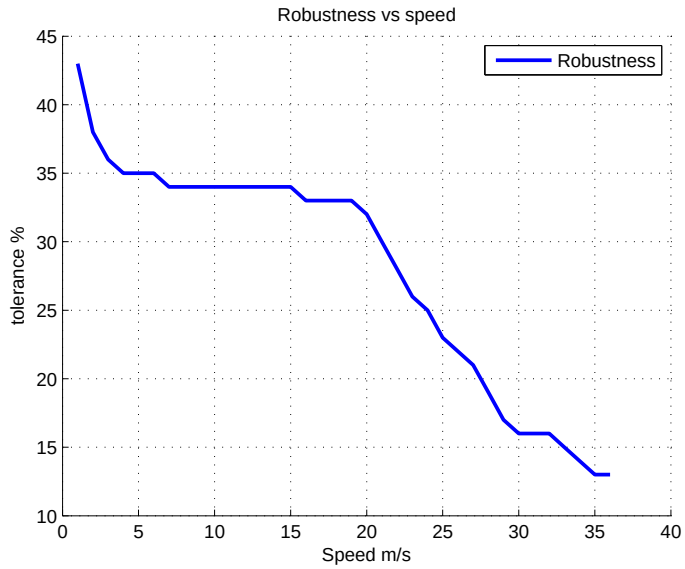

Figure 5.5: Robustness with respect of increasing speed.

control system [53] and makes also use of vehicle lateral speed, with the proposed nested PID control. CarSim vehicle uses detailed nonlinear tire models according to combined slip theory and takes into account the major kinematics and compliance effects of the suspensions (nonlinear spring models) and steering systems. The vehicle has a nonlinear second order speed depending rack and pinion ratio steering system; for the active steering a realistic actuator with a bandwidth of 10Hz is considered. The first simulation, shown in Fig. 5.7, concerns a path following in the case of a typical highway road curvature profile and a vehicle speed of 31 $[m/s]$. In Fig. 5.7 the XY-trajectory, the path following error, the steering angle and the yaw rate are shown for the vehicle controlled by the CarSim driver model and by the proposed control. To emphasize the simulation results only a detail of the path following manoeuvre is depicted as shown in the first subplot of Fig. 5.7: in that curve the vehicle reach a lateral acceleration of 7.8 $[m/s^2]$. Both controllers achieve the

path following however, as shown in the second subplot of Fig. 5.7, we may observe a more accurate lane keeping and a reduced path following maximum error in the lateral direction of 70% obtained by the proposed control law.

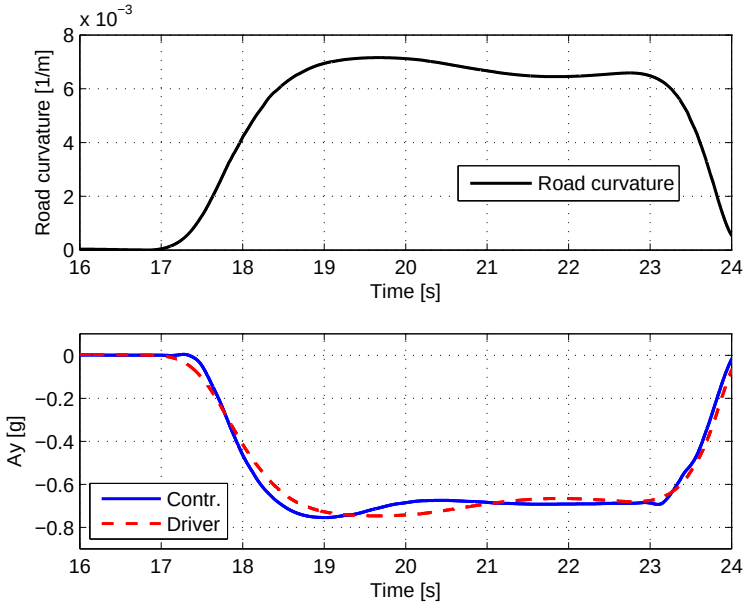

Figure 5.6: Target road curvature and lateral acceleration in a standard CarSim® path following manoeuvre ($v = 31$ $[m/s]$).

Both controllers achieve the path following: the error of the proposed control system is smaller than the error of the CarSim® simulated driver.

To analyze the performance of the proposed controlled system with respect to tire-road adherence variations a μ-split braking manoeuvre is performed ($\mu = 0.1$ on the left hand side and $\mu = 0.8$ on the right hand side in the CarSim model). A sudden braking action of 15 $[MPa]$ at a velocity of 40 $[m/s]$ is given on both the vehicle with the MPC and the vehicle with the nested PID control strategy: the proposed control system ensures the lane keeping (first subplot of Fig. 5.9) while

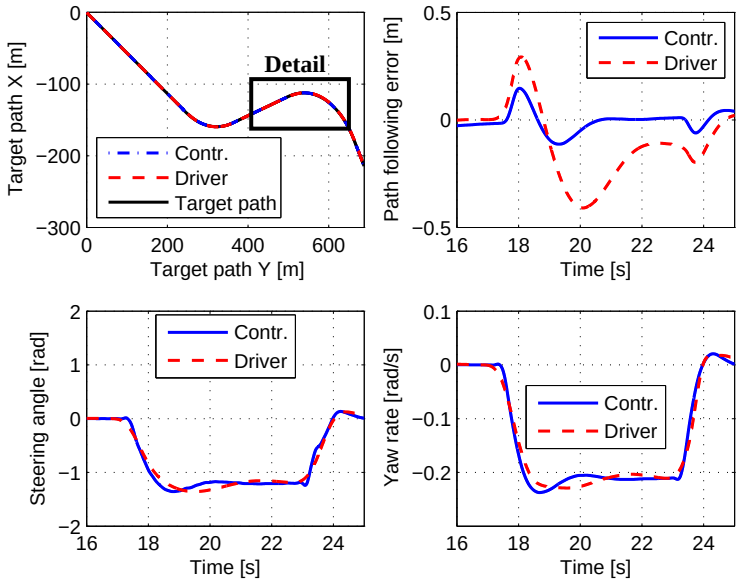

Figure 5.7: Standard CarSim® path following manoeuvre ($v = 31$ $[m/s]$).

the vehicle controlled by the CarSim driver model leaves the lane. The CarSim steering action saturates at the maximum allowed mechanical constrain that is equal to 720 $[deg]$ while we may observe the oscillations on the steering signal, provided by the proposed control, due to the ABS that prevents wheel lock while ensuring greater decelerations (third subplot of Fig. 5.9).

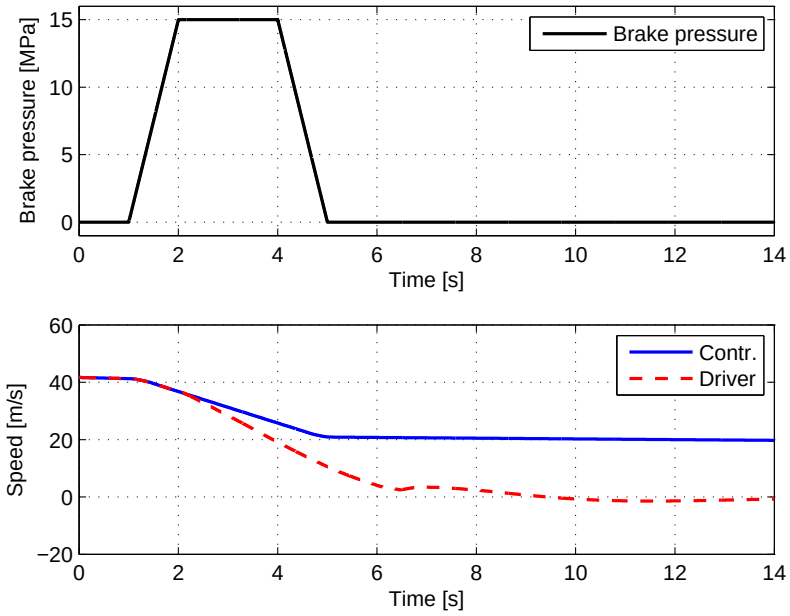

Figure 5.8: Braking pressure and vehicle speed for the μ-split braking manoeuvre.

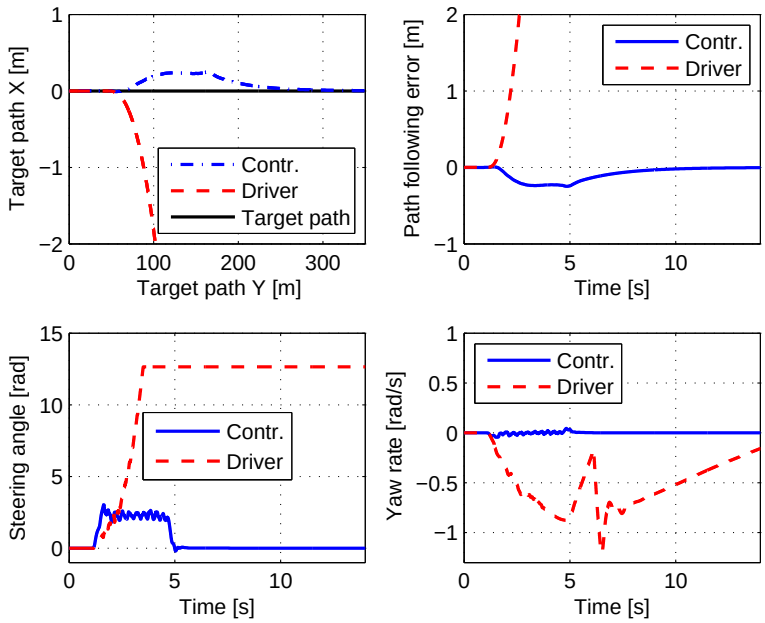

Figure 5.9: μ-split braking manoeuvre.

Chapter 6

Conclusions

6.1 Global Chassis Control Integration

In this Ph.D. thesis the following control systems are designed and validated by simulation:

- A PI steering control on the front wheels and a PI steering control on the rear wheels along with an additive feed forward reference signal for the vehicle sideslip angle in order to decouple vehicle sideslip and yaw rate dynamics from the desired yaw rate and vehicle sideslip angle reference signals. The PI controllers feed back the yaw rate tracking error. Chapter 3 shows that the proposed control system assigns real stable eigenvalues to a widely used linear model of the vehicle steering dynamics for any value of longitudinal speed in understeering vehicles.

- An integrated control of front and rear active differentials with an active front steering from the yaw rate and the wheel speed measurements in order to improve vehicle dynamics (by suppressing resonances and enlarging the bandwidth of the yaw rate tracking dynamics), safety and reduce driver effort. The control of the electronic differentials is not only aimed at keeping the wheel speed

differences at desired values but it is also integrated with the active steering control (a PI action from the yaw rate error) to produce a yaw moment (also depending on the yaw rate error) which improves the vehicle steering dynamics since the corresponding eigenvalues can be placed to be all real at every speed to prevent oscillations.

- A vision based lane keeping control for autonomous vehicles. As a first step, on the basis of lateral displacements at a look ahead distance provided by a vision system, a reference yaw rate signal is designed using PID control techniques; as a second step the steering angle is designed as a PI control on the yaw rate tracking error. The robustness of the proposed control with respect to speed variations and parameter uncertainties such as mass, front and rear cornering stiffnesses has been analyzed. Simulations in the CarSim environment illustrate the performance achieved by the proposed lane keeping control strategy both on a standard path and during a μ-split braking manoeuvre: the proposed controller is compared with the MPC used in CarSim as steering control which also requires the vehicle lateral speed and orientation. Future work will explore the interactions of the proposed controller with the driver both during normal driving and in emergency conditions.

A common output based approach is followed in the design of the control laws presented in this thesis (no lateral speed measurements or observer are required): the high variability of the physical vehicle parameters and the variable tire-road adherence conditions together with the good performance obtained by the proposed controls reinforce this approach.

6.2 New Control Avenues

Many sections of this thesis have hinted to possible future research topics. Following the current increasing production of four wheel steering vehicles [16] and [19] and the develop of high quality vision systems an integrated controlled 4WS vision based vehicle can be designed in order to combine the additional measure given by the camera with the generation of the yaw rate and/or the vehicle sideslip reference, as shown in Fig. 6.1 for autonomous vehicle.

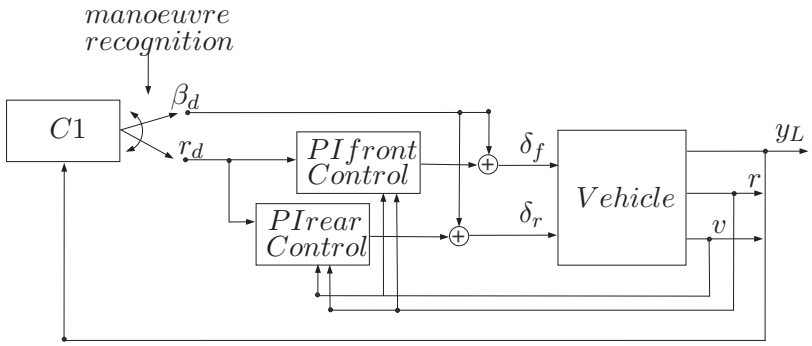

Figure 6.1: Vision based Four wheel steering vehicle.

Moreover, future works, will explore also the interactions with the driver both during normal driving and in emergency situations.

Also the works done on the active or semiactive differentials can be integrated in the framework of 4WS; due to the high number of actuators the control design of the overactuated system can be analyzed following an optimal control theory approach. However, the introduction of electric vehicles allow to directly control the torque at each wheel giving more degree of freedom to the designer and removing the mechanical constraints. The increasing number of electric vehicles is supported by

electric motors that often achieve 90% energy conversion efficiency over the full range of speeds and power of interest. They can also be combined with regenerative braking systems that have the ability to convert kinetic energy back into stored electricity. This can be used to reduce the wear on brake systems (and consequent brake pad dust) and reduce the total energy requirement. Another advantage is that electric vehicles typically have less vibration and noise pollution than a vehicle powered by an internal combustion engine. For this and other reasons, the control of electric vehicle can be a very interesting field of research.

Chapter 7

Appendix

7.1 Appendix - Asymptotic Decoupling Control

Table 7.1: Vehicle nomenclature:

v	vehicle velocity
v_x	longitudinal speed
v_y	lateral speed
β	vehicle sideslip angle
r	vehicle yaw rate
a_y	lateral acceleration
δ_p	driver steering angle
δ_f	front steer angle
δ_r	rear steer angle
CG	centre of gravity
m	vehicle mass
J	vehicle inertia vertical axle

l_f	distance front axle - CG
l_r	distance rear axle - CG
L	$l_f + l_r$
μ	adherence coefficient
$f_{s,l}$	lateral, longitudinal forces
ω_i	angular wheel speed
$\alpha_{f,r}$	front,rear tire sideslip
$\lambda_{f,r}$	long. front,rear sideslip
c_{yf}	lat. front cornering stiffness
c_{yr}	lat. rear cornering stiffness
c_{xf}	long. front cornering stiffness
c_{xr}	long. rear cornering stiffness
$B_{x,y\,f}$	Pacejka parameter
$B_{x,y\,r}$	Pacejka parameter
$C_{x,y\,f}$	Pacejka parameter
$C_{x,y\,r}$	Pacejka parameter
$D_{x,y\,f}$	Pacejka parameter
$D_{x,y\,r}$	Pacejka parameter
$E_{x,y\,f}$	Pacejka parameter
$E_{x,y\,r}$	Pacejka parameter

Table 7.2: Vehicle parameters for the linear model (2.27):

m	1300	[kg]	J	1296	[kg m^2]
l_f	0.88	[m]	l_r	1.32	[m]
c_f	9.417e+4	[N/rad]	c_r	7.946e+4	[N/rad]
T_f	1.465	[m]	T_r	1.470	[m]
R_w	0.334	[m]	J_w	0.9	[kg m^2]

Table 7.3: Pacejka tire model:

B_f	11.459	B_r	11.459
C_f	1.400	C_r	1.400
D_f	6562.8	D_r	5156.8
E_f	-0.5	E_r	-0.7

Table 7.4: Matrix M entries:

M_{11}	$\frac{Ll_rc_fc_rmv^2-(l_rl_fmv^2-L^3c_r+l_f^2mv^2)c_f^2}{Jmv\left(\left(l_rl_f+l_f^2\right)c_f+l_rmv^2\right)}$
M_{12}	0
M_{13}	0
M_{21}	$\frac{c_f\left(c_r{l_r}^2+c_f{l_f}^2\right)L}{J\left(l_rmv^2+l_rc_fl_f+c_f{l_f}^2\right)}$
M_{22}	$-\frac{c_rc_fL}{Jmv}$
M_{23}	$\frac{c_rc_fL}{Jmv}$
M_{31}	0
M_{32}	$-\frac{c_rl_r}{J}$
M_{33}	$\frac{c_fl_f}{J}$

7.2 Appendix - Integrated Control: Active Steering and Differentials

Table 7.5: Vehicle parameters for the linear model (4.8):

m	1862	[kg]	J	2488	[kg m^2]
l_f	1.18	[m]	l_r	1.77	[m]
c_{xf}	9.97e+4	[N]	c_{xr}	6.63e+4	[N]
c_{yf}	9.69e+4	[N/rad]	c_{yr}	6.90e+4	[N/rad]
T_f	1.57	[m]	T_r	1.57	[m]
R_w	0.38	[m]	J_w	1.1	[kg m^2]

Table 7.6: Pacejka tire model coefficients:

B_{yf}	12.45	B_{yr}	12.75
C_{yf}	1.42	C_{yr}	1.44
D_{yf}	5482	D_{yr}	3752
E_{yf}	-1.65	E_{yr}	-1.86
B_{xf}	13.80	B_{xr}	13.80
C_{xf}	1.30	C_{xr}	1.30
D_{xf}	5555	D_{xr}	3695
E_{xf}	-0.26	E_{xr}	-0.26

7.3 Appendix - Vision Based Autonomous Vehicles

Table 7.7: Vehicle parameters for the linear model (5.2):

m	2023	[kg]	J	6286	[kg m^2]
l_f	1.26	[m]	l_r	1.90	[m]
c_f	2.864e+5	[N/rad]	c_r	1.948e+5	[N/rad]

Table 7.8: Pacejka tire model:

B_f	11.459	B_r	11.459
C_f	1.400	C_r	1.400
D_f	6562.8	D_r	5156.8
E_f	-0.5	E_r	-0.7

Table 7.9: Substitutions

$h_7 = 1251.7$ $h_6 = 7.4\ 10^5$ $h_5 = 582\ 10^5$ $h_4 = 3981\ 10^5$

$h_3 = 11231\ 10^5$ $h_2 = 7434\ 10^5$ $h_1 = 1373\ 10^5$ $h_0 = 1.3\ 10^5$

List of Figures

List of Tables

Bibliography

[1] Y. Furukawa, N. Yuhara, S. Sano, H. Takeda, "A Review of Four-Wheel Steering Studies from the Viewpoint of Vehicle Dynamics and Control", Vehicle System Dynamics Vol. 18, pp. 151-186, 1989.

[2] Y. Shibahata, "Progress and Future Direction of Chassis Control Technology, Honda R&D, Tochigi R&D Centre - Proceedings of IFAC Symposium Advances in Automotive Control Salerno (Italy) pp. 9-14, March 2004.

[3] H. H. Chen, "Motor Vehicle with Supplementary Rear Steering Having Open and Closed Loop Modes", Delphi Technologies - Troy, Mi, United States Patent Pub. No. US 2002/0042671 A1 Aug 3/2001.

[4] A. B. Hac, "Rear Steering Control For Vehicles with Front and Rear Steering", Delphi Technologies - Troy, Mi, United States Patent Pub. No. US 2003/6,553,293 B1 Jan 3/2002.

[5] J. Ackermann, "Robust Car Steering by yaw rate control", IEEE Conference on Decision and Control, pp. 2033-2034, 1990.

[6] J. Ackermann, "Robust Decoupling, Ideal Steering Dynamics and Yaw Stabilization of 4WS Cars", Automatica, Vol. 30, No. 11, pp. 1761-1668, 1994.

[7] Y. Jia, "Robust control with decoupling performance for steering and traction of 4ws under velocity-varying motion", IEEE Trans. Contr. Syst. Technol., Vol. 8, no. 3, pp. 554-569, 2000.

[8] D. J. Leith, W. E. Leithead and M. Vilaplana, "Robust Lateral Controller for 4-Weel-Steer Cars with Actuator Constraints", Proceeding of 36^{th} IEEE Conference on Decision and Control, Seville, Spain, pp. 5101-5106, 2005.

[9] M. G. Skarpetis, F. N. Koumboulis, F. S. Barmpokas and G. E. Chamilothoris, "Decoupling Control Algorithms for 4ws Vehicles", Proceeding of 2006 International Conference on Mechatronics, Budapest, pp. 499-504, July 2006.

[10] R. Marino and F. Cinili, "Input-Output Decoupling Control by Measurement Feedback in Four-Wheel-Active-Steering Vehicles", IEEE Conference on Decision and Control, San Diego, CA, USA, 2006.

[11] G. Baumgarten, "Motor vehicle steering system having a yaw rate controller", Bayerische Motoren Werke, United States Patent Pub. No. US 20040070268 April 15/2004.

[12] A. Pauly, G. Baumgarten, "Overlay steering system and method for motor vehicles", Bayerische Motoren Werke, United States Patent Pub. No. US 6854558 Feb. 15/2005.

[13] H. B. Pacejka, "Tire and Vehicle Dynamics", Elsevier - Butterworth Heinemann, 2004.

[14] T. D. Gillespie, "Fundamentals of Vehicle Dynamics", SAE International 1992.

[15] S. Glaser, L. Nouveliere, B. Lussetti, "Speed Limitation on an Advanced Curve Warning System", Proceeding of the 2007 IEEE Intelligent Vehicle Symposium, Istanbul, Turkey, June 13-15, 2007.

[16] L. Lionel, P. Richard, "Method and System for Controlling a Vehicle Equipped with a Controlled Braking System and with a Four-Wheel Steering System", Renault, European Patent Office Pub. No. WO2008040889 Feb 04/2008.

[17] R. Schwarz, W. Dick, T. Meissner, F. Martin, "Dynamic Steering and Quattro with Sport Differential - Two Perfect Partners for Highest Agility and Active Safety", Proceeding of the 2008 FISITA Word Automotive Congress, Munich, Germany, September 14-19, 2008.

[18] T. C. Meissner, J. Fuchs, R. Schwarz, "Propulsion System for All-Wheel Drive Motor Vehicle", United States Patent Pub. No. US 0221425 Sep. 27/2007 .

[19] M. Wallbrecher, P. Herold, T. Thalhammer, "The New Steering System of BMW - The Integral-Active-Steering Synthesis of Agility and Sovereignty", Proceeding of the 2008 FISITA Word Automotive Congress, Munich, Germany, September 14-19, 2008.

[20] D. M. Bevly, J. Ryu, and J. C. Gerdes, "Integrating i.n.s. sensors with gps measurements for continuous estimation of vehicle sideslip, roll, and tire cornering stiffness", IEEE Trans. Intell. Transport. Syst., Vol. 7, no. 4, pp. 483-493, Dec. 2006.

[21] J. C. Hsu, R. H. Lin, and E. C. Yeh, "Vision-based motion measurement by directly extracting image features for vehicular steer-

ing control", Proceeding of the I MECH E Part D Journal of Automobile Engineering, Vol. 211, no. 4, pp. 277-289, Jul. 1997.

[22] H. Cherouat and S. D. M. Braci, "Vehicle velocity, side slip angles and yaw rate estimation", in Proc. of IEEE ISIE, Dubrovnik, Croatia, Jun. 2005.

[23] J. Farrelly and P. Wellstead, "Estimation of vehicle lateral velocity", in Proceeding of the 1996 IEEE Intern. Conf. on Control Applications, Deaborn, MI, Sep. 1996.

[24] L. R. Ray, "Nonlinear state and tire force estimation for advanced vehicle control", IEEE Trans. Contr. Syst. Technol., Vol. 3, no. 1, pp. 117-124, Mar. 1995.

[25] A. Ungoren, H. E. Tseng, and H. Peng, "A study on lateral speed estimation methods", Int. J. Vehicle Autonomous Systems, Vol. 2, no. 1, pp. 126-144, Feb. 2004.

[26] A. Hac and M. D. Simpson, "Estimation of vehicle side slip angle and yaw rate", SAE Technical Paper Series, no. 2000-01-0696, 2000.

[27] L. Imsland, T. A. Johansen, T. I. Fossen, H. F. Grip, and J. C. Kalkkuhl, "Vehicle velocity estimation using nonlinear observers", Automatica, Vol. 42,no. 12, pp. 2091Ű2013, September 2006.

[28] G. Genta, "Meccanica dell' Autoveicolo", Torino: Levrotto - Bella, 2000.

[29] M. Guiggiani, "Dinamica del Veicolo", Torino: Citta' Studi Edizioni, 2002.

[30] S. Frediani, R. Gianoglio and F. Giuliano, "System for the Active Control of a Motor Vehicle Differential", US Patent Number. 6,393,351 B2, Applicant Centro Ricerche Fiat, May 2002.

[31] Y. Ushiroda, K. Sawase and K. Suzuki, "Development of super AYC", New Technologies, n° 15, pp.73-76, 2003.

[32] F. Cheli, M. Giaramita, F. Resta, M. Zanchetta, G. C. Travaglio, "A New Control Strategy for a Semi-Active Differential", 16th IFAC World Congress, Prague, July 3-8, 2005.

[33] M. Canale, L. Fagiano, M. Milanese, P. Borodani, "Robust Vehicle Yaw Control Using Active Differential and Internal Model Control Techniques", Control Engineering Practice, Vol. 15 pp. 923Ű941, 2007.

[34] R. Marino, S. Scalzi, F. Cinili, "A Nonlinear Semiactive Rear Differential Control in Rear Wheel Drive Vehicles", Proceeding of the 26^{th} Chinese Control Conference, Zhangjiajie, China, July 26-31, 2007.

[35] M. Nagai, M. Shino, F. Gao, "Study on Integrated Control of Active Front Steer Angle and Direct Yaw Moment", JSAE Review, Vol. 23, pp. 309-315, 2002.

[36] J. Shi, "Integrated Global Chassis Control - A Top-Down Design Approach", Proceeding of FISITA World Automotive Congress, Yokohama, Japan, October 22-27, 2006.

[37] D. Li, X. Shen and F. Yu, "Study on the Chassis Control Integration Based on Tire Slip Ratio Regulation and Active Steering Control", Proceeding of FISITA World Automotive Congress, Yokohama, Japan, October 22-27, 2006.

[38] Y. Hattori, "Optimum Vehicle Dynamics Control Based on Tire Driving and Braking Forces", Toyota CRDL, Vol. 38, No. 4, 2003.

[39] M. Hancock, J. Kasac, J. Deur, B. Novakovic, "Optimization of Global Chassis Control Variables", Proceeding of the 17^{th} World Congress IFAC, Seoul, Korea, July 6-11, 2008.

[40] J. Gerhard, M. C. Laiou, M. Monnigmann, W. Marquardt, "Robust Yaw Control Design with Active Differential and Active Roll Control Systems", Advances in Automotive Control, IFAC, Salerno, Italy, April 19-23, 2004.

[41] R. Morselli, R. Zanasi, G. Sandoni, "Mechanical and Active Car Differentials: Detailed and Reduced Dynamic Models", 4TH MATHMOD, Vienna, pp. 1011-1020, February 5-7, 2003.

[42] T. Raste, R. Bauer, P. Rieth, "Global Chassis Control: Challenges and Benefits within the Networked Chassis", Proceeding of FISITA World Automotive Congress, Munich, Germany, September 14-19, 2008.

[43] M. Shiebahn, M. Lakehal, P. Zegelaar, O. Hofmann, "Coordination of Multiple Active Systems for Improved Vehicle Dynamics Coltrols", Proceeding of FISITA World Automotive Congress, Munich, Germany, September 14-19, 2008.

[44] R. Jihoon, J. Jinhee, K. Hyoungsoo, O. Seungkyu, L. Jongil, "A Proposal on the Advanced Unified Chassis Control System for the Enhancement of Vehicle Dynamics Control", Proceeding of FISITA World Automotive Congress, Munich, Germany, September 14-19, 2008.

[45] T.H. Hwang, K. Park, S.J. Heo, S.H. Lee, J.C. Lee, "Design of Integrated Chassis Control Logics for AFS and ESP", International Journal of Automotive Technology, Vol. 9, No. 1, pp.17-27, 2008.

[46] R. Marino, S. Scalzi, F. Cinili, "Active Front and Rear Steering Control in Four Wheel Steering", 31st FISITA Transactions 2006 - Paper no. F2006V089T.

[47] R. Marino, S. Scalzi, and F. Cinili, "Nonlinear PI front and rear steering control in four wheel steering vehicles", Vehicle System Dynamics Vol. 45, No. 12, pp. 1140-1168 October 2007.

[48] R. Marino, S. Scalzi, "Asymptotic Sideslip and Yaw Rate Decoupling Control in Four Wheel Steering Vehicles", submitted to Control Engineering Practice, March 2008.

[49] R. Marino, S. Scalzi, "Integrated Active Front Steering and Semiactive Rear Differential Control in Rear Wheel Drive Vehicles", Proceeding of the 17^{th} World Congress IFAC, Seoul, Korea, July 6-11, 2008.

[50] R. Marino, S. Scalzi, "Integrated Control of Active Steering and Electronic Differentials in Four Wheel Drive Vehicles", submitted to Automatica, December 2008.

[51] P. Kokotovic, H. Khalil, J. O'Reilly, "Singular Perturbation Methods in Control: Analysis and Design", Academic Press, London, 1986.

[52] R. Marino, P.Tomei, "Non Linear Control Design, Geometric, Adaptive, Robust", London, UK, Prentice Hall, pp. 362-363, 1995.

[53] C.C. MacAdam, "Application of an Optimal Preview Control for Simulation of Closed-Loop Automobile Driving", IEEE Transactions on Systems, Man, and Cybernetics, Vol.11, June 1981.

[54] N. M. Enache, M. Netto, S. Mammar, B. Lusetti, "Driver Steering Assistance for Lane Departure Avoidance", Accepted in Control Engineering Practice, 7 October 2008.

[55] N. M. Enache, M. Netto, S. Mammar, "Driver Steering Assistance for Lane Departure Avoidance Based on Hybrid Automata and on Composite Lyapunov Function", Submitted for publication to IEEE Trans. on Intelligent Transportation Systems, January 28, 2008.

[56] T. Raharijaona, G. Duc, S. Mammar, "H_∞ Controller Synthesis and Analysis with Application to Lateral Driving Assistance", IFAC Symposium on Advance in Automotive Control, Salerno, Italy, April 2004.

[57] J. Kang, R. Y. Hindiyeh, S. Moon, J. C. Gerdes, K. Yi, "Design and Testing of a Controller for Autonomous Vehicle Path Tracking Using GPS/INS Sensors", Proceedings of the 17th IFAC World Congress, Seoul, Korea, July 6-11, 2008.

[58] P. Falcone, F. Borrelli, J. Asgari, H. E. Tseng and D. Hrovat, "Predictive Active Steering Control for Autonomous Vehicle Systems", IEEE Transactions on Control Systems Technology, Vol. 15, NO. 3, May 2007.

[59] A. Takahashi, N. Asanuma, "Introduction of HONDA ASV-2 (Advanced safety Vehicle-Phase 2)", Proceedings of the IEEE Intelligent Vehicles Symposium. Dearborn (MI), USA, October 3-5, 2000.

[60] A. Broggi, M. Bertozzi, A. Fascioli, C.G. Lo Bianco, A. Piazzi, "The ARGO Autonomous Vehicle's Vision and Control Systems", International Journal of Intelligent Control and Systems. Vol. 3, No. 4, pp. 409-441, 1999.

[61] T. B. Foote, L. B. Cremean, J. H. Gillula, G. H. Hines, D. Kogan, K. L. Kriechbaum, J. C. Lamb, J. Leibs, L. Lindzey, C. E. Rasmussen, A. D. Stewart, J. W. Burdick, and R. M. Murray, "Alice: An information-rich autonomous vehicle for high-speed desert navigation", Journal of Field Robotics, Vol. 23, No. 9, Sept. 2006.

[62] M. Montemerlo, S. Thrun, H. Dahlkamp, D. Stavens, A. Aron, J. Diebel, P. Fong, J. Gale, M. Halpenny, G. Hoffmann, K. Lau, C. Oakley, M. Palatucci, V. Pratt, P. Stang, S. Strohband, C. Dupont, L.-E. Jendrossek, C.Koelen, C.Markey,C.Rummel,J.vanNiekerk, E. Jensen, P. Alessandrini, G. Bradski, B. Davies, S. Ettinger, A. Kaehler, A. Nefian, and P. Mahoney, "Stanley: the robot that won the DARPA grand challenge", Journal of Field Robotics, Vol. 23 , No. 9, Sept. 2006.

[63] V. Cerone, M. Milanese, D. Regruto, "Combined Automatic Lane Keeping and Driver's Steering Through a 2-DOF Control Strategy", IEEE Transactions on Control Systems Technology, Vol. 17, No. 1, pp. 135-142 Jan. 2009.

[64] V. Cerone, A. Chinu, D. Regruto, "Experimental results in vision-based lane keeping for highway vehicles", Proceedings of the American Control Conference. Anchorage, AK May 8-10, 2002.

[65] E.E. Sandoz, P.V. Kokotović, "Continuous Path Following Control for Underactuated Systems With Bounded Actuation", Proceedings of the 2007 IEEE Intelligent Vehicles Symposium. Istanbul, Turkey, June 13-15 2007.

[66] C. Hatipoğlu, K. Redmill and Ümit Özgüner, "Steering and Lane Change: A Working System", IEEE Conf. on Intelligent Transportation Systems, pp. 272-277, Boston, MA, 1997.

[67] Nishira, Hikaru, Seto, Yoji, Yamamura, Yoshinori, Kawabe, Taketoshi, "Research on predictive lane-changing algorithm using model predictive control", Proceeding of FISITA World Automotive Congress, Yokohama, Japan, October 22-27 2006.

[68] L. Liu, M. Nagai, P. Raksincharoensak, "On Torque Control of Vehicle Handling and Steering Feel for Avoidance Maneuver with Electric Power Steering", Proceedings of the 17th World Congress, The International Federation of Automatic Control. Seoul, Korea, July 6-11, 2008.

[69] M. Vidyasagar , H. Kimura, "Robust Controllers for Uncertain Linear Multivariable Systems", Automatica, Vol. 22, No. 1, pp. 85-94, January 1986.

[70] S. Paoletti, O.M. Grasselli and L. Menini, "A Comparison Between Classical Robust Stability Conditions", International Journal Robust and Nonlinear Control, Vol. 14, pp. 249-271, 2004.

[71] C. Ching Yu and W. L. Luyben, "Conditional stability in cascade control", Industrial & Engineering Chemistry Fundamentals, Vol. 25, No. 1, pp. 171-174, 1986.